The Dissertation Committee for Bethany Leeann Tiner Certifies that this is the approved version of the following dissertation:

Induction of Long-Term Immune Responses to Protect Mice against Pneumonic Plague: Development and Testing of Novel Live-Attenuated Mutants of *Yersinia pestis* CO92

Committee:

Ashok Chopra, Ph.D., C.Sc.

Vladimir Motin, Ph.D.

Johnny Peterson, Ph.D.

Yingzi Cong, Ph.D.

Vernon Tesh, Ph.D.

David Niesel, Ph.D.,

Senior Vice President and Dean, Graduate School

Induction of Long-Term Immune Responses to Protect Mice against Pneumonic Plague: Development and Testing of Novel Live-Attenuated Mutants of *Yersinia pestis* CO92

by

Bethany Leeann Tiner, B.S.

Dissertation

Presented to the Faculty of the Graduate School of

The University of Texas Medical Branch

for the Degree of

Doctor of Philosophy in Microbiology and Immunology

The University of Texas Medical Branch

June 2016

Dedication

To my husband, Peter, for his love and inspiration, and to my parents, Wayne and Roxanne, for their love, laughter, and support over the years

Acknowledgements

I wish to thank the members of my committee, Drs. Ashok Chopra, Vladimir Motin, Johnny Peterson, Yingzi Cong, and Vernon Tesh, for their support and advice through the duration of my work. I especially want to thank Dr. Motin and Dr. Cong for their assistance and providing reagents for the plasminogen-activator protease activity assay and for the long-term immune responses flow cytometry analysis, respectively. Also, I want to thank Dr. Wallace Baze for his help in the histopathological analysis of tissue sections and Dr. Vsevolod Popov for his help in performing and analyzing TEM imaging. Additionally, thank you to the past and present members of Dr. Chopra's laboratory for their help and support during my project, especially Dr. Jian Sha, Dr. Duraisamy Ponnusamy, Dr. Elena Kozlova, Dr. Tatiana Erova, Dr. Christina van Lier, Miss Jourdan Anderson, Mr. Eric Fitts, and Miss Michelle Kirtley. My eternal gratitude is extended to Dr. Chopra and Dr. Sha for all their guidance over the years. I would also like to acknowledge the Department of Microbiology and Immunology, especially the program director Dr. Lynn Soong, the program coordinator Ms. Aneth Zertuche, and the secretarial staff for their assistance and support. I sincerely thank the Sealy Center for Vaccine Development (SCVD) and the Jeane B. Kempner Foundation for providing me pre-doctoral fellowship support. The McLaughlin Endowment also awarded me the McLaughlin Scholar Award. Thank you to the SCVD as well as Dr. Alan Barrett and Dr. Gregg Milligan for selecting, financing, and advising me as an intern at the World Health Organization (WHO) in Geneva, Switzerland. I also want to thank my mentors and the members of the Global Influenza Programme and Pandemic Influenza Programme at the WHO for expanding my perspective on global health. Finally, I would like to thank my parents, Mr. and Mrs. Wayne Tiner, for their support and strength not only through graduate school but throughout my life, and my husband, Mr. Peter Kundert, for his encouragement, love, and patience even during arduous times.

Combinational deletion of three membrane protein-encoding genes highly attenuates *Yersinia pestis* while retaining immunogenicity in a mouse model of pneumonic plague

Publication No._____1_____

Bethany Leeann Tiner, Ph.D.

University of Texas Medical Branch, April 2015

Supervisor: Ashok Chopra, Ph.D., C.Sc.

Abstract:

Previously, we showed that deletion of genes encoding Braun lipoprotein (Lpp) and MsbB attenuated *Y. pestis* CO92 in mouse and rat models of bubonic and pneumonic plague. While Lpp activates Toll-like receptor-2, MsbB encoding acyltransferase modifies lipopolysaccharide. Here, we deleted the *ail* gene (encoding Attachment Invasion Locus) from the wild-type (WT) CO92 or its *lpp* single and Δ*lpp* Δ*msbB* double mutants. While the Δ*ail* single mutant was minimally attenuated, when compared to the WT bacterium in a mouse model of pneumonic plague, the Δ*lpp* Δ*ail* double and the Δ*lpp* Δ*msbB* Δ*ail* triple mutant were increasingly attenuated, with the latter unable to kill mice at a 50% lethal dose (LD_{50}) equivalent to 6800 of WT CO92. The mutant-infected animals developed balanced T_H1- and T_H2-based immune responses based on antibody isotyping. The triple mutant cleared from mouse organs rapidly with a concurrent decrease in the production of various cytokines and histopathological lesions. When surviving animals infected with the increasing doses of the triple mutant were subsequently challenged on day 24 with the bioluminescent WT CO92 (20-28 LD_{50}), 40 to 70% of the mice survived with efficient

clearing of the invading pathogen as visualized in real time by *in vivo* imaging. The rapid clearance of the triple mutant, when compared to that of WT CO92, from animals was related to decreased adherence and invasion of human-derived HeLa and A549 alveolar epithelial cells and to its inability to survive intracellularly in these cells as well as in MH-S murine alveolar and primary human macrophages. An early burst of cytokine production in macrophages elicited by the triple mutant compared to WT CO92, and the mutant's sensitivity to the bactericidal effect of human serum would further augment bacterial clearance. Together, deletion of the *ail* gene from the Δ*lpp* Δ*msbB* double mutant severely attenuated *Y. pestis* CO92 to evoke pneumonic plague in a mouse model while retaining required immunogenicity needed for subsequent protection against infection.

Intramuscular immunization of mice with a live-attenuated triple mutant of *Yersinia pestis* CO92 induces robust humoral and cell-mediated immunity to completely protect animals against pneumonic plague

Publication No._____2_____

Bethany Leeann Tiner, Ph.D.

University of Texas Medical Branch, December 2015

Supervisor: Ashok Chopra, Ph.D., C.Sc.

Abstract:

Earlier, we showed that the Δ*lpp* Δ*msbB* Δ*ail* triple mutant of *Yersinia pestis* CO92 deleted for genes encoding Braun lipoprotein (Lpp), an acyltransferase (MsbB), and the Attachment Invasion Locus (Ail), respectively, was avirulent in a mouse model of pneumonic plague. In this study, we further evaluated the immunogenic potential of the Δ*lpp* Δ*msbB* Δ*ail* triple mutant and its derivative by different routes of vaccination. Mice were immunized *via* the subcutaneous (s.c.) or the intramuscular (i.m.) route with two doses (2 x 10^6 CFU/dose) of the above-mentioned triple mutant with 100% survivability of the animals. Upon subsequent pneumonic challenge with 70-92 LD_{50} of WT CO92, all of the mice survived when immunization occurred by the i.m. route. Since Ail has both virulence and immunogenic potential, a mutated version of Ail devoid of its virulence properties was created, and the genetically modified *ail* replaced the native *ail* gene on the chromosome of the Δ*lpp* Δ*msbB* double mutant, creating a Δ*lpp* Δ*msbB::ailL2* vaccine strain. This newly generated mutant was similarly attenuated as the Δ*lpp* Δ*msbB* Δ*ail* triple mutant when administered by the i.m. route, and provided 100% protection to animals

against subsequent pneumonic challenge. Not only did both of the above-mentioned mutants cleared rapidly from the initial i.m. site of injection in animals with no histopathological lesions, the immunized mice did not exhibit any disease symptoms during immunization and after subsequent exposure to WT CO92. These two mutants triggered balanced Th1- and Th2- based antibody responses and cell-mediated immunity. A substantial increase in IL-17 from T-cells of vaccinated mice, a cytokine of the Th17 cells, further augmented their vaccine potential. Thus, both Δ*lpp* Δ*msbB* Δ*ail* triple and Δ*lpp* Δ*msbB::ailL2* mutants represent excellent vaccine candidates for plague, with the latter mutant still retaining Ail immunogenicity but much diminished virulence potential.

Immunization of mice with new live-attenuated mutants of *Yersinia pestis* CO92 induces protective long-term humoral- and cell-mediated immunity against pneumonic plague

Publication No._____3_____

Bethany Leeann Tiner, Ph.D.

University of Texas Medical Branch, June 2016

Supervisor: Ashok Chopra, Ph.D., C.Sc.

Abstract:

We showed recently that the live-attenuated Δ*lpp* Δ*msbB* Δ*ail* and Δ*lpp* Δ*msbB::ailL2* mutants of *Yersinia pestis* CO92 provided short-term protection to mice against developing subsequent lethal pneumonic plague. These mutants were either deleted for genes encoding Braun lipoprotein (Lpp), an acetyltransferase (MsbB), and the attachment invasion locus (Ail) (Δ*lpp* Δ*msbB* Δ*ail*) or contained a modified version of the *ail* gene with diminished virulence (Δ*lpp* Δ*msbB::ailL2*). Here, long-term immune responses were examined after intramuscular immunization of mice with the above-mentioned mutants, as well as the newly constructed Δ*lpp* Δ*msbB* Δ*pla* mutant, deleted for the plasminogen-activator protease (*pla*) gene instead of *ail*. *Y. pestis*-specific IgG levels peaked between day 35 and 56 in the mutant-immunized animals and were sustained until the last tested day 112. Splenic memory B cells peaked earlier (day 42) before declining in the Δ*lpp* Δ*msbB::ailL2* mutant-immunized mice while being sustained for 63 days in the Δ*lpp* Δ*msbB* Δ*ail* and Δ*lpp* Δ*msbB* Δ*pla* mutant-immunized animals. Splenic $CD4^+$ T cells increased in all immunized mice by day 42 with differential cytokine production among the immunized

groups. On day 120, animals were exposed intranasally to wild-type (WT) CO92, and 80-100% of the immunized mice survived pneumonic challenge. Animals immunized with the above-mentioned three mutants had increased innate as well as $CD4^+$ responses immediately after WT CO92 exposure, and coupled with sustained antibody production, indicated the role of both arms of the immune response in protection. These data warrant further testing of these *Y. pestis* live-attenuated vaccine candidates in higher animal models.

TABLE OF CONTENTS

LIST OF TABLES ***XIV***

LIST OF FIGURES ***XV***

LIST OF ABBREVIATIONS ***XVIII***

CHAPTER 1 ***1***

Introduction ***1***
Vaccines against the Plague 2
Live-attenuated Vaccine Development in our Laboratory 3
Braun Lipoprotein (Lpp) and Acyltransferase (MsbB) 4
Plasminogen-Activator Protease (Pla) 6
Attachment Invasion Locus (Ail) 7
Specific Aims 9

CHAPTER 2 ***10***

Materials and Methods ***10***
Bacterial strains and plasmids. 10
Deletion of the *ail* gene. 10
Mutation of the *ail* gene. 14
Creation of the Δ*lpp* Δ*msbB* Δ*pla* mutant of *Y. pestis* CO92. 15
Complementation of the Δ*ail* mutant strains of *Y. pestis* CO92. 15
Absence of Ail and unchanged level of Lpp in the membranes of *Y. pestis* CO92 Δ*ail* mutants. 17
Growth kinetics and membrane alteration of the *Y. pestis* CO92 triple mutant. 17
Sensitivity of the *Y. pestis* CO92 mutants to gentamicin. 17
Evaluation of the essential *Y. pestis* virulence factors in various mutants of *Y. pestis* CO92. 18
Type 3 Secretion System (T3SS) 18
Capsular Antigen (F1) 19
Plasminogen-Activator Protease (Pla) 20
Serum resistance of various mutants of *Y. pestis* CO92. 21
Adherence, invasion, and intracellular survival of various *Y. pestis* CO92 mutants in HeLa and A549 epithelial cells. 22
Intracellular survival of mutant strains in murine alveolar macrophages and human monocyte-derived macrophages. 23
Animal studies with the *Y. pestis* CO92 mutant strains. 24
i) Attenuation and survival analysis of *Y. pestis* CO92 mutant strains. 24
ii) Bacterial dissemination and histopathological studies with infection triple mutant of *Y. pestis* CO92. 25
iii) Cytokine and chemokine levels in mice after intranasal administration of the triple mutant of *Y. pestis* CO92. 26
iv) Intramuscular and Subcutaneous Immunization. 26
v) Antibody responses after immunization. 27

vi) Protection assays. 27
vii) Histopathological analysis of immunized mice. 28
viii) Progression of infection. 28
ix) T-cell proliferative responses and cytokine production 30
x) Long term humoral and cell-mediated immune responses. 30
Statistical analysis. 32

CHAPTER 3 ***34***

Combinational deletion of three membrane protein-encoding genes highly attenuates Yersinia pestis while retaining immunogenicity in a mouse model of pneumonic plague ***34***
Introduction 34
Results 35
In vitro characterization of Δ*ail* mutants of *Y. pestis* CO92. 35
The Δ*lpp* Δ*msbB* Δ*ail* triple mutant of *Y. pestis* CO92 produces essential *Y. pestis* virulence and immunogenic factors. 36
Evaluation of *Y. pestis* CO92 Δ*ail* mutants in a pneumonic plague mouse model. 40
Bacterial dissemination and histopathological lesions in mice challenged by the intranasal route with Δ*lpp* Δ*msbB* Δ*ail* triple mutant of *Y. pestis* CO92. 46
The Δ*lpp* Δ*msbB* Δ*ail* triple mutant of *Y. pestis* CO92 evokes reduced inflammatory cytokines in a pneumonic plague mouse model. 49
The Δ*ail* mutants of *Y. pestis* CO92 have host-dependent serum sensitivities. 50
Decreased adherence and invasion of *Y. pestis* CO92 Δ*ail* mutants in the epithelial cells. 51
Host-dependent survivability of *Y. pestis* CO92 Δ*ail* mutants in murine and human macrophages and epithelial cells. 53
Host-dependent inflammatory cytokine secretion by *Y. pestis* CO92 Δ*ail* mutants in infected macrophages. 56
Discussion 58

CHAPTER 4 ***66***

Intramuscular immunization of mice with a live-attenuated triple mutant of Yersinia pestis CO92 induces robust humoral and cell-mediated immunity to completely protect animals against pneumonic plague ***66***
Introduction 66
Results 67
Evaluation of protection provided by intramuscular immunization of mice with the Δ*lpp* Δ*msbB* Δ*ail* triple mutant in a pneumonic plague model. 67
In vitro characterization of the Δ*lpp* Δ*msbB::ailL2* mutant of *Y. pestis* CO92. 69
Evaluation of protection provided by intramuscular or subcutaneous immunization of mice with the Δ*lpp* Δ*msbB* Δ*ail* triple or the Δ*lpp* Δ*msbB::ailL2* mutant in a pneumonic plague model. 71
Histopathological analysis of mouse tissues after intramuscular immunization with the Δ*lpp* Δ*msbB* Δ*ail* triple and the Δ*lpp* Δ*msbB::ailL2* mutant and post exposure to WT *Y. pestis* CO92 in a pneumonic plague model. 75
Progression of infection and histopathological lesions in mice intramuscularly infected with the Δ*lpp* Δ*msbB* Δ*ail* triple and the Δ*lpp* Δ*msbB::ailL2* mutant of *Y. pestis* CO92. 78
Activation of T cells by the Δ*lpp* Δ*msbB* Δ*ail* triple and the Δ*lpp* Δ*msbB::ailL2* mutant of *Y. pestis* CO92 after intramuscular or subcutaneous immunization of mice. 81
Discussion 83

CHAPTER 5 ***90***

Immunization of mice with new live-attenuated mutants of Yersinia pestis CO92 induces protective long-term humoral- and cell-mediated immunity against pneumonic plague ***90***
Introduction 90
Results 91
Attenuation in virulence of the Δ*lpp* Δ*msbB* Δ*pla* mutant of *Y. pestis* CO92. 91
Evaluation of long-term humoral immunity in mice after immunization with live-attenuated mutants of *Y. pestis* CO92. 92
Long-term cell-mediated immunity after immunization of mice with live-attenuated mutants of *Y. pestis* CO92. 96
Evaluation of long-term protection against pneumonic plague provided by immunization of mice with live-attenuated mutants of *Y. pestis* CO92. 98
Evaluation of the immediate innate immune response of vaccinated mice after exposure to WT *Y. pestis* CO92 in a pneumonic plague model. 100
Evaluation of cytokine producing $CD4^+$ T cells in immunized mice after exposure to WT *Y. pestis* CO92 in a pneumonic plague model. 101
Discussion 104

CHAPTER 6 ***109***

Conclusions and Future Directions ***109***

REFERENCES ***111***

VITAE ***123***

LIST OF TABLES

Table 2.1. Bacterial strains and plasmids used in this study.....12

Table 2.2. Sequences of primers used in this study.....16

LIST OF FIGURES

Figure 1.1. Outer Membrane of *Yersinia pesits*.....4

Figure 3.1. Ail and Lpp production and transmission electron microscopic analysis. 35

Figure 3.2. Growth curve of WT *Y. pestis* CO92 and its Δ*lpp* Δ*msbB* Δ*ail* triple mutant.....36

Figure 3.3. Functionality of the T3SS and production/enzymatic activity of the Pla protease.....37

Figure 3.4. Production of F1 antigen.....40

Figure 3.5. Survival analysis and antibody responses of mice infected with WT *Y. pestis* CO92 and its mutant strains in a pneumonic plague model. 41

Figure 3.6. Virulence potential of and subsequent protection conferred by the Δ*lpp* Δ*msbB* Δ*ail* triple mutant *Y. pestis* CO92 in a pneumonic plague mouse model.....43

Figure 3.7. Survival analysis and subsequent protection conferred by high doses of Δ*lpp* Δ*msbB* Δ*ail* triple mutant of *Y. pestis* CO92 in a pneumonic plague mouse model. 45

Figure 3.8. Dissemination of WT CO92 and its Δ*lpp* Δ*msbB* Δ*ail* triple mutant in a mouse model of pneumonic plague. 47

Figure 3.9. Histopathology of mouse tissues following pneumonic infection with WT CO92 or its Δ*lpp* Δ*msbB* Δ*ail* triple mutant. 48

Figure 3.10. Cytokine/chemokine analysis on the sera and lung homogenates of mice in a pneumonic plague mouse model.....49

Figure 3.11. Serum resistance and Ail production by various *Y. pestis* CO92 strains.....51

Figure 3.12. Adherence and invasion of WT *Y. pestis* CO92 and its mutant strains. 52

Figure 3.13. Adherence and invasion of WT *Y. pestis* CO92 and its mutant strains. 53

Figure 3.14. Intracellular survival of various *Y. pestis* CO92 mutant strains in epithelial cells and macrophages.....55

Figure 3.15. Inflammatory cytokine production by macrophages infected with various *Y. pestis* CO92 strains. 57

Figure 4.1. Immunity conferred by the Δ*lpp* Δ*msbB* Δ*ail* triple mutant to mice *via* intramuscular immunization. 68

Figure 4.2. Ail associated virulence activities in the Δ*lpp* Δ*msbB::ailL2* mutant. 70

Figure 4.3. Immunity conferred by the Δ*lpp* Δ*msbB* Δ*ail* and Δ*lpp* Δ*msbB::ailL2* mutants to mice *via* intramuscular and subcutaneous routes of immunization.....73

Figure 4.4. Antibody responses in mice elicited by the Δ*lpp* Δ*msbB* Δ*ail* or the Δ*lpp* Δ*msbB::ailL2* mutant *via* intramuscular or subcutaneous route of immunization.....75

Figure 4.5. Histopathological analysis of mouse organs after immunization. 76

Figure 4.6. Histopathological analysis of immunized mouse organs after WT CO92 challenge. 77

Figure 4.7. Progression of infection in mice intramuscularly infected with various *Y. pestis* CO92 strains. 79

Figure 4.8. Histopathological alterations in mice intramuscularly infected with various Y. pestis CO92 strains. 80

Figure 4.9. T-cell proliferation. 82

Figure 4.10. T-cell cytokine production. 83

Figure 5.1. Survival analysis and protection conferred by vaccination of mice with high doses of the Δ*lpp* Δ*msbB* Δ*pla* mutant of *Y. pestis* CO92 in a pneumonic plague mouse model. 92

Figure 5.2. Long-term humoral immune responses in mice immunized with live-attenuated mutants of *Y. pestis* CO92. 95

Figure 5.3. Long-term cell-mediated immune responses in mice immunized with live-attenuated mutants of *Y. pestis* CO92. 97

Figure 5.4. Survival analysis of immunized mice after exposure to WT *Y. pestis* CO92 in a pneumonic plague model. 99

Figure 5.5. Innate immune responses in immunized mice after exposure to WT *Y. pestis* CO92 in a pneumonic plague model. 100

Figure 5.6. Cell-mediated immune responses in immunized mice after exposure to WT *Y. pestis* CO92 in a pneumonic plague model. 102

LIST OF ABBREVIATIONS

aa	Amino Acid
Ail	Adhesion Invasion Locus
ANOVA	Analysis of Variance
APC	Antigen Presenting Cells
ATCC	American Type Culture Collection
A549	Human Alveolar Epithelial Cells
CDC	Centers for Disease Control and Prevention
CFU	Colony Forming Unit
DMEM	Dulbecco Modified Eagle Medium
DPBS	Dulbecco Phosphate-buffered Saline
EGTA	Ethylene Glycol Tetra-acetic Acid
EV76	Live-Attenuated Plague Vaccine which lacks the *pgm* locus
FBS	Fetal Bovine Serum
FDA	Food and Drug Administration
F1	Fraction 1 Capsular Antigen
F1-V	Fusion Protein Containing F1 and LcrV Antigens
F-12K	Kaighn's Medium
GSBS	Graduate School of Biomedical Sciences
H&E	Hemotoxylin & Eosin
HeLa	Human Cervical Epithelial Cells
HIB	Heart Infusion Broth
HMDM	Human Monocyte-derived Macrophages
IFN	Interferon
IgG	Immunoglobulin G
IL	Interleukin
i.m.	Intramuscular
iMF	Monocyte-derived Macrophages
i.n.	Intranasal
KIM/D27	Mutant of *Y. pestis* KIM Strain which lacks the *pgm* locus
LB	Luria-Bertani Medium
LcrV	Low Calcium Response V Antigen
LD_{50}	Minimum lethal dose that kills 50% of animals
Lpp	Braun Lipoprotein
LPS	Lipopolysaccharide
L2	Loop L2 of Ail
MHC-II	Major Histocompatibility Complex II
MH-S	Murine Alveolar Macrophages
MIC	Minimum Inhibitory Concentration
MOI	Multiplicity of Infection
MsbB	Acyltransferase
NHP	Nonhuman Primate
OD	Optical Density

PBMC	Peripheral Blood Mononuclear Cells
PBS	Phosphate-Buffered Saline
pgm	Pigmentation Locus
Pla	Plasminogen-Activator Protease
PMA	Phorbol 12-Myristate 13-Acetate
SBA	Sheep Blood Agar
s.c.	Subcutaneous
SDS-PAGE	Sodium Dodecyl Sulfate Polyacrylamide Gel Electrophoresis
TCA	Tricholoracetic Acid
TEM	Transmission Electron Microscopy
TNF	Tumor Necrosis Factor
T3SS	Type Three Secretion System
UTMB	University of Texas Medical Branch
WHO	World Health Organization
WT CO92	Wild-type *Yersinia pestis* CO92 Strain

Chapter 1

Introduction

Pathogenic yersiniae lead to two types of diseases: yersiniosis (typified by gastroenteritis caused by *Yersinia enterocolitica* and *Y. pseudotuberculosis*) (1) and plague (caused by *Y. pestis*) (2, 3). *Y. pestis* evolved from *Y. pseudotuberculosis* within the last 20,000 years by acquiring additional plasmids and pathogenicity islands as well as by deactivating some genes (4-6). These evolutionary adaptations allowed the plague bacterium to maintain a lifecycle in both the flea and rodents/mammals and to confer the ability to survive in the blood instead of the intestine (3). Plague manifests itself in three forms: bubonic (acquired from an infected rodent through a flea bite), pneumonic (acquired either directly by aerosol transmission from an infected host's lungs through respiratory droplets or secondarily from bubonic plague), and septicemic (severe bacteremia either directly due to a flea bite or subsequent to bubonic or pneumonic plague) (2). The latter two forms of plague are almost always fatal without treatment or if the administration of antibiotics is delayed (7, 8).

Historically, *Y. pestis* has caused three pandemics and over 200 million deaths worldwide: the 541 AD Justinian Plague which spread from Ethiopia to Europe, the 1347 Black Death plague which decimated Europe, and the 1894 plague originating in mainland China (9, 10). *Y. pestis* is currently classified as a reemerging pathogen by the World Health Organization (WHO) due to climate changes and shifts in its rodent carrier ranges having caused increased outbreaks in recent years (11). *Y. pestis* is classified as a Tier-1 select agent by the Centers for Disease Control and Prevention (CDC) due to the ease of

weaponizing the organism and its associated high mortality rate in humans (8, 9, 12). Currently, there are only two FDA-approved antibiotics for plague (levofloxacin [2012] and moxifloxacin [2015]) (13-15). Alarmingly, antibiotic-resistant strains of *Y. pestis* have been isolated from plague patients; and according to state documents, it is known that drug-resistant strains have been engineered in laboratories for possible use by terrorists (9). Therefore, vaccination is the optimal strategy for human protection against this deadly disease. However, there are currently no FDA-licensed plague vaccines available in the United States (16-18).

VACCINES AGAINST THE PLAGUE

Most current attempts to develop plague vaccines are recombinant subunit vaccines consisting of a low-calcium response V (LcrV) antigen as well as the capsular antigen F1. While these F1-V based vaccines are highly efficacious against pneumonic plague in rodents and macaques, this protection becomes variable in African green monkeys (7, 19-26). Furthermore, LcrV is highly divergent among *Y. pestis* strains (2, 27) and F1-deficient strains are still capable of causing disease (28, 29). Thus, the F1-V-based vaccines cannot provide optimal protection against all plague-causing *Y. pestis* strains (30, 31).

Although a heat-killed plague vaccine composed of the *Y. pestis* 195/P strain was in use in the United States until 1999, the production of this vaccine was discontinued because it was effective only against the bubonic and not the pneumonic plague. It was also highly reactogenic in humans (19, 32). The most effective live-attenuated vaccine which is currently administered is the EV76 strain and its various derivatives. Originally, the EV strain was isolated from a human case of bubonic plague in Madagascar which was then passaged for 6 years in order to create the EV76 vaccine (33). Various live-attenuated

Y. pestis EV76 vaccine strains, which lack the 102-kb chromosomal region encoding the pigmentation locus (*pgm*) required for iron utilization and haemin storage, provide protection against both bubonic and pneumonic plague and are being used in some parts of the world where plague is endemic (16).

The EV76 strain contains both *lcrV* and the F1 operon (34) which may explain why the protection it confers is superior compared to other live-attenuated strains. Developing live-attenuated mutants with genomic differences from EV76 could provide understanding about the variability of immunogenic and protective effectiveness of such EV-based plague vaccines. However, these EV76-based vaccines are not genetically uniform and are also highly reactogenic (35). They thus do not meet the standards for FDA approval. Also problematic is that EV NIIEG, a subculture of EV76 used for immunization, is highly virulent during intravenous inoculation of mice even though it is avirulent by other routes of administration (36). In addition, the Δ*pgm* mutants of *Y. pestis* (e.g., KIM/D27 strain) may not be safe because of a reported case of fatal infection in an individual with hemochromatosis (37, 38).

LIVE-ATTENUATED VACCINE DEVELOPMENT IN OUR LABORATORY

Our recent efforts to develop novel live-attenuated vaccines led to the deletion and/or modification of the genes encoding Braun lipoprotein (Lpp), an acetyltransferase (MsbB), the attachment invasion locus (Ail), and the plasminogen-activator protease (Pla) (39-42). All of these proteins are located in the outer membrane of *Y. pestis* (**Fig. 1.1**). Our past efforts included the development of both the Δ*lpp* Δ*msbB* and Δ*lpp* Δ*pla* double mutants. The focus of this project was on the creation of triple mutants of *Y. pestis*, primarily the Δ*lpp* Δ*msbB* Δ*ail* triple mutant and its derivative, Δ*lpp* Δ*msbB::ailL2*, in order to examine Ail's role in virulence and immunogenicity. The Δ*lpp* Δ*msbB* Δ*pla* triple mutant

(which has native Ail intact) was also developed and its vaccine potential was compared to that of the Δ*lpp* Δ*msbB* Δ*ail* and Δ*lpp* Δ*msbB::ailL2* mutants.

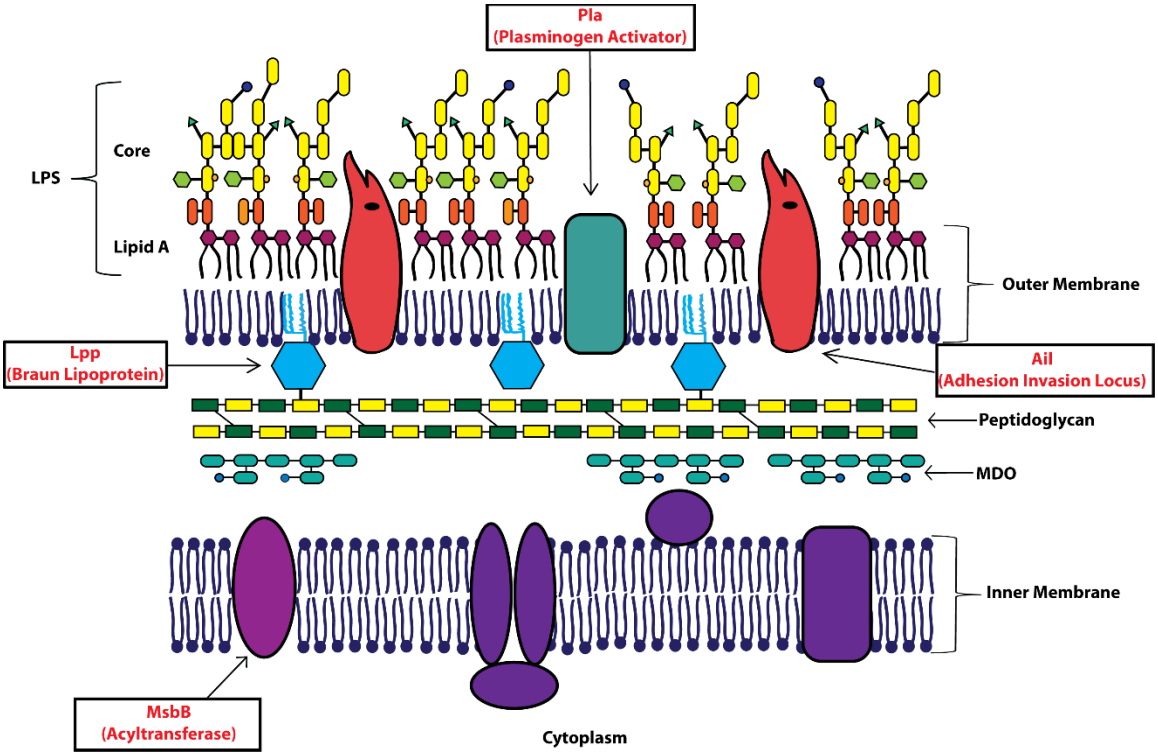

Figure 1.1. Outer Membrane of *Yersinia pesits*
Schematic representation of the membrane of *Y. pestis*. At the human host temperature (37ºC), the LPS is tetraacylated instead of hexaacylated. *Y. pestis* LPS also lacks the O-antigen. Important membrane components for this study are highlighted in red (Lpp, MsbB, Ail, and Pla).

Braun Lipoprotein (Lpp) and Acyltransferase (MsbB)

Lpp and lipopolysaccharide (LPS) are the most abundant components of the outer membrane of gram-negative bacteria in the *Enterobacteriaceae* family to which *Y. pestis* belongs (43, 44). Both Lpp and LPS trigger toxic and biological responses in the hosts through interaction of their lipid domains with toll-like receptor (TLR)-2 and -4, respectively, and by evoking the production of inflammatory cytokines such as tumor necrosis factor (TNF-α), interleukin 6 (IL-6), and interferon gamma (IFN-γ) (45, 46). Also, the complement and coagulation cascades are activated by both Lpp and LPS, and the

production of other damaging inflammatory mediators contributes to the severity of infection (45, 47-49). Our earlier studies have indicated that *Y. pestis* strains which lack Lpp have decreased ability to survive in macrophages (40, 50-52).

While Lpp links the peptidoglycan layer to the outer membrane of *Y. pestis* (53), MsbB is an acyltransferase located in the inner membrane of the bacterial cell wall and catalyzes the addition of lauric acid (C_{12}) to the lipid A moiety of LPS, thus increasing its biological potency (54-57). *Y. pestis* synthesizes a rough LPS devoid of the O antigen and exists in different acylated forms depending upon bacterial growth temperatures (54, 58-64). For example, the lipid A of *Y. pestis* LPS shifts from a hexa-acylated form at 21-27ºC (flea temperature) to a tetra-acylated form at 37ºC (human temperature) due in part to the inactivity of MsbB at 37ºC, which prevents the activation of TLR-4 (54-57).

Δlpp Δmsbb

In our earlier study, we investigated the effects of deletion of *lpp* and *msbB* genes in the pathogenesis of a highly virulent *Y. pestis* CO92 strain (42). Both Δ*lpp* single and Δ*lpp* Δ*msbB* double mutants exhibited significant attenuation (70 to 100%) when compared to the wild-type (WT) bacterium in pneumonic and bubonic plague mouse models at 3 50% lethal dose (LD_{50}) (42). Importantly, only animals initially challenged with the double mutant in a pneumonic plague model were significantly protected (55%) upon subsequent pneumonic infection with 10 LD_{50} of WT CO92 (42). The attenuated phenotype of the Δ*lpp* Δ*msbB* double mutant in mouse models correlated with its reduced survivability in murine RAW 264.7 macrophages (42). Furthermore, the Δ*lpp* Δ*msbB* double mutant evoked reduced levels of inflammatory cytokines compared to the WT bacterium in a pneumonic plague mouse model, which coincided with overall decreased dissemination of the mutant

to the peripheral organs of mice (42). However, while the Δ*lpp* Δ*msbB* double mutant was much more impaired in its ability to disseminate compared to the Δ*lpp* single mutant, substantial numbers of the double mutant were still detected at the initial infection site (lungs) in some mice 3 days post-infection (p.i.) (42). Similarly, the Δ*lpp* Δ*msbB* double mutant persisted in the spleen of mice by day 6 p.i. when animals were challenged by the subcutaneous route (42), suggesting the need to delete additional virulence factor-encoding gene(s) from this Δ*lpp* Δ*msbB* double mutant to increase attenuation.

Plasminogen-Activator Protease (Pla)

Encoded by the *pla* gene of the pPCP-1 plasmid of *Y. pestis*, the surface protease Pla belongs to the omptin family. The Pla protease cleaves plasminogen into plasmin and degrades the plasmin inhibitor, α2-anti-plasmin (65-67). This causes the dissolution of fibrin clots, which in turn allows bacteria to disseminate to deep tissues during plague infection (68, 69). The Δ*pla* single mutant is deficient in dissemination as well as the ability to colonize lung tissues in large numbers (40, 70-73).

pCP-1$^-$/Δ*lpp* and Δ*lpp* Δ*pla*

When pPCP-1 was cured from the Δ*lpp* isogenic mutant, this pPCP-1$^-$/Δ*lpp* isogenic mutant was attenuated in a mouse model of pneumonic plague infection (74). A Δ*lpp* Δ*pla* double mutant of *Y. pestis* CO92 was recently developed and characterized by our laboratory (40). Δ*lpp* Δ*pla* was highly attenuated with 100% of mice surviving when administered with doses up to 5 x 10^5 colony forming units (CFU) through the subcutaneous or intranasal route (10000 and 1000 LD_{50} equivalents of WT CO92, respectively) (40). After exposure, mice were able to clear the Δ*lpp* Δ*pla* mutant rapidly

and to generate adequate humoral and cell-mediated immune responses which protected them upon WT CO92 pneumonic plague exposure (40).

Attachment Invasion Locus (Ail)

Y. pestis must be able to survive in the blood to establish an infection and to increase its chances of transmission, and, consequently, the organism must have evolved ways to evade and disarm the host immune system. Ail, also referred to as OmpX, is a major contributor of serum resistance and complement evasion in *Y. pestis* (75-78) and accounts for 20-30% of the total outer membrane proteins in yersiniae at 37ºC (79-81). Ail proteins of *Y. enterocolitica* and *Y. pestis* are approximately 69% homologous (78) and bind, as well as regulate, several mediators of the complement system, e.g., Complement Protein 4-binding protein (82-84) and Complement Factor H (FH) (85-87). In addition to serum resistance, Ail of *Y. pestis* facilitates adhesion/invasion of bacteria to the host cells (77, 78, 88-90), inhibits inflammatory responses (76, 88), and assists in the translocation of damaging *Yersinia* outer membrane proteins (Yops) to the host cells (88, 89, 91, 92). Ail is a ~17 kDa outer membrane protein with four extracellular loops, and the loop 2 (L2) has been reported to be mainly responsible for Ail-mediated bacterial serum resistance and adherence/invasion of the host cells (39, 75-78, 88-92).

Ail was also identified by mass-spectrometric analysis along with several other outer membrane antigens, to which antibodies were generated when rats were exposed to the WT CO92 by the intranasal route to mimic pneumonic plague and then rescued by an antibiotic levofloxacin given 24 h post infection for 6 days (93). Importantly, immunization of rats with recombinant Ail protein provided partial protection to animals from the lethal

challenge dose of WT CO92 in a pneumonic plague model, indicating that Ail also has some immunogenic potential (93).

These studies led us to develop triple Δ*lpp* Δ*msbB* Δ*ail* isogenic mutant and its derivative, Δ*lpp* Δ*msbB::ailL2,* to directly discern Ail's role in both virulence and immunogenicity. Also, our goal was to measure these strains' potential to induce long-term humoral and cell-mediated immune responses necessary to protect mice against the pneumonic plague. Consistent with our hypothesis, these mutants as well as a recently developed Δ*lpp* Δ*msbB* Δ*pla* mutant (which has native Ail intact) were highly attenuated and safe when administered to mice, and they stimulated long-term protective immunity.

SPECIFIC AIMS

Hypothesis:
The Δ*lpp* Δ*msbB* Δ*ail* isogenic mutant and its derivatives will be greatly attenuated serving as potential vaccine candidates against pneumonic plague by triggering both humoral and cell-mediated immune responses

Aim 1: To determine the extent of and characterize the attenuation of the triple isogenic Δ*lpp* Δ*msb*B Δ*ail* mutant of *Y. pestis* CO92

Aim 2: To determine the vaccine potential and the correlates of protection for the Δ*lpp* Δ*msbB* Δ*ail* mutant of *Y. pestis* CO92 in protecting against the pneumonic plague

Aim 3: To evaluate long-term humoral and cell-mediated immune responses generated by live-attenuated mutants of *Y. pestis* CO92 needed for the protection against the pneumonic plague

Publications addressing the aims of my project (reproduced with permission):

1. **Tiner BL,** Sha J, Kirtley ML, Erova TE, Popov VL, Baze WB, van Lier CJ, Ponnusamy D, Andersson JA, Motin VL, Chauhan S, Chopra AK. 2015. Combinational deletion of three membrane protein-encoding genes highly attenuates *Yersinia pestis* while retaining immunogenicity in a mouse model of pneumonic plague. Infect Immun. 83(4):1318-38.
2. **Tiner BL**, Sha J, Ponnusamy D, Baze WB, Fitts EC, Popov VL, van Lier CJ, Erova TE, Chopra AK**.** 2015. Intramuscular Immunization of Mice with a Live-Attenuated Triple Mutant of Yersinia pestis CO92 Induces Robust Humoral and Cell-Mediated Immunity To Completely Protect Animals against Pneumonic Plague. Clin Vaccine Immunol **22:**1255-1268.
3. **Tiner BL**, Sha J, Cong Y, Chopra AK**.** 2016. Immunization of mice with new live-attenuated mutants of *Yersinia pestis* CO92 induces protective long-term humoral- and cell-mediated immunity against pneumonic plague. npj Vaccines. (under review).

Chapter 2

Materials and Methods

Bacterial strains and plasmids.

All bacterial strains and plasmids used in this study are listed in **Table 2.1**. *Y. pestis* was grown in heart infusion broth (HIB) (Difco, Voigt Global Distribution Inc., Lawrence, KS) at 28ºC with constant agitation (180 rpm). On the solid surface, *Y. pestis* was grown on either HIB agar or 5% sheep blood agar (SBA) plates (Teknova, Hollister, CA). Luria-Bertani (LB) medium was used for growing recombinant *Escherichia coli* at 37ºC with agitation. Strains containing plasmid pBR322 or its tetracycline sensitive (Tc^S) variant were grown in media with the addition of 100 µg/ml ampicillin. All of our studies were performed in a Tier-1 select agent facility within the Galveston National Laboratory (GNL), UTMB. Restriction endonucleases and T4 DNA ligase were obtained from Promega (Madison, WI). Advantage cDNA PCR kits were purchased from Clontech (Palo Alto, CA), and all digested plasmid DNA or DNA fragments from agarose gels were purified by using QIAquick kits (Qiagen, Inc., Valencia, CA). All tissue culture cell lines were obtained from the American Type Culture Collection (ATCC, Manassas, VA).

Deletion of the *ail* gene.

The up- and down- stream DNA sequences flanking the *ail* gene were polymerase chain reaction (PCR) amplified by using Aup5-Aup3 and Adn5-Adn3 primer pairs (**Table 2.2**), respectively, with genomic DNA of *Y. pestis* CO92 as the template. Additionally, primers Km5-Km3 (**Table 2.2**) specific for the pKD13 plasmid were used to amplify the kanamycin resistance gene (Km^r) cassette with flippase (FLP) recombinase recognition

sites (94, 95). The upstream DNA flanking fragment to the *ail* gene, the Km^r gene cassette, and the downstream *ail* flanking DNA fragment were ligated in that order by using appropriate restriction enzyme sites and cloned into the pDMS197 suicide vector (96). The resulting recombinant pDMS197-Δ*ail* plasmid (**Table 2.1**) was then transformed into the WT CO92, the Δ*lpp* single, and the Δ*lpp* Δ*msbB* double mutant of *Y. pestis* CO92 via electroporation (Genepulser Xcell; Bio-Rad, Hercules, CA). Transformants were plated on LB agar plates containing 5% sucrose and 100 µg/ml kanamycin, and Km^r colonies were screened by using PCR to ensure genomic replacement of the *ail* gene with the antibiotic-resistant cassette. The correct clones were retransformed with the pFlp2 plasmid which contains the FLP recombinase to remove the Km^r gene cassette. The pFlp2 plasmid was eventually cured by growing colonies on 5% sucrose (42), leading to the generation of the single (Δ*ail*), double (Δ*lpp* Δ*ail*), and triple (Δ*lpp* Δ*msbB* Δ*ail*) mutants. Subsequent PCR analysis with primers (Up5-Dn3, Ail5-Ail3) and genomic sequencing with the SqAil primer (**Table 2.2**) further confirmed the in-frame deletion of the *ail* gene from all three mutant strains.

Table 2.1. Bacterial strains and plasmids used in this study

Strain or plasmid	Genotype and /or relevant characteristics	Reference and Source[a]
Strains		
Y. pestis CO92		
WT CO92	Virulent WT *Y. pestis* isolated in 1992 from a fatal pneumonic plague case, biovar Orientalis, and naturally resistant to polymyxin B	CDC
WT:pBR322	WT *Y. pestis* CO92 transformed with pBR322 (Tc^s)	(40)
WT CO92 *luc2*	WT *Y. pestis* with chromosomally integrated luciferase operon *via* Tn*5*, which retains similar virulence potential as the WT CO92 and used as a bioluminescent reporter strain	(97)
WT CO92-*lux*	WT *Y. pestis* with chromosomally integrated luciferase operon downstream of the conserved *glmS* gene *via* Tn*7*, which retains similar virulence potential as the WT CO92 and used as a bioluminescent reporter strain	This study
WT KIMD/27	Mutant of *Y. pestis* KIM Strain which lacks the *pgm* locus	Laboratory Stock
Δ*caf1*	*caf* gene deletion mutant of *Y. pestis* CO92	(28)
Δ*lpp*	*lpp* gene deletion mutant of *Y. pestis* CO92	(51)
Δ*lpp*:Tn*7*-*lpp*	Δ*lpp* CO92 mutant complemented strain with *lpp in cis* by using the targeted Tn*7*	(74)
Δ*lpp* Δ*msbB*	*lpp* and *msbB* double gene deletion mutant of *Y. pestis* CO92	(42)
Δ*lpp*Δ*msbB:*pBR322	Δ*lpp* Δ*msbB* CO92 double mutant transformed with pBR322 (Tc^s)	This study
Δ*ail*	*ail* in-frame gene deletion mutant of *Y. pestis* CO92	This study
Δ*ail*:pBR322	Δ*ail* CO92 mutant transformed with pBR322 (Tc^s)	This study
Δ*ail:*pBR322-*ail*	Δ*ail* CO92 mutant complemented with pBR322-*ail* (Tc^s)	This study
Δ*lpp* Δ*ail*	*lpp* and *ail* double gene deletion mutant of *Y. pestis* CO92	This study
Δ*lpp* Δ*msbB* Δ*ail-Km*	*Y. pestis* CO92 intermediate *lpp, msbB* and *ail* triple gene deletion mutant that carried a Km^r cassette in place of the *ail* gene	This study
Δ*lpp* Δ*msbB* Δ*ail*	*lpp, msbB* and *ail* triple gene deletion mutant of *Y. pestis* CO92	This study
Δ*lpp* Δ*msbB* Δ*ail-lux*	Δ*lpp* Δ*msbB* Δ*ail* with chromosomally integrated luciferase operon downstream of the conserved *glmS* gene *via* Tn*7*, which was used as a bioluminescent reporter strain	This study
Δ*lpp*Δ*msbB*Δ*ail*:pBR322	Δ*lpp* Δ*msbB* Δ*ail* CO92 triple mutant transformed with pBR322 (Tc^s)	This study

Δ*lpp*Δ*msbB*Δ*ail*:pBR322-*ail*	Δ*lpp* Δ*msbB* Δ*ail* CO92 triple mutant complemented with pBR322-*ail* (Tc^s)	This study
Δ*lpp* Δ*msbB::ailL2*	*lpp* and *msbB* double gene deletion mutant with a mutated *ail* gene *ailL2*	This study
Δ*lpp* Δ*msbB::ailL2-lux*	Δ*lpp* Δ*msbB::ailL2* with chromosomally integrated luciferase operon downstream of the conserved *glmS* gene *via* Tn*7*, which was used as a bioluminescent reporter strain	This study
Δ*pla*	*pla* in-frame gene deletion mutant of *Y. pestis* CO92	(40)
Δ*lpp* Δ*pla*	*lpp* and *pla* double gene deletion mutant of *Y. pestis* CO92	(40)
Δ*lpp* Δ*msbB* Δ*pla*	*lpp*, *msbB* and *pla* triple gene deletion mutant of *Y. pestis* CO92	This study
E. coli DH5α *λpir*	Contains the *λpir* gene (lysogenized with *λpir* phage) and it is used for the cloning and propagation of plasmid with R6K origin of replication	Laboratory stock
Plasmids		
pDMS197	Suicide vector with a conditional R6K origin of replication (*ori*) and a levansucrase gene (*sacB*) from *Bacillus subtilis* used for homologous recombination	(96)
pDMS197-Δ*ail*	Recombinant plasmid containing the upstream and downstream regions surrounding the *ail* gene-coding region along with the Km^r cassette	This study
pDMS197-*ailL2*	pDMS197 vector containing the mutated *ail* gene [*ailL2*] with its flanking sequences, used to generate the Δ*lpp* Δ*msbB::ailL2* mutant	This study
pKD13	Template plasmid for PCR amplification of the Km^r gene cassette flanked by FLP recombinase recombination target sites	(95)
pFlp2	Vector that produces the FLP recombinase to remove the Km^r gene cassette from the mutants (Ap^r)	(94)
pBR322 (native)	Cloning vector for complemetation (Tc^r Ap^r)	GE Healthcare
pBR322 (modified)	Variant of pBR322 (Tc^s Ap^r)	(98)
pBR322-*ail*	Recombinant plasmid containing the *ail* gene-coding region and its putative promoter inserted in the Tc^r cassette in vector pBR322 used to complement the Δ*ail* mutants of *Y. pestis* CO92 (Tc^s)	This study
pUC4K	Template plasmid used as a source of the Km^r cassette	Amersham Pharmacia Biotech
pTNS2	Helper plasmid that expresses the transposase complex to facilitate efficient transposition	(99)
pUC18-mini-Tn*7*T-*lux*-Gm	pUC18 based plasmid containing mini-Tn*7* transposon, the luciferase operon (*lux*) and the gentamicin (Gm) resistance cassette	(99)
pUC18R6KT-mini-Tn*7*T	pUC18 based plasmid with a conditional R6K origin of replication (*ori*) containing mini-Tn*7* transposon	(99)
pUC18R6KT-mini-Tn*7*T-*lux*	pUC18R6KT-mini-Tn*7*T based plasmid containing the luciferase operon (*lux*)	This study

pUC18R6KT-mini-Tn*7*T- *lux*-Km	pUC18R6KT-mini-Tn*7*T-*lux* based plasmid containing the Km^r cassette, used to create various bioluminescent reporter strains of *Y. pestis*	This study

[a]CDC = Centers for Disease Control and Prevention

Mutation of the *ail* gene.

Four aa residues (Lysine-88, Aspartate-91, Aspartate-93, and Phenyalanine-94) in L2 of Ail were changed to alanine by using polymerase chain reactions (PCRs). Briefly, the primer pairs Aup5-mAup3 and mAdn5-Adn3 (**Table 2.2**) were used to introduce specific mutations within L2 region of the *ail* gene, as well as to amplify the mutated *ail* gene with its up- and down- stream DNA sequences, respectively. The mutated *ail* gene, designated as *ailL2*, with its up- and down-stream flanking DNA sequences were joined together by PCR with the primer pair Aup5-Adn3 (**Table 2.2**). The above-mentioned PCR product was subsequently cloned into the suicide vector pDMS197 (96), which generated the recombinant plasmid pDMS197-*ailL2* (**Table 2.1**).

Previously, we constructed an intermediate *lpp*, *msbB*, and *ail* triple gene deletion mutant (Δ*lpp* Δ*msbB* Δ*ail-Km*) of *Y. pestis* CO92 (**Table 2.1**) that carried a kanamycin resistance gene (Km^r) cassette (95) in place of the *ail* gene (39). Therefore, the recombinant suicide vector pDMS197-*ailL2* was electroporated into the Δ*lpp* Δ*msbB* Δ*ail-Km* strain (Genepulser Xcell; Bio-Rad, Hercules, CA) (39). The transformants that were sensitive to kanamycin (Km^s) and resistant to 5% sucrose were picked up and screened by PCR with the primer pair Up5-Dn3 (**Table 2.2**) (39) to ensure genomic replacement of the Km^r cassette with the *ailL2* gene. Genomic DNA sequencing with the primer SqAil (**Table 2.2**) (39) was used to further confirm replacement and to ensure no alteration in the *ailL2* surrounding regions in the Δ*lpp* Δ*msbB::ailL2* mutant, when compared to that of the native *ail* gene in the Δ*lpp* Δ*msbB* double mutant.

Creation of the Δ*lpp* Δ*msbB* Δ*pla* mutant of *Y. pestis* CO92.

The in-frame deletion of the *msbB* gene from the Δ*lpp* Δ*pla* double mutant of *Y. pestis* CO92 was prepared using the suicide vector pDMS197 followed by homologous recombination as described previously by our laboratory (42). The in-frame deletion of the *msbB* gene was confirmed by polymerase chain reaction (PCR) analysis employing specific primers (42) as well as by DNA sequencing of the flanking regions to the *msbB* gene on the chromosome.

Complementation of the Δ*ail* mutant strains of *Y. pestis* CO92.

By using Apbr5-Apbr3 primers (**Table 2.2**), the coding region of the *ail* gene with its promoter was PCR amplified with genomic DNA of WT CO92 as the template. The amplified DNA fragment was cloned into the pBR322 vector, creating the recombinant pBR322-*ail* plasmid (**Table 2.1**). Through electroporation, the pBR322-*ail* plasmid was transformed into the Δ*ail* single and Δ*lpp* Δ*msbB* Δ*ail* triple mutant strains, resulting in the creation of the complemented Δ*ail*:pBR322-*ail* and Δ*lpp* Δ*msbB* Δ*ail*:pBR322-*ail Y. pestis* strains (**Table 2.1**). These complemented strains were sensitive to tetracycline due to the replacement of a large portion of the tetracycline resistance (Tc^r) cassette from the plasmid pBR322 with the *ail* gene. The tetracycline-susceptible (Tc^s) variant of the pBR322 vector (98) without the *ail* gene was also electroporated into WT CO92, Δ*ail* single, Δ*lpp* Δ*msbB* double, and the Δ*lpp* Δ*msbB* Δ*ail* triple mutants for generating empty vector controls (e.g., WT:pBR322, Δ*ail:*pBR322, Δ*lpp* Δ*msbB:*pBR322, and Δ*lpp* Δ*msbB* Δ*ail*: pBR322, respectively) (**Table 2.1**).

Table 2.2. Sequences of primers used in this study

Primer or primer pair	Primer sequences[a] (5′–3′)	Purpose
Aup5-Aup3	TATGAGCTCACGACGCACAAGACTCTGGC (SacI), AACGGATCCCCATCCAGATTGTTATAAC (BamHI)	PCR amplification of upstream flanking DNA fragment to the *ail* gene of *Y. pestis* CO92
Adn5-Adn3	ATGAAGCTTCCTAACGTCCTCCTAACCATG (HindIII), GCATCCGTCAATGGTACCAG (KpnI)	PCR amplification of downstream flanking DNA fragment to the *ail* gene of *Y. pestis* CO92
Km5-Km3	ATTCCGGGGATCCGTCGACC (BamHI), CTTAAGCTTGTGTAGGCTGGAGCTGCTTC (HindIII)	PCR amplification of the Km^r gene cassette with FLP recombinase recognition target sites from plasmid pKD13 at both ends
Aup5-mAdn3	TATgagctcACGACGCACAAGACTCTGGC (SacI), TAGTACTT**AGCAGCACCAGCAATAAGTGCGAA**TCCGTCAA	PCR amplifies the upstream flanking DNA fragment to the loop 2 region of the *ail* gene and introduces specific mutations in the loop 2
mAdn5-Adn3	TTGACGGA**TTCGCACTTATTGCTGGTGCTGCT**AAGTACTA, GCATCCGTCAATggtaccAG (KpnI)	PCR amplifies the downstream flanking DNA fragment to the loop 2 region of the *ail* gene and introduces specific mutations in the loop 2
Aup5-Adn3	TATgagctcACGACGCACAAGACTCTGGC (SacI), GCATCCGTCAATggtaccAG (KpnI)	Primer pair used to join the *ailL2* with its upstream and downstream flanking DNA fragments by PCR
Up5-Dn3	ATGCCCACATCGTTACCACC, CCGTAATCCATGGTGATCTG	Primer pair located outside the flanking DNA sequences of the *ail* gene used to verify gene deletion; also used to verify the correct replacement of Km^r cassette with *ailL2* on the chromosome of the Δ*lpp* Δ*msbB* Δ*ail-Km*
Ail5-Ail3	TAATGTGTATGCCGAAGGC, TTGGAGTATTCATATGAAGC	PCR amplification of the coding region of the *ail* gene from *Y. pestis* CO92
Apbr5-Apbr3	CGGGATCCCGCAAGGTCAATGGGGCTATTG (BamHI), ACGCGTCGACTTAGAACCGGTAACCCGCGC (SalI)	PCR amplification of the *ail* gene of *Y. pestis* CO92 including its promoter for integration in the pBR322 vector for complementation
P1-P2	GGTGGCACCGAACAATGAAT, CATTACGCTGACTTGACGGG	PCR confirmation of the insertion of the *lux* operon at the attTn*7* region of *Y. pestis* CO92
SqAil	GGAATACTGTACGAATATCC	Primer located 108 bp upstream of the *ail* gene; used to confirm correct deletion of the *ail* gene as well as the correct integration of *ailL2* with its adjacent regions in the Δ*lpp* Δ*msbB::ailL2* mutant by chromosomal DNA sequencing

[a] Bold bases denote loop 2 region, underlined bases denote mutations and the lower case letters represent restriction enzyme sites

Absence of Ail and unchanged level of Lpp in the membranes of *Y. pestis* CO92 Δ*ail* mutants.

The generated mutant strains were grown overnight in HIB medium at 28ºC with shaking at 180 rpm, and the resulting bacterial cell pellets (representing similar CFU) were dissolved by boiling in SDS-PAGE sample buffer. An aliquot of the samples was then analyzed by immunoblotting by using polyclonal antibodies to Ail and monoclonal antibodies to Lpp that were available in the laboratory (51, 93). As a loading control for the Western blots, the presence of DnaK in the bacterial pellets of the mutants and WT CO92 was assessed by using anti-DnaK monoclonal antibodies (Enzo, Farmingdale, NY).

Growth kinetics and membrane alteration of the *Y. pestis* CO92 triple mutant.

The WT CO92 and its Δ*lpp* Δ*msbB* Δ*ail* triple mutant were grown in 100 ml of HIB medium contained in 500 ml HEPA filter TOP polycarbonate Erlenmeyer culture flasks (Triforest Labware, Irvine, CA) at 28ºC with constant shaking (180 rpm). Samples from each flask were taken at 1- to 2-h intervals until the cultures reached their plateau phases. The CFU were determined by plating (28). For visualization of the membrane alteration, bacterial strains were grown to an exponential phase at 28ºC (OD_{600} of 0.6). The cells were washed, pelleted, fixed, and subjected to transmission electron microscopy (40).

Sensitivity of the *Y. pestis* CO92 mutants to gentamicin.

The minimum inhibitory concentration (MIC) of gentamicin against WT *Y. pestis* CO92:pBR322, the Δ*ail*:pBR322, Δ*ail*:pBR322-*ail*, Δ*lpp* Δ*msbB:*pBR322, Δ*lpp* Δ*msbB* Δ*ail*:pBR322, and Δ*lpp* Δ*msbB* Δ*ail*:pBR322-*ail* mutants was determined by using Etest (bioMérieux, Inc., Durham, NC) (42). Briefly, the bacterial cultures were spread evenly onto 5% SBA and LB agar plates, and pre-defined gentamicin (range, 0.016 to 256 μg/ml)

Etest strips were placed onto the plates. The plates were incubated for 48 h at 28°C, and the MICs were recorded.

Evaluation of the essential *Y. pestis* virulence factors in various mutants of *Y. pestis* CO92.

Type 3 Secretion System (T3SS)

The intactness and functionality of the T3SS, crucial in plague pathogenesis and immunity, were then evaluated. Through the T3SS, the plague bacterium secretes Yops, such as YopE, YopH, and LcrV (low calcium response V antigen), in response to a low calcium signal. Consequently, the overnight grown WT CO92, the Δ*ail* single, the Δ*lpp* Δ*msbB* double, and the Δ*lpp* Δ*msbB* Δ*ail* triple mutants were diluted 1:20 and grown in either HIB or calcium-depleted Modified M9 Medium (42 mM Na_2HPO_4, 22 mM KH_2PO_4, 8.6 mM NaCl, 18.6 mM NH_4Cl, 0.001 mg/ml $FeSO_4$, 0.0001% thiamine, 1 mM $MgSO_4$, 0.4% dextrose, and 1% casamino acids) at 28ºC with shaking (180 rpm) for 3 h and then at 37ºC for 2 h.

When the bacteria were grown in HIB, 5 mM of ethylene glycol tetra-acetic acid (EGTA, Sigma-Aldrich, St. Luis, MO) was added to trigger the low calcium response 5 min before harvesting the cultures. Aliquots of the cultures grown in either media (representing similar CFU) were removed and 1 ml of the supernatants was precipitated with 55 µl of 100% tricholoracetic acid (TCA) on ice for 2 h. The TCA precipitates were dissolved in SDS-PAGE buffer and analyzed by immunoblotting with antibodies to YopE, LcrV (Santa Cruz Biotechnology, Santa Cruz, CA), and YopH (Agrisera, Stockholm, Sweden) (40, 42, 51). The anti-DnaK monoclonal antibody (Enzo) was employed to probe

bacterial pellets to ensure that the bacterial supernatants were obtained from similar number of bacteria across the tested strains.

To evaluate translocation of T3SS effectors by the *Y. pestis* mutants, a digitonin extraction assay was used (51). Briefly, overnight-grown *Y. pestis* cultures from HIB were diluted in Dulbecco Modified Eagle Medium (DMEM) with 10% Fetal Bovine Serum (FBS). The diluted bacteria were cultivated at 28°C for 30 min and then 37°C for 60 min. The HeLa cells (in a twelve-well plate) were then infected with the above *Y. pestis* cultures at a multiplicity of infection (MOI) of 30. After 4 h of infection at 37°C, the cells were washed twice with phosphate-buffered saline (PBS), and lysed with 200 μl of digitonin (1% in PBS). The cells were dislodged from the surface of the plate, collected, and centrifuged at 13,000 rpm for 5 min to obtain supernatant and the pellet fractions. The YopE polyclonal antibodies were then used to detect YopE in both the fractions, while anti-actin (Santa Cruz Biotechnology) and anti-DnaK monoclonal antibodies were employed to the supernatant and pellet fractions, respectively, to monitor equivalent sample loading during Western blot analyses.

Capsular Antigen (F1)

For examining F1 production by WT CO92 and its triple mutant, the 37ºC grown bacteria were subjected to a commercially available plague detection kit, the *Yersinia pestis* (F1) Tetracore *RedLine Alert*^{TM} kit (Tetracore, Rockville, MD), as we previously described (28). A Δ*caf1*-negative mutant of CO92 devoid of F1 antigen was used as a control (28). We further analyzed F1 production by the WT CO92 and its triple mutant by flow cytometry (28). Briefly, the above-mentioned *Y. pestis* cultures (10^6 CFU/sample) were fixed with 4% paraformaldehyde. After washing with PBS, the bacteria were incubated

with a primary antibody to the F1 antigen (Santa Cruz Biotechnology), followed by the secondary antibody (goat anti-mouse IgG1) conjugated with Alexa Fluor 488. The bacterial cells were then washed and resuspended in 500 µl of FACS buffer (1% FBS in PBS) before analysis. Samples were read on the LSRII Fortessa (UTMB Core Facility) and analyzed with FlowJo (Ashland, OR). We also examined F1 production by WT CO92 and its Δ*caf1*-negative and the Δ*lpp* Δ*msbB* Δ*ail* triple mutants by immunofluorescence (IF) staining by using anti-F1-antibodies and microscopy (28).

Plasminogen-Activator Protease (Pla)

Pla surface protease of *Y. pestis* is a multifunctional protein that contributes to bacterial adherence to host cells and intracellular survival, complement resistance, and bacterial dissemination by virtue of possessing fibrinolytic and coagulase activities (40, 68, 74, 92, 100-103). To examine whether deletion or mutation of three membrane protein-encoding genes (*lpp*, *msbB*, *ail*, *ailL2*) from WT CO92 altered Pla levels, we performed Western blot analysis. The overnight grown various *Y. pestis* strains were diluted 1:20 in fresh HIB and grown at 28ºC with shaking (180 rpm) for 3 h and then at 37ºC for 2 h. The bacterial cell pellets were harvested and dissolved in SDS-PAGE sample buffer. An aliquot of the samples was then analyzed by immunoblotting by using polyclonal antibodies to Pla that were available in the laboratory (93). The anti-DnaK monoclonal antibody was also employed to monitor equivalent sample loading during Western blot analyses.

To ensure that Pla was properly displayed on the bacterial surface and enzymatically active, we measured its protease activity by using a fluorimetric assay with the Pla substrate (104). Briefly, strains were plated on HIB agar plates at 28ºC for 36 h. The strains were then re-plated on fresh HIB agar plates and incubated at either 28ºC or 37ºC (representing

flea and human body temperature, respectively) for 20-22 h. Bacteria from each plate were suspended in PBS and adjusted to optical densities (OD_{600}) of 0.1 (5 x 10^7 CFU/ml) and 0.5 (2.5 x 10^8 CFU/ml) by using BioRad SmartSpec^{Tm} 300. For each strain, 50 µl of the suspension was added to the wells in triplicate of a black microtiter plate (Costar Corning Incorporated, Corning, NY). The hexapeptide substrate, DABCYL-Arg-Arg-Ile-Asn-Arg-Glu(EDANS)-NH_2, at a final concentration of 2.5 µg/well was added to the bacterial cells. The kinetics of substrate cleavage by Pla displayed on the bacterial surface was measured every 15 min for 2 h in a fluorimetric assay (Extinction/Emission 360nm/460nm) at 37ºC by using BioTek Synergy HT spectrophotometer (BioTek Instruments, Inc., Winooski, WT).

Serum resistance of various mutants of *Y. pestis* CO92.

Normal human and mouse sera were purchased from Sigma-Aldrich, and the non-human primate sera were collected from naïve animals that were housed in the GNL. Prior to use, an aliquot of each serum was also heated at 56ºC for 30 min to inactivate complement and served as a control. Various *Y. pestis strains* were grown overnight, harvested, and then diluted in PBS to an OD_{600} of 0.8 (~4 x 10^8 CFU/ml). A 50-µl volume of the diluted bacteria (~2 x 10^7 CFU) was mixed with either 200 µl of normal (unheated) or heated sera. The samples were incubated at 37ºC for 2 h with shaking at 500 rpm. The number of surviving bacteria (CFU) in each sample was determined by serial dilutions and plating on SBA plates (40, 42). Percent bacterial survival was calculated by dividing the average CFU in samples incubated in normal serum by the average CFU in samples incubated in the heat-inactivated serum and multiplying by 100.

Adherence, invasion, and intracellular survival of various *Y. pestis* CO92 mutants in HeLa and A549 epithelial cells.

The 12-well tissue culture plates were seeded with either HeLa (from human cervix) or A549 (human alveolar) epithelial cells at a concentration of 4 x 10^5 in 1 ml of DMEM + 10% FBS or F-12K (Kaighn's) Medium + 10% FBS medium, respectively (101, 105). The cells were incubated at 37ºC/5% CO_2 until a confluent monolayer was established.

Overnight grown bacterial strains were used to infect host cells at an MOI of 100. The plates were centrifuged at 1200 rpm for 10 min to ensure bacterial contact with the host cells. After 2 h of incubation, one set of the triplicate wells was not washed, and the total number of bacteria used for infection that were present in the culture medium and those adhering to and/or invading the host cells was recovered by scraping and vortexing the host cells. Another set of triplicate wells was gently washed twice with 1 mL of Dulbecco phosphate-buffered saline (DPBS) and the adherent and invaded bacteria in the host cells were then enumerated after lysing epithelial cells with 1 ml of ice-cold water.

The last set of the host cells was similarly washed twice with DPBS, and the gentamicin (50 µg/ml) protection assay was used to discriminate between the invading and extracellular bacteria (101). After 1 h of incubation in the gentamicin-containing medium to kill extracellular bacteria, the host cells were washed twice with 1 ml of DPBS and the intracellular bacteria were then enumerated after adding 1 ml of ice-cold water to each well (101). The percentage of invasion and adhesion was then determined.

The intracellular survival of various CO92 mutants in HeLa and A549 cells was assessed in a manner similar to that of the invasion assay. The 0 h samples corresponded to a time point immediately after the gentamicin treatment. The intracellular bacteria in

HeLa and A549 cells were then enumerated by serial dilution and plating after 12 h of incubation in media containing 10 µg/ml gentamicin (51).

Intracellular survival of mutant strains in murine alveolar macrophages and human monocyte-derived macrophages.

Murine MH-S alveolar macrophages were infected with WT CO92 and its mutant strains at an MOI of 10. After 30 min of infection, the host cells were treated for 45 min with 20 µg/ml gentamicin to kill extracellular bacteria. The surviving bacteria inside the macrophages were then enumerated immediately after the gentamicin treatment (0 h time point), and subsequently at 2 and 4 h of incubation in a medium containing 10 µg/ml gentamicin. The number of bacteria present inside the macrophages was determined by serial dilution and plating (51).

Human buffy coats were obtained from three different healthy individuals in 10 ml Vacutainer tubes without additive (Becton Dickinson Labware, Franklin Lakes, NJ) from the UTMB blood bank. The EDTA-treated blood was handled under endotoxin-free conditions, diluted 1:1 with PBS, and peripheral blood mononuclear cells (PBMC) purified by centrifugation over a Ficoll-sodium diatrizoate solution (Ficoll-Paque™ PLUS, GE Healthcare Bio-sciences AB, Uppsala, Sweden). Monocytes were then purified from PBMC by positive selection using human CD14 microbeads and the magnetic column separation system from Miltenyi Biotec (Auburn, CA). Monocyte-derived macrophages (iMF) were subsequently differentiated from purified $CD14^+$ monocytes.

Briefly, monocytes were cultured in RPMI-1640 medium supplemented with 10% FBS, L-glutamine, HEPES, sodium pyruvate, penicillin-streptomycin, and granulocyte macrophage-colony stimulating factor (GM-CSF) (100 ng/ml, Leukine Sargramostium

Genzyme Corp., Cambridge, MA). Monocytes were seeded in 24-well tissue-culture plates at 10^6 cells/ml and adherent iMF were obtained at 6 days of culture.

These human monocyte-derived macrophages (HMDM) were infected with WT CO92 and its mutant strains at an MOI of 1. The infected macrophages were incubated at 37°C with 5% CO_2 for 45 min, followed by 1 h of treatment with 10 μg/ml gentamicin. The surviving bacteria inside the macrophages were enumerated immediately after the gentamicin treatment (0 h time point), and subsequently at 2 h and 4 h (51). The concentration of gentamicin used in the gentamicin protection assay was optimized for each host cell type used in this study.

Supernatants from infected macrophages during the intracellular survival assay were collected at each of the time point tested and filtered. A Bio-Rad mouse 6-plex assay kit (IL-1β, IFN-γ, IL-10, IL-17, IL-6, and TNF-α) or a Bio-Rad human 8-plex assay kit (GM-CSF, IFN-γ, IL-2, IL-4, IL-6, IL-8, IL-10, and TNF-α) was used to measure cytokine and chemokine levels.

Animal studies with the *Y. pestis* CO92 mutant strains.

Six-to-eight-week old, female Swiss-Webster mice (17 to 20 g) were purchased from Taconic Laboratories (Germantown, NY). All of the animal studies were performed in the Animal Biosafety Level (ABSL)-3 facility under an approved UTMB Institutional Animal Care and Use Committee protocol.

i) Attenuation and survival analysis of *Y. pestis* CO92 mutant strains.

Mice (n=10 per group) were challenged intranasally (i.n.) with 1.3 x 10^4 CFU [representing 26 50% LD_{50} of the WT bacterium, with 1 LD_{50} corresponding to 500 CFU (40)] of WT CO92, Δ*ail* single, Δ*lpp* Δ*msbB* and Δ*lpp* Δ*ail* double, or the Δ*lpp* Δ*msbB*

Δ*ail* triple mutant strains. Also, the animals were challenged by the i.n. route with the Δ*lpp* Δ*msbB* Δ*ail* triple mutant at higher doses of 4.0 x 10^4, 1.7 x 10^5, 5.9 x 10^5, 1.8 x 10^6, and 3.4 x 10^6 CFU (corresponding to 80, 340, 1180, 3600, and 6800 LD_{50}s of the WT CO92). Mice (n= 5 per group) were challenged by the i.n. route with one dose of 2.5 x 10^6 CFU/40 μL or 5.0 x 10^6 CFU/40 μL of WT CO92 or the Δ*lpp* Δ*msbB* Δ*pla* mutant. All mice were assessed for morbidity and/or mortality as well as clinical symptoms over the duration of each experiment (22-30 days p.i.).

ii) Bacterial dissemination and histopathological studies with infection triple mutant of *Y. pestis* CO92.

Mice infected with 2.5 x 10^6 CFU (representing 5000 LD_{50} of the WT CO92) of the Δ*lpp* Δ*msbB* Δ*ail* triple mutant or the WT CO92 by the i.n. route were euthanized by using a mixture of ketamine and xylazine followed by cervical dislocation on days 2, 3, and 6 p.i. For each time point, five mice per group were used, and the lungs, liver, and the spleen were removed immediately following animal sacrifice. The blood was collected from these animals by cardiac puncture. The tissues were homogenized in 1 ml of PBS, and serial dilutions of the homogenates were spread on the SBA plates to assess dissemination of the bacteria to peripheral organs (42).

Portions of each organ (lung, liver, and spleen) from 5 mice at each time point were also removed and immersion fixed in 10% neutral buffered formalin (51, 74). The tissues were processed and sectioned at 5 μm, and the samples were mounted on slides and stained with hematoxylin and eosin (H&E). Tissue lesions were scored on the basis of a severity scale, which correlated with estimates of lesion distribution and the extent of tissue involvement (minimal, 2 to 10%; mild, >10 to 20%; moderate, >20 to 50%; severe, >50%),

as previously described (51, 74). The histopathological evaluation of the tissue sections was performed in a blinded fashion.

iii) Cytokine and chemokine levels in mice after intranasal administration of the triple mutant of *Y. pestis* CO92.

Concurrently, blood was collected from infected (with WT CO92 versus the Δ*lpp* Δ*msbB* Δ*ail* triple mutant) animals on days 2, 3, and 6 p.i. (for cytokine analysis). Blood was also collected from all animals prior to infection and on day 14 p.i. to determine antibody responses. Serum samples were filtered by using Costar 0.1-μm centrifuge tube filters (Corning Inc.). The levels of following cytokine/chemokines, namely IL-12, IFN-γ, IL-4, IL-5, IL-6, and TNF-α in the sterile serum samples were analyzed by using a mouse 6-plex Bioplex assay (eBioscience, San Diego, CA).

iv) Intramuscular and Subcutaneous Immunization.

Mice were immunized by the i.m. route with one or two doses of 2 x 10^6 CFU/100 μL of the Δ*lpp* Δ*msbB* Δ*ail*, the Δ*lpp* Δ*msbB::ailL2*, and/or the Δ*lpp* Δ*msbB* Δ*pla* mutants. The mutants were administered in a 50 μL volume in each of the hind legs. When two doses of each vaccine strain were administered, they were injected twenty-one days apart (on days 0 and 21). Mice receiving only one dose were injected on the same day when the other animals received their second vaccine dose (on day 21). Mice which were immunized by the s.c. route with two doses of 2 x 10^6 CFU/100 μL of the Δ*lpp* Δ*msbB* Δ*ail* triple or the Δ*lpp* Δ*msbB::ailL2* mutant strains were injected at one site twenty-one days apart (on days 0 and 21). All mice were assessed for morbidity and/or mortality over the duration of vaccination.

v) Antibody responses after immunization.

Blood was collected by the retro-orbital route from vaccinated mice two weeks after each immunization regardless of route (on days 14 and/or 35). For gauging long-term antibody responses after i.m. immunization, retro-orbital bleeding of all mice occurred on days 14, 35, 56, 81, and 112. Pre-immunization blood samples served as a control. Sera were separated and filtered by using Costar 0.1-μm centrifuge tube filters (Corning Inc., Corning, NY). ELISA plates were coated with the F1-V fusion protein (1 ng/μl, BEI Resources, Manassas, VA) (39, 40, 42). Total IgG and antibody isotypes against F1-V (capsular antigen F1 and a type 3 secretion system [T3SS] component low calcium response V antigen [LcrV]) in the sera (1:5 serially diluted) of immunized mice were then determined as we previously described (106).The sera were serially diluted (either 1:5 or 1:10) and horseradish peroxidase (HRP)-conjugated secondary antibodies were used to determine total-IgG titers and IgG isotype responses employing goat anti-mouse IgG-HRP, IgG1-HRP, IgG2a-HRP, and IgG2b-HRP (SouthernBiotech, Birmingham, AL). The substrate 3,3′,5,5′-Tetramethylbenzidine (TMB) (ThermoScientific, Waltham, MA) was used for color development, and the plates were read at 450 nm using a spectrophotometer (106).

vi) Protection assays.

Survivors after initial i.n. infection with the mutants were subsequently challenged with 1 x 10^4 to 1.4 x 10^4 CFU (20 to 28 LD_{50} of the bioluminescent WT *Y. pestis* CO92 *luc2* strain) (97), which contains the luciferase (*luc*) gene and its substrate, allowing *in vivo* imaging of mice in terms of bacterial dissemination in real time. Twenty-one days after the last i.m. or s.c. immunization (day 42), the immunized mice were anesthetized with a

mixture of xylazine-ketamine and then exposed by the i.n. route to 3.5 x 10^4 to 4.6 x 10^4 CFU/40 μL (70 to 92 LD_{50}) of WT CO92 *luc2*.

Naïve mice of the same age were used as controls for each experiment. On days 3 and 7 post WT exposure, all animals were imaged by using an *in vivo* imaging system (IVIS) 200 bioluminescent and fluorescence whole-body imaging workstation (Caliper Corp. Alameda, CA) in the ABSL-3 facility.

vii) Histopathological analysis of immunized mice.

Immunized mice (n=2) which received two doses of the vaccine by either the i.m. or the s.c. route were euthanized three weeks after the second vaccine dose (on day 42). Similarly, three mice from each of the immunized groups that survived pneumonic challenge with 70 LD_{50} of WT CO92 *luc2* strain were sacrificed on day 54 post challenge. Age-matched naïve uninfected mice (n=2) were also euthanized as a control. Lungs, liver, and the spleen were harvested from these mice, fixed in 10% neutral buffered formalin (51, 74), and tissues processed and sectioned at 5 μm. The samples were mounted on slides and stained with hematoxylin and eosin (H&E). Tissue lesions were scored on the basis of a severity scale, which correlated with estimates of lesion distribution and the extent of tissue involvement (minimal, 2 to 10%; mild, >10 to 20%; moderate, >20 to 50%; severe, >50%), as previously described (51, 74). The histopathological evaluation of the tissue sections was performed in a blinded fashion.

viii) Progression of infection.

To monitor progression of infection in real time, various bioluminescent stains of *Y. pestis* CO92 were constructed by using the Tn*7*-based system (74). The Tn*7*- based system integrates the target gene in a site-specific manner downstream of the conserved *glmS*

(glucosamine-6-phosphate synthase) gene on the bacterial chromosome (107, 108). Briefly, the *lux* operon was removed from the plasmid pUC18-mini-Tn*7*T-*lux*-Gm by *Spe*I/*Kpn*I restriction enzyme digestion and sub-cloned into plasmid pUC18R6KT-mini-Tn*7*T (99) resulting in a derivative, designated as pUC18R6KT-mini-Tn*7*T-*lux* (**Table 2.1**).

Subsequently, the Km^r cassette from the pUC4K plasmid (*Bam*HI digestion) was inserted into pUC18R6KT-mini-Tn*7*T-*lux*, thus, resulted in the creation of the pUC18R6KT-mini-Tn*7*T-*lux*-Km plasmid (**Table 2.1**). The electrocompetent cells of WT CO92, Δ*lpp* Δ*msbB* Δ*ail* triple, and the Δ*lpp* Δ*msbB::ailL2* mutant strains were electroporated with mixed (2 to 1) pTNS2 and pUC18R6KT-mini-Tn*7*T-*lux*-Km plasmids (74, 97, 99)**,** and selected for Km^r and luminescence. The insertion of *lux* at the attTn*7* region was confirmed by PCR using primer pair P1-P2 (**Table 2.2**) which specifically amplified the region between *Y. pestis glmS* gene and the Tn*7* insertion cassette (74). Luminescence intensity of each strain was determined by relative luminescence unit (RLU) measurement (Spectramax M5e, Molecular Devices, Sunnyvale, CA) (97).

Mice (n=3) were then infected with 2 x 10^6 CFU/100 μL of the above generated bioluminescent stains: Δ*lpp* Δ*msbB* Δ*ail-lux*, Δ*lpp* Δ*msbB::ailL2-lux*, or the WT CO92-*lux* (**Table 2.1**) by the i.m. route. The IVIS images were taken immediately after challenge and then every 12 h until 48 h p.i. After 48 h, mice were euthanized and the muscles, lungs, liver, and the spleen were removed immediately following animal sacrifice. The tissues were homogenized in 1 ml of PBS, and serial dilutions of the homogenates were spread on the SBA plates to assess dissemination of the bacteria to peripheral organs (42). Portions

of each organ from 3 mice at each time point were also removed for histopathological analysis (51, 74).

ix) T-cell proliferative responses and cytokine production

Mice (n=5) were infected by the i.m. or the s.c. route with *Y. pestis* KIM/D27 (*pgm* locus minus strain) (**Table 2.1**), the Δ*lpp* Δ*msbB* Δ*ail* triple, or the Δ*lpp* Δ*msbB::ailL2* mutant strains of *Y. pestis* CO92 at a dose of 1 x 10^3 CFU/100 μL. The T-cell proliferation in response to heat-killed WT CO92 antigens (pulsed) was measured on day 21 p.i., as we previously described (40, 42). T-cells from uninfected mice as well as un-pulsed T cells served as negative controls. The T-cell culture supernatants were collected at 48 h to measure cytokine/chemokine production by using a mouse 6-plex assay kit (Bio-Rad Laboratories Inc.). After 72 h of incubation, 1μCi of [^{3}H] thymidine was added into each well, and the cells harvested 16 h later using a semi-automated sample harvester, FilterMate Harvester (PerkinElmer, Waltham, MA), followed by the measurement of radioactive counts (TopCount NXT, PerkinElmer).

x) Long term humoral and cell-mediated immune responses.

Organ harvesting.

Groups of mice (n=5 per group per time point) were used to determine the kinetics of immune cell responses after i.m. immunization with mutants of *Y. pestis* CO92. Another set of mice (n=3 per time point) were inoculated with PBS which served as a naïve, age matched control. Spleens were isolated from mice on days 42, 63, and/or 84. Subsequently, immunized and control mice (n=8-10 per group) were exposed to 1.2 x 10^4 CFU/40 μL (24 LD_{50}) of the bioluminescent WT *Y. pestis* CO92 *luc2* strain. Spleens were isolated from these mice (n=3-4 per group) on day 124 (4 days p.i.), and from surviving animals (n=4-6

per group) and from PBS, non-exposed control mice (n=3) on day 141 (21 days p.i.). Single cell suspensions were prepared by forcing the spleens through nylon cell strainers and by suspending the cells in RPMI 1640 medium with 10% fetal bovine serum. Cells were collected by centrifugation, with blood cells being removed by using red blood cell lysis buffer (Sigma-Aldrich; St. Louis, MO).

Flow cytometry analysis.

All cells were stained with Ghost Dye-APC/Cy7 (Tonbo biosciences; San Diego, CA) to gate for live cell populations. Splenic cells (1×10^6) were incubated with 0.5 μg/sample anti-mouse CD16/32 antibody (BioLegend; San Diego, CA) for 10 min on ice to prevent non-specific binding of monoclonal antibodies to the Fc receptors. The surface of the B cells was stained with monoclonal anti-mouse CD19-FITC (B cell surface marker; BioLegend), anti-mouse CD38-PE/Cy7 (memory B cell marker; BioLegend), and anti-mouse IgG-PE (mature, isotype-switched B cell marker; Southern Biotech; Birmingham, AL) for 30 min in the dark at 4°C.

To measure T cell kinetics, splenic cells were pretreated with ionomycin (750 ng/mL) and phorbol 12- myristate 13-acetate (PMA, 50 ng/sample), and then incubated 2 h later with Brefeldin A (0.7 μg/sample) to accumulate intracellular cytokines. The surface of the T cells was stained with monoclonal anti-mouse CD4-PE/Dazzle594 (BioLegend) and anti-mouse CD8-FITC (BioLegend) for 30 min in the dark at 4°C to distinguish $CD4^+$ and $CD8^-$ expressing cells. Stained cells were centrifuged, washed, and permeabilized with Foxp3 staining buffer set (eBioscience; San Diego, CA). T cells were stained with anti-mouse IFN-γ-Percp/Cy5.5 (BioLegend), anti-mouse IL-17A-PE/Cy7 (BioLegend), and anti-mouse Foxp3-PacificBlue (eBioscience) for 30 min in the dark at 4°C.

To determine innate immune responses, the surface of DCs was stained with monoclonal anti-mouse CD11c-PE/Dazzle594 (BioLegend), anti-mouse CD11b-Percp/Cy5.5 (BioLegend), anti-mouse CD80-Pacific Blue (BioLegend), anti-mouse CD86-FITC (BioLegend), and anti-mouse MHC-II-PE (Tonbo Biosciences) for 30 min in the dark at 4°C.

All stained cells were fixed with 1% paraformaldehyde in PBS, examined for sterility, and then subjected to flow cytometry. Suitable isotype antibodies for all experiments were used as controls. The differential cell population was acquired on flow cytometer (LSRII Fortessa) and analyzed using FACS diva software.

Protection assay.

Intramuscularly immunized mice were exposed by the i.n. route with 1.2 x 10^4 CFU/40 μL (24-36 LD_{50}) of the bioluminescent WT *Y. pestis* CO92 *luc2* strain on day 120. Mice inoculated with PBS were used as age-matched, naïve controls. On days 123 and 130 (day 3 and 10 p.i.), the animals which were challenged with 1.2 x 10^4 CFU were imaged by using an *in vivo* imaging system (IVIS) 200 bioluminescent and fluorescence whole-body imaging workstation (Caliper Corp.; Alameda, CA) in the ABSL-3 facility to examine dissemination and progress of infection. Spleens were isolated from surviving mice and subjected to flow cytometry analysis as described above.

Statistical analysis.

For majority of the experiments, one-way analysis of variance (ANOVA) was used with the Bonferroni correction except for the intracellular survival experiments in which Tukey's *post hoc* test was employed for data analysis. For the flow cytometry analysis of total cell populations, one-way analysis of variance (ANOVA) and two-way ANOVA were

used with the Tukey's *post hoc* test for data analysis. We used Kaplan-Meier survival estimates for animal studies, and p values of ≤ 0.05 were considered significant for all of the statistical tests used. The standard deviations were derived from three independently performed experiments with three replicates per experiment for *in vitro* assays.

Chapter 3

Combinational deletion of three membrane protein-encoding genes highly attenuates *Yersinia pestis* while retaining immunogenicity in a mouse model of pneumonic plague[1][2]

Introduction

It has been reported that the virulence potential of Ail is modulated by the LPS core saccharide length, and that Ail's biological activity could be masked by LPS (77). However, since the LPS of *Y. pestis* lacks O antigen, Ail is believed to contribute significantly in the pathogenesis of *Y. pestis* infections (6). Indeed, the recent study of Kolodziejek et al. showed that Ail of *Y. pestis* CO92 contributed to virulence in a rat model of pneumonic plague (77). Thus, we aimed at whether deletion of the *ail* gene from WT CO92 or its Δ*lpp* single and Δ*lpp* Δ*msbB* double mutants would further attenuate the bacterium. Our data showed that the Δ*lpp* Δ*msbB* Δ*ail* triple mutant of *Y. pestis* CO92 was severely attenuated while retaining immunogenicity, thus providing an excellent scaffold from which other virulence genes can be deleted to generate novel live-attenuated vaccine strains for plague in the future.

---

[1] Reproduced with permission from the following source: Infection and Immunity (http://www.iai.asm.org); **Tiner BL**, Sha J, Kirtley ML, Erova TE, Popov VL, Baze WB, van Lier CJ, Ponnusamy D, Andersson JA, Motin VL, Chauhan S, Chopra AK. 2015. Combinational Deletion of Three Membrane Protein-Encoding Genes Highly Attenuates Yersinia pestis while Retaining Immunogenicity in a Mouse Model of Pneumonic Plague. Infect Immun **83:**1318-1338.

[2] **Author Contributions:** Bethany Tiner was involved in the creation of all mutants, in microscopic analysis and western blot analysis of the mutants, in virulence determination assays (F1 production, T3SS, adherence, invasion, serum resistance, and intracellular survival), and in all *in vivo* studies. Dr. Jian Sha (Assistant Professor) was involved in mutant creation, virulence determination assays (T3SS, adherence, invasion, serum resistance, and intracellular survival), and in all *in vivo* studies. Christina van Lier, Sadhana Chauhan, and Dr. Vladamir Motin were involved in the Pla Protease Assay. Christina van Lier, Dr. Duraisamy Ponnusamy (McLaughlin postdoctoral fellow), Jourdan Andersson, and Michelle Kirtley were involved in *in vivo* studies and intracellular survival assays. Dr. Wallace Baze was involved in histopathological analysis while Dr. Vsevolod Popov assisted in transmission electron microscopy. Dr. Tatiana Erova was involved in preparing *ail* complementation strain as well as the dissemination experiments.

Results

In vitro characterization of Δ*ail* mutants of *Y. pestis* CO92.

The in-frame deletion of the *ail* gene from WT CO92, Δ*lpp* single, and the Δ*lpp* Δ*msbB* double mutants of *Y. pestis* CO92 was confirmed through PCR analysis by using specific primers (**Table 2.2**), as well as by DNA sequencing of the flanking regions of the *ail* gene on the chromosome. The above-mentioned genetic manipulations resulted in the creation of authentic Δ*ail* single, Δ*lpp* Δ*ail* double, and the Δ*lpp* Δ*msbB* Δ*ail* triple mutants of *Y. pestis* CO92. As shown in **Fig. 3.1A**, Ail-specific antibodies detected the correct size protein in WT CO92 and its Δ*lpp* Δ*msbB* double mutant, but not in the Δ*ail* single, Δ*lpp* Δ*ail* double, and the Δ*lpp* Δ*msbB* Δ*ail* triple isogenic mutants. Importantly, deletion of the *ail* gene from WT CO92 did not affect the production of Lpp (**Fig. 3.1A**).

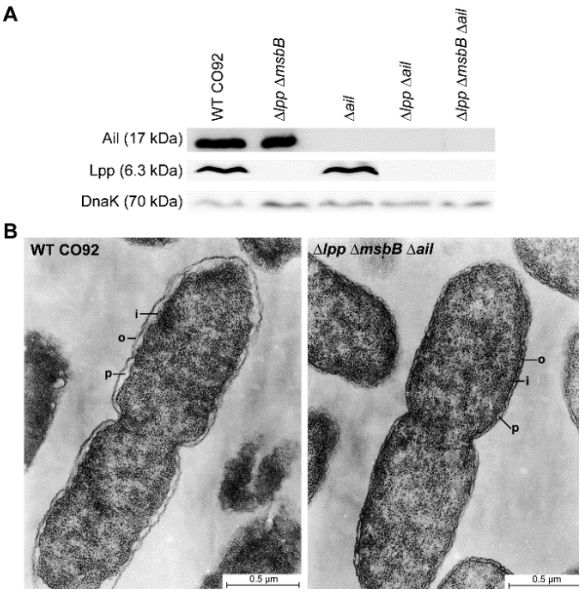

Figure 3.1. Ail and Lpp production and transmission electron microscopic analysis. Overnight grown *Y. pestis* cultures (at 37ºC) were collected, and the production of Ail and Lpp in the whole cell lysates was analyzed by immunoblotting using antibodies to Ail and Lpp. Anti-DnaK antibodies were used as a loading control for Western blots (A). The WT CO92 and its Δ*lpp* Δ*msbB* Δ*ail* triple mutant were grown to exponential growth phase at 28ºC and subjected to transmission electron microscopic analysis (B). o=bacterial outer membrane, i=bacterial inner membrane, p=periplasmic space. Scale=0.5 µm.

Since both Ail and Lpp are outer membrane proteins and MsbB encoding acyltransferase modifies LPS, the WT CO92 and its Δ*lpp* Δ*msbB* Δ*ail* triple mutant were subjected to transmission electron microscopy to evaluate if there were any membrane alterations. Except for finding that the Δ*lpp* Δ*msbB* Δ*ail* triple mutant had somewhat

decreased periplasmic space compared to WT CO92 (**Fig. 3.1B**), no other abnormalities were apparent. The growth kinetics of the triple mutant was also examined, and the Δ*lpp* Δ*msbB* Δ*ail* triple mutant entered log phase at an earlier time point and grew faster initially than the WT CO92 strain; however, both strains had similar CFU by 16 h (**Fig. 3.2**).

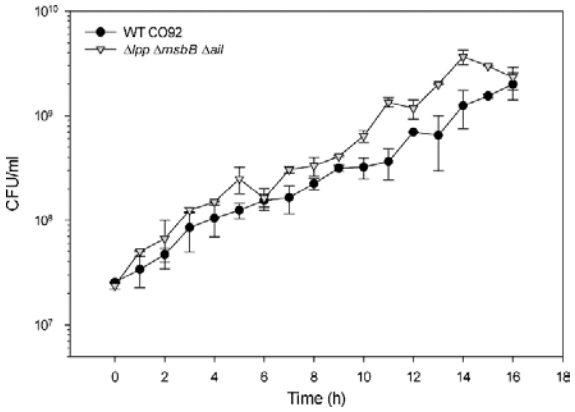

Figure 3.2. Growth curve of WT *Y. pestis* CO92 and its Δ*lpp* Δ*msbB* Δ*ail* triple mutant. The organisms were grown at 28°C in HIB medium and the samples taken at 1- to 2- h intervals until the cultures reached their saturation phases. The CFU were determined by plating on SBA plates for 48 h at 28°C. The error bars represent means ± standard deviations.

<u>The Δ*lpp* Δ*msbB* Δ*ail* triple mutant of *Y. pestis* CO92 produces essential *Y. pestis* virulence and immunogenic factors.</u>

The T3SS is an essential virulence mechanism in *Y. pestis*. Through the T3SS, an immunoreactive antigen (LcrV) as well as other Yops, such as YopE and YopH (which destroy actin monofilaments and interfere with phagocyte signal transduction machinery, respectively), are secreted. Therefore, the T3SS-dependent protein secretion in response to a low calcium signal was measured for the generated *ail* mutants. This *in vitro* assay mimics the environment during eukaryotic host cell contact with the bacterial T3SS needles. In a calcium-depleted M9 medium, the Δ*lpp* Δ*msbB* Δ*ail* triple mutant showed significantly increased levels of YopH and YopE in the culture supernatants compared to WT CO92 and its Δ*lpp* Δ*msbB* double mutant (**Fig. 3.3A**). While an increased level of YopH was also noted in the supernatant of the Δ*ail* single mutant, the YopE level in the culture medium was not as pronounced when compared to that of the Δ*lpp* Δ*msbB* double mutant and the

WT CO92 (**Fig. 3.3A**). There was no significant difference in the levels of LcrV in the culture supernatants across the strains tested (**Fig. 3.3A**).

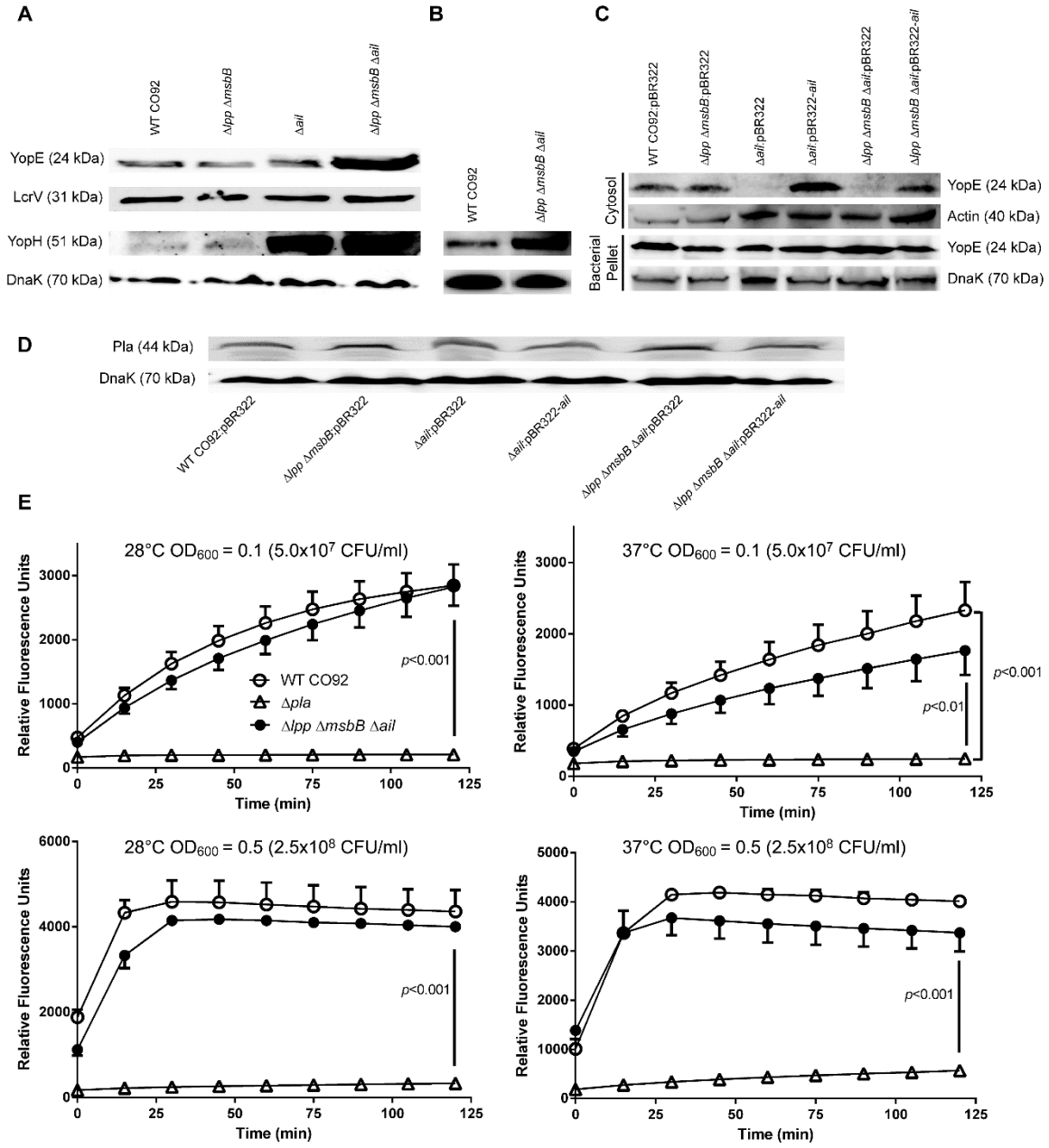

Figure 3.3. Functionality of the T3SS and production/enzymatic activity of the Pla protease. Overnight HIB grown cultures of various *Y. pestis* strains were diluted 1:20 in modified M9 medium or fresh HIB and continued to grow at 28°C for 3 h, followed by additional 2 h of incubation at 37°C. Production of YopH, LcrV, and YopE in M9 medium (**A**) or YopH in HIB chelated for calcium (**B**) was measured by Western blot analysis using their specific antibodies. The anti-DnaK antibodies were employed to examine bacterial pellets to ensure bacterial supernatants were obtained from similar number of bacteria across the tested strains. For the translocation studies, overnight-grown HIB cultures of various *Y. pestis* strains were diluted, sensitized to DMEM by growth at 28°C for 30 min, followed by additional 1 h of incubation at 37°C. HeLa cells were then infected with the above-mentioned cultures at an MOI of 30. After 4 h of infection, the

cytosolic fraction of the host cells was separated from the pellet and probed with anti-YopE antibodies. The anti-actin and anti-DnaK antibodies were also employed to the supernatant and pellet fractions, respectively, to monitor equal loading of the samples during Western blot analyses (**C**). Pla production in various *Y. pestis* CO92 stains was examined with specific antibodies to Pla, and anti-DnaK antibodies were used as a loading control (**D**). For measuring Pla activity, the tested *Y. pestis* CO92 strains were mixed with the Pla substrate (DABCYL-Arg-Arg-Ile-Asn-Arg-Glu(EDANS)-NH_2) and the kinetics of substrate cleavage was measured. The Δ*pla* single mutant of CO92 was employed as a negative control during the assay. The kinetics of each reaction was plotted with arithmetic means ± standard deviations (**E**). Statistical analysis on Pla activity data was performed by One-way ANOVA with a Bonferroni *post-hoc* test. Statistically significant *p* values are shown between the groups by a vertical line.

To demonstrate that the higher level of the specific effector, YopH, observed in the culture supernatant of the Δ*lpp* Δ*msbB* Δ*ail* triple mutant (**Fig. 3.3A**) was not due to the leakiness of the bacterial cell membrane and the T3SS itself, we examined secretion of YopH by the triple mutant grown in HIB medium after induction of a low calcium signal. As noted from **Fig. 3.3B**, 5 min after the addition of EGTA, YopH was detected in the supernatants of WT CO92 and its Δ*lpp* Δ*msbB* Δ*ail* triple mutant, however, no detectable level of YopH was present in un-induced culture supernatants (data not shown). Importantly, compared to the WT bacterium, there was a significant increase in the level of YopH in the supernatant of the Δ*lpp* Δ*msbB* Δ*ail* triple mutant (**Fig. 3.3B**).

To simulate *in vivo* conditions and to measure translocation of Yops, HeLa cells were infected with various mutant strains of *Y. pestis*. A digitonin extraction assay was used to evaluate translocation of YopE into the host cells. While the WT CO92 and its Δ*lpp* Δ*msbB* mutant bacteria had similar levels of YopE translocation, the *ail* deletion mutants (both Δ*ail* and Δ*lpp* Δ*msbB* Δ*ail*) had significantly decreased translocation of YopE into the cytosol of the host cells (**Fig. 3.3C**). The YopE translocation was restored in the *ail* deletion mutants when complemented with the corresponding gene *in trans* (**Fig. 3.3C**). The decreased level of YopE translocation from the *ail* deletion mutants was not due to differential expression of the *yopE* gene or the number of bacteria that were used to infect

HeLa cells as all of them had similar levels of YopE and DnaK in the cell pellet fraction (**Fig. 3.3C**).

Pla, another important virulence factor of *Y. pestis*, is a multifunctional protein (40, 68, 74, 92, 100, 101). To evaluate whether the levels of Pla remained unaltered in the Δ*ail* mutants, Western blot analysis was performed. Essentially, similar levels of Pla protein were noted in various mutant strains tested (Δ*ail* single-, Δ*lpp* Δ*msbB* double-, Δ*lpp* Δ*msbB* Δ*ail* triple-, as well as the *ail* complemented- mutant strains) compared to that of WT CO92 at 37ºC, a temperature that increases Pla production and activity (80, 109, 110) (**Fig. 3.3D**). To confirm the Western blot data and to ensure that the Pla activity was fully retained by the Δ*lpp* Δ*msbB* Δ*ail* triple mutant compared to the WT CO92 strain, the mutant bacteria were exposed to a fluorogenic hexapeptide Pla substrate. This substrate was selected from the library of fluorogenic peptides by positional screening methods (104). Both the WT CO92 and its Δ*lpp* Δ*msbB* Δ*ail* triple mutant cleaved the substrate in a time-dependent manner following essentially similar kinetics both at 28ºC and 37ºC at the two tested bacterial concentrations (**Fig. 3.3E**). As a control, a Pla-negative mutant (Δ*pla*) of CO92 did not cleave the substrate.

The capsular antigen (F1) is not only a major immunoreactive protein of *Y. pestis*, but it also exhibits antiphagocytic properties (111). Thus, the F1 production was verified in WT CO92 versus its triple mutant by using a commercially available plague immunochromatographic dipstick (impregnated with F1 antibodies) test which allows for rapid, *in vitro* qualitative identification of *Y. pestis*. Both the WT CO92 and its triple Δ*lpp* Δ*msbB* Δ*ail* mutant produced similar-intensity, purple color bands at the reaction and control lanes, whereas the Δ*caf1* mutant (negative control) was only positive at the control

lane (**Fig. 3.4A**). To confirm these results, the presence of F1 on bacterial cells was verified by IF staining with F1-specific antibodies followed by flow cytometry and microscopy (28). As noted from **Fig. 3.4B&C**, F1 was detected on the surfaces of both the WT CO92 and its Δ*lpp* Δ*msbB* Δ*ail* triple mutant, while the Δ*caf1* mutant was negative for the presence of F1.

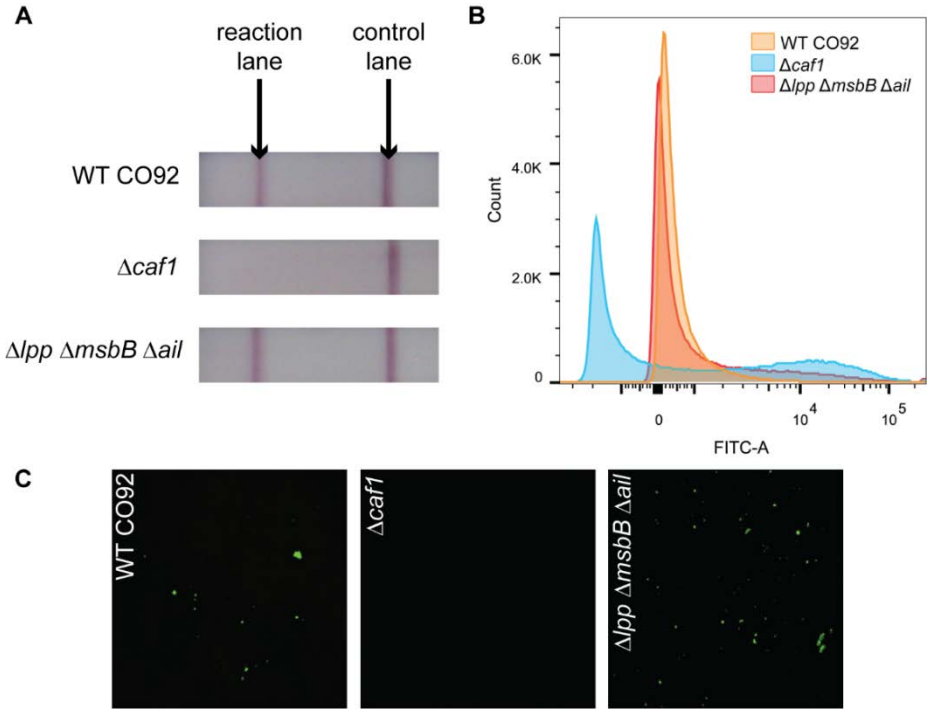

Figure 3.4. Production of F1 antigen.
Selected overnight *Y. pestis* cultures were diluted 1:20 in fresh HIB and continued to be grown at 28°C for 3 h, followed by an additional 2 h of incubation at 37°C. The F1 production was examined by using either immunochromatographic reaction dipsticks (**A**) or probed by immunofluorescence staining with anti-F1 antibodies followed by flow cytometric analysis (**B**) and microscopy **(C)**. The Δ*caf1* mutant CO92 was employed as a negative control. Magnification= ×400 **(C)**.

<u>Evaluation of *Y. pestis* CO92 Δ*ail* mutants in a pneumonic plague mouse model.</u>

To gauge the virulence potential of the Δ*ail* mutant strains, mice (n=10/group) were infected by the i.n. route with similar doses (1.3 x 10^4 CFU, representing 26 LD_{50} of the WT bacterium) of the Δ*ail* single-, Δ*lpp* Δ*ail* and Δ*lpp* Δ*msbB* double-, or the Δ*lpp* Δ*msbB* Δ*ail* triple-mutant strains as well as the WT CO92. While animals inoculated with the WT CO92 died by day 4 p.i., all of the mice infected with the Δ*ail* single mutant died by day

10 p.i., showing an increased mean time to death (**Fig. 3.5A**), confirming an earlier report of Kolodziejek et al. (77). Mice infected with the Δ*lpp* Δ*ail* and Δ*lpp* Δ*msbB* double mutants, or the Δ*lpp* Δ*msbB* Δ*ail* triple mutant had increased survival rates (20, 40, and 100%, respectively). Clinically, animals infected with the WT CO92 or mutants that provided minimal attenuation in mice had ruffled fur, hunched back, and lethargy, and they were unable to groom and tended to hurdle together.

To evaluate specific immunity that was developed to *Y. pestis*, sera from all of the surviving mice infected with various mutants of CO92 (**Fig. 3.5A**) were collected on day 14 p.i. Animals challenged with the WT CO92 or the Δ*ail* single mutant could not be bled, since there were no survivors. Based on the ELISA data, sera from mice challenged with Δ*lpp* Δ*msbB* and Δ*lpp* Δ*ail* double mutants exhibited high total IgG titers (1:3125) to the F1-V antigen (**Fig. 3.5B**), while this titer was low (1:25) when animals were infected with the Δ*lpp* Δ*msbB* Δ*ail* triple mutant (**Fig. 3.5B**).

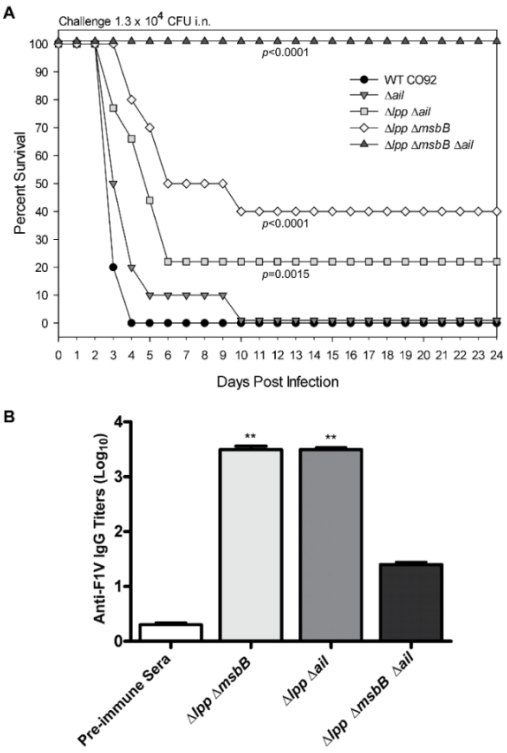

Figure 3.5. Survival analysis and antibody responses of mice infected with WT *Y. pestis* CO92 and its mutant strains in a pneumonic plague model.

Female Swiss Webster mice (10 per group) were challenged by the intranasal (i.n.) route with 1.3 x 10^4 CFU of WT *Y. pestis* CO92 or its various mutants. The survival of mice was plotted and analyzed by the Kaplan Meier survival estimates. The statistically significant *p* values when comparing various mutants and the WT CO92-infected mice are indicated under each curve (**A**). Mice were bled 14 days p.i., and the total IgG responses to F1-V antigen were determined by an ELISA. The arithmetic means ± standard deviations are plotted. "**" indicates statistical significance with $p < 0.001$ when compared to pre-immune serum (**B**).

The extent of attenuation in the virulence potential of the Δ*lpp* Δ*msbB* Δ*ail* triple mutant was then ascertained by infecting mice by the i.n. route with increasing doses ranging from 4.0 x 10^4 to 5.9 x 10^5 CFU, representing 80 to 1180 LD_{50} of the WT bacterium (**Fig. 3.6A**). A group of animals that received 32 LD_{50} of WT CO92 served as a control, and all of them died by day 4 p.i. The Δ*lpp* Δ*msbB* Δ*ail* triple mutant was unable to kill mice at all of these doses and thus resulted in 100% survival rates (**Fig. 3.6A**). Importantly, the total IgG titers (on day 14 p.i.) in the sera progressively increased (up to 1:625) when the animals were challenged with increasing doses (80 to 1180 LD_{50}s of the WT CO92) of the Δ*lpp* Δ*msbB* Δ*ail* triple mutant (**Fig. 3.6B**).

To further assess specific immunity induced in mice after initial infection with the Δ*lpp* Δ*msbB* Δ*ail* triple mutant strain (**Fig. 3.6A**), the surviving animals were subsequently challenged on day 24 p.i. with 1.0 x 10^4 CFU (20 LD_{50}) of the WT CO92 *luc2* strain. Age-matched naïve mice were used as a control, and 90% of them died by day 4 p.i. (**Fig. 3.6A**). There was an increase in time to death and somewhat of a dose-dependent protection, which was maximal in animals that were initially infected with 5.9 x 10^5 CFU (1180 LD_{50} of WT CO92) of the triple mutant (50% of the mice survived) compared to the naïve animals during the WT CO92 *luc2* strain re-challenge (**Fig. 3.6A**).

The surviving mice were imaged on day 3 p.i by using an *in vivo* imaging system and the first animal on the left in each imaging panel was uninfected and served as a control (**Fig. 3.6C**). While the WT CO92 *luc2* strain disseminated to the whole body in 6 out of 9 naïve animals (**Fig. 3.6C-I**), the bioluminescent strain was confined at the initial infection site (lungs) in those animals that were first infected with the Δ*lpp* Δ*msbB* Δ*ail* triple mutant

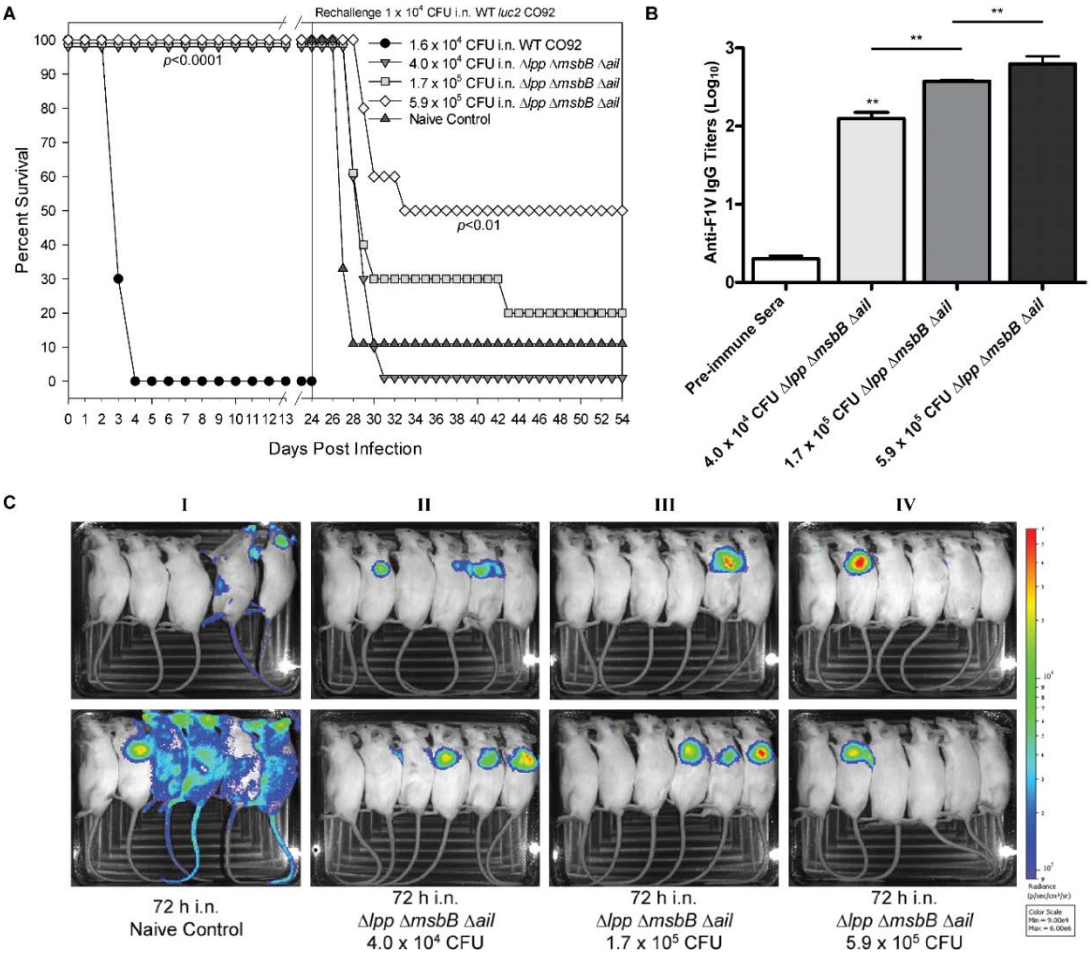

Figure 3.6. Virulence potential of and subsequent protection conferred by the Δ*lpp* Δ*msbB* Δ*ail* triple mutant *Y. pestis* CO92 in a pneumonic plague mouse model.
Female Swiss Webster mice (n=9 or 10/group) were challenged by the i.n. route with various indicated doses of the Δ*lpp* Δ*msbB* Δ*ail* triple mutant or 1.6 x 10^4 CFU of WT *Y. pestis* CO92. The surviving animals with age-matched naïve mice were then re-challenged on Day 24 p.i. with 1 x 10^4 CFU of WT CO92 *luc2* strain. The statistically significant *p* values are in comparison to WT CO92-infected mice during the initial challenge or to naïve control animals during the WT CO92 *luc2* re-challenge (**A**). The total IgG responses to the F1-V antigen were examined in the sera at day 14 post initial infection. "**" indicates statistical significance with $p < 0.001$ as compared to pre-immune serum or between different doses of the triple mutant used for initial infection (**B**). The animals after re-challenge were imaged at 72 h for bioluminescence (panels I-IV). The bioluminescence scale is within the figures and ranges from most intense (red) to least intense (violet). The animal on left in each imaging panel represents an uninfected control (**C**).

before being challenged with the WT CO92 *luc2* strain (**Fig. 3.6C-Panels II-IV**). As the dose of the initial infection with the triple mutant was increased from 4 x 10^4 to 1.7 x 10^5 CFU, the number of animals that were positive for bioluminescence decreased from 6/10 to 4/10 animals subsequent to WT CO92 *luc2* strain challenge (**Fig. 3.6C-Panels II & III**). At the highest infection dose of the triple mutant (5.9 x 10^5 CFU), only 2/10 mice were

positive for bioluminescence as a result of subsequent CO92 *luc2* challenge, with 80%, 60%, and 50% of the animals found to survive on days 7, 8, and 10, respectively (**Fig. 3.6A**). Since half of the animals did not succumb to infection, these data indicated clearing of the WT CO92 *luc2* strain (**Fig. 3.6C-Panel IV**).

In our subsequent experiment, i.n. initial infection doses of the Δ*lpp* Δ*msbB* Δ*ail* triple mutant given to the mice were increased to 1.8 x 10^6 and 3.4 x 10^6 CFU which corresponded, respectively, to 3600 and 6800 LD_{50}s of the WT CO92. As noted from **Fig. 3.7A**, even the highest dose of the triple mutant was unable to kill mice, while the control animals infected with a much lower dose of the WT CO92 (26 LD_{50}) died by day 4 (**Fig. 3.7A**). As expected, in the sera of mice infected with the highest challenge dose (3.4 x 10^6 CFU) of the Δ*lpp* Δ*msbB* Δ*ail* triple mutant strain, the total IgG and IgG isotype (IgG1, IgG2a, and IgG2b) antibody titers to F1-V antigen were sustained at 1:625 (**Fig. 3.7B**), indicating a balanced T_H1 and T_H2 response. The total IgG titers were higher (1:1000) when the ELISA plates were coated with the whole cells and reflected the presence of antibodies to other *Y. pestis* antigens along with F1 and V (**Fig. 3.7B**).

As expected, protection levels increased to 70% when the animals were initially infected with the Δ*lpp* Δ*msbB* Δ*ail* triple mutant at a dose of 3.4 x 10^6 CFU (6800 LD_{50} of the WT CO92) and then challenged i.n. on day 24 with a higher dose (28 LD_{50} or 1.4 x 10^4 CFU) of the WT CO92 *luc2* strain (**Fig. 3.7A**). Mice (n=5-10) were imaged with in *vivo* imaging system again (**Fig. 3.7C**). On day 3 post-challenge, 5/5 of naïve animals were positive for bioluminescence, while WT CO92 *luc2* disseminated throughout the animal body in 4/5 mice (**Fig. 3.7C-Panel I**). Only two of the ten animals which had received the triple mutant at the highest dose before being challenged with the WT CO92 *luc2* strain,

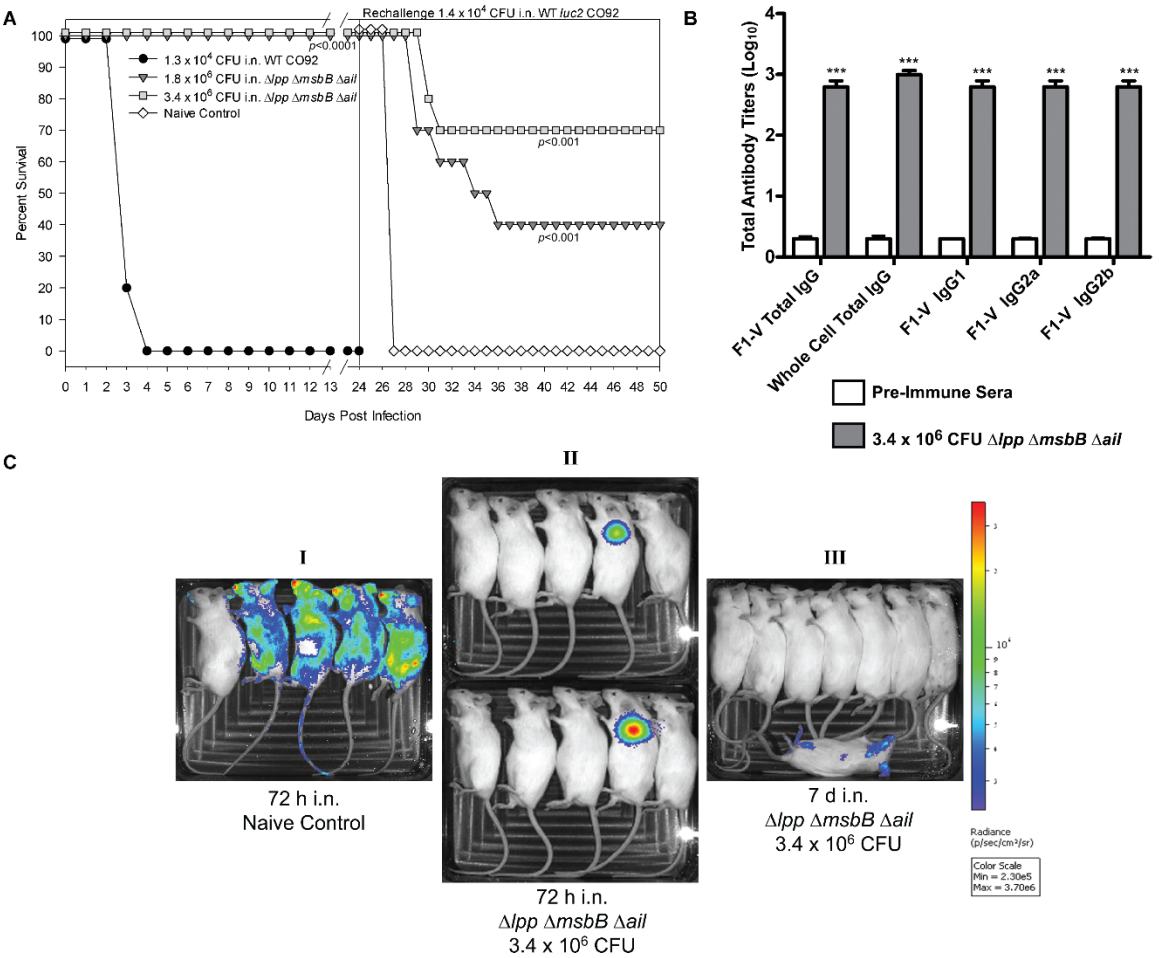

Figure 3.7. **Survival analysis and subsequent protection conferred by high doses of Δ*lpp* Δ*msbB* Δ*ail* triple mutant of *Y. pestis* CO92 in a pneumonic plague mouse model.**
Female Swiss Webster mice (5-10 per group) were infected by the i.n. route with various doses of the Δ*lpp* Δ*msbB* Δ*ail* triple mutant or 1.3 x 10^4 CFU of WT *Y. pestis* CO92. Surviving mice with age-matched naïve animals were then re-challenged on Day 24 p.i. with 1.4 x 10^4 CFU of WT CO92 *luc2* strain. The statistically significant *p* values are in comparison to the WT CO92-infecteded mice in initial challenge or to naïve control mice during the WT CO92 *luc2* re-challenge (**A**). The total IgG responses to the F1-V antigen or the whole bacteria were examined in the sera at day 14 post initial infection. The antibody isotypes to F1-V antigen were further delineated by using isotyping specific secondary antibodies. "***" indicates statistical significance with $p < 0.0001$ as compared to pre-immune serum (**B**). The animals were imaged on day 3 and/or 7 post re-challenge for bioluminescence (panels I-III). The bioluminescence scale is within the figures and ranges from most intense (red) to least intense (violet) (**C**).

were positive for bioluminescence (**Fig. 3.7C-Panel II**) and these animals subsequently died by day 6 (**Fig. 3.7A**). On day 7 p.i., another mouse succumbed to infection and was positive for bioluminescence (**Fig. 3.7C-Panel III**). The low bioluminescence detected in the dead animal was possibly due to lack of oxygen and low body temperature that diminished bioluminescence (97). Importantly, the remainder of the 7 mice that were

previously infected with 3.4 x 10^6 CFU of the Δ*lpp* Δ*msbB* Δ*ail* triple mutant were devoid of bioluminescence after subsequent challenge with WT CO92 *luc2* strain, indicating clearance of the infecting pathogen (**Fig. 3.7C-Panel III**). Collectively, these data suggested that the increased humoral immune response generated by the triple mutant in mice seemed to correlate with the subsequent enhanced protection of animals when challenged with the WT CO92.

Bacterial dissemination and histopathological lesions in mice challenged by the intranasal route with Δ*lpp* Δ*msbB* Δ*ail* triple mutant of *Y. pestis* CO92.

Mice were either challenged with 2.5 x 10^6 CFU of WT CO92 (5000 LD_{50}) or its Δ*lpp* Δ*msbB* Δ*ail* triple mutant. Animals were sacrificed on day 2, 3, and 6 p.i., and their lungs, liver, spleen, and the blood harvested and subjected to bacterial load determination. Mice challenged with WT bacteria had a high bacterial load in each of these organs on both day 2 (ranged from 1.1 x 10^7 to 1.7 x 10^9 CFU/organ) and day 3 (1.3 x 10^9 to 2.8 x 10^9 CFU/organ). No data were collected on day 6 since all of the mice succumbed to infection within 80 h. Animals challenged with the Δ*lpp* Δ*msbB* Δ*ail* triple mutant had minimal- to-no bacterial load in the organs examined except in the lungs on day 2 (ranged from 2.8 x 10^2 to 1.9 x 10^3 CFU/organ) (**Fig. 3.8**).

Organs from the infected mice were also removed for histopathological analysis. Between 48 and 60 h p.i., two of the five WT bacteria-infected mice succumbed to infection and their organs were not harvested. The remaining three mice succumbed to infection between 60 and 72 h p.i., and their lungs had mild-to-moderate neutrophilic inflammation (arrow). All of the animals had bacteria present in their lungs (asterisk), and one had mild diffuse congestion. The alveoli of all of the lungs had a moderate level of hemorrhage

(arrowhead) with few alveolar spaces observed (**Fig. 3.9**). The lungs of Δ*lpp* Δ*msbB* Δ*ail* triple mutant-infected mice appeared normal, with only one animal having minimal histiocytic infiltration of the alveolus by day 3 p.i. There were no noticeable bacteria or edema present in the lungs of triple mutant-infected mice (**Fig. 3.9**). However, the lungs of the Δ*lpp* Δ*msbB* Δ*ail*-infected mice did have minimal-to-mild neutrophilic infiltration on day 2 p.i. (data not shown). The residual lesions in the triple-mutant infected mice resolved by day 6 p.i. (data not shown).

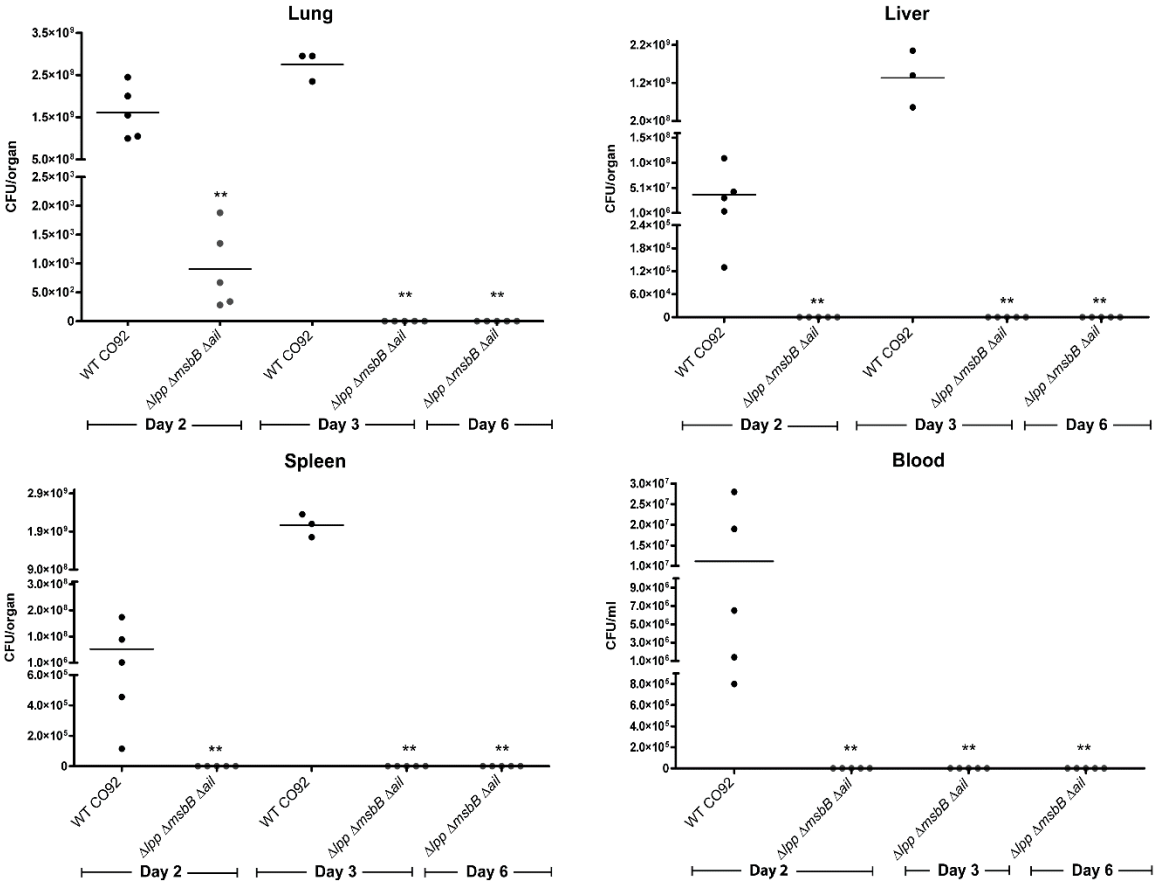

Figure 3.8. Dissemination of WT CO92 and its Δ*lpp* Δ*msbB* Δ*ail* triple mutant in a mouse model of pneumonic plague.
Female Swiss Webster mice were challenged by the i.n. route with 2.5 x 10^6 CFU of the WT *Y. pestis* CO92 or its Δ*lpp* Δ*msbB* Δ*ail* triple mutant. Organs and the blood were harvested from mice (n=5) on days 2, 3, and 6 p.i. The bacterial loads in different organs and blood in each individual mouse were plotted and the arithmetic means are indicated by the horizontal bars. "**" indicates statistical significance with $p<0.001$ as compared to WT CO92 on each day (Day 6 was compared to Day 3 WT CO92).

All of the livers of WT-infected animals had bacteria (asterisk), some necrosis (arrowhead), and neutrophilic infiltration (arrow). These lesions were non-existent or minimal in the livers of Δ*lpp* Δ*msbB* Δ*ail* triple mutant-infected mice on day 3 p.i. (**Fig. 3.9**). All of the spleens of WT-infected mice had bacteria (asterisk), mild lymphoid depletion of the marginal zone in the white pulp, and mild-to-marked diffuse rarefaction (+) or loss of normal cell population of the red pulp with fibrin present. The red pulp of these spleens also had moderate level of hemorrhage on day 3 p.i. (**Fig. 3.9**). The spleens of the Δ*lpp* Δ*msbB* Δ*ail* triple mutant-infected mice were essentially normal with occasional animals having either minimal neutrophilic inflammation of the red pulp or mild depletion of the white pulp (**Fig. 3.9**). These changes in the spleens of animals infected with the triple mutant could be related to the generation of an immune response.

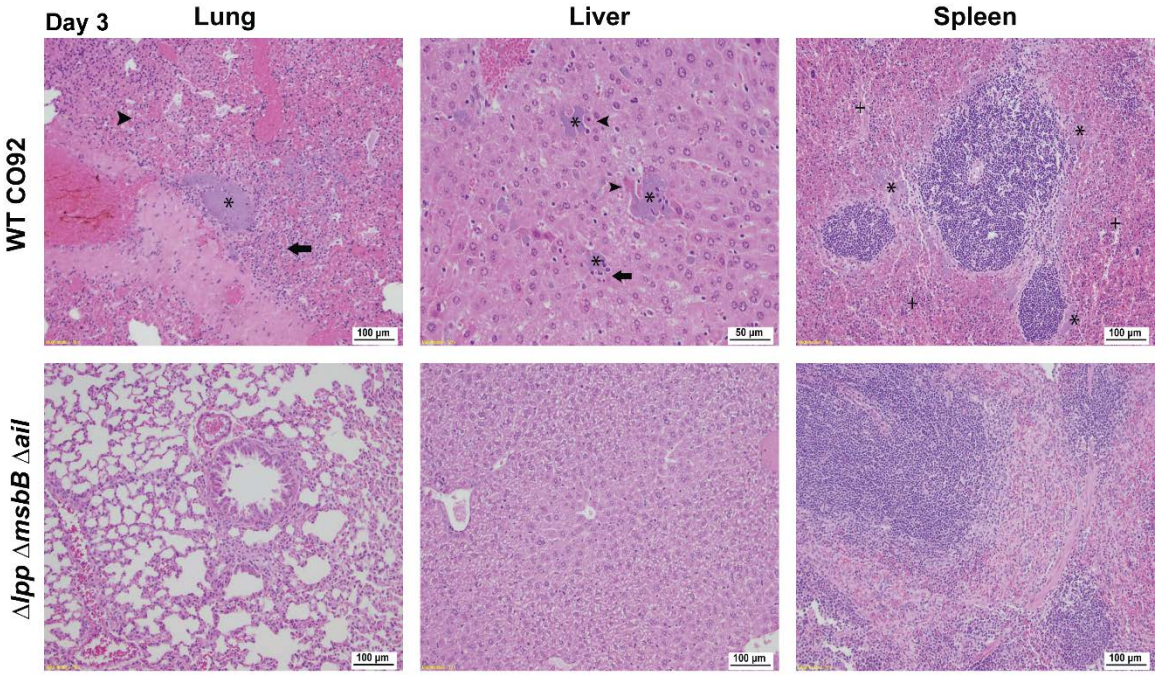

Figure 3.9. Histopathology of mouse tissues following pneumonic infection with WT CO92 or its Δ*lpp* Δ*msbB* Δ*ail* triple mutant.

Female Swiss Webster mice were challenged by the i.n. route with 2.5 x 10^6 CFU of WT *Y. pestis* CO92 or its Δ*lpp* Δ*msbB* Δ*ail* triple mutant. On days 2, 3, and 6 p.i., a portion of the lungs, liver, and the spleen (n=3-5) was stained with H&E, and evaluated by using light microscopy in a blinded fashion. Only data for day 3 are shown. The presence of bacteria, neutrophilic infiltration, hemorrhage/necrosis, and rarefied red pulp is indicated by the asterisks, arrows, arrowhead and the plus symbols (+), respectively. The scale for each panel is indicated.

The Δ*lpp* Δ*msbB* Δ*ail* triple mutant of *Y. pestis* CO92 evokes reduced inflammatory cytokines in a pneumonic plague mouse model.

Samples of the lung homogenates and sera collected from the above-mentioned infected animals were assessed for cytokine production by using an eBioscience 6-plex Bioplex assay. There was a statistically significant difference in the presence of TNF-α, IFN-γ, and IL-6 in both the lungs and the sera between the WT- and the triple Δ*lpp* Δ*msbB* Δ*ail* mutant- infected animals on both days 2 and 3 p.i. (**Fig. 3.10**). In the lungs, TNF-α and IFN-γ levels from WT-infected animals were >50-100 fold higher than those in the triple mutant-infected animals, whereas their IL-6 levels were >1000-fold higher (**Fig. 3.10-Panel A**). In the serum, TNF-α and IFN-γ levels from WT-infected mice were >50 fold higher than those in the triple mutant-infected animals, whereas their IL-6 levels were >300 fold higher (**Fig. 3.10-Panel B**). These reduced cytokine levels in the mutant-infected mice correlated with its rapid clearance (**Fig. 3.8**).

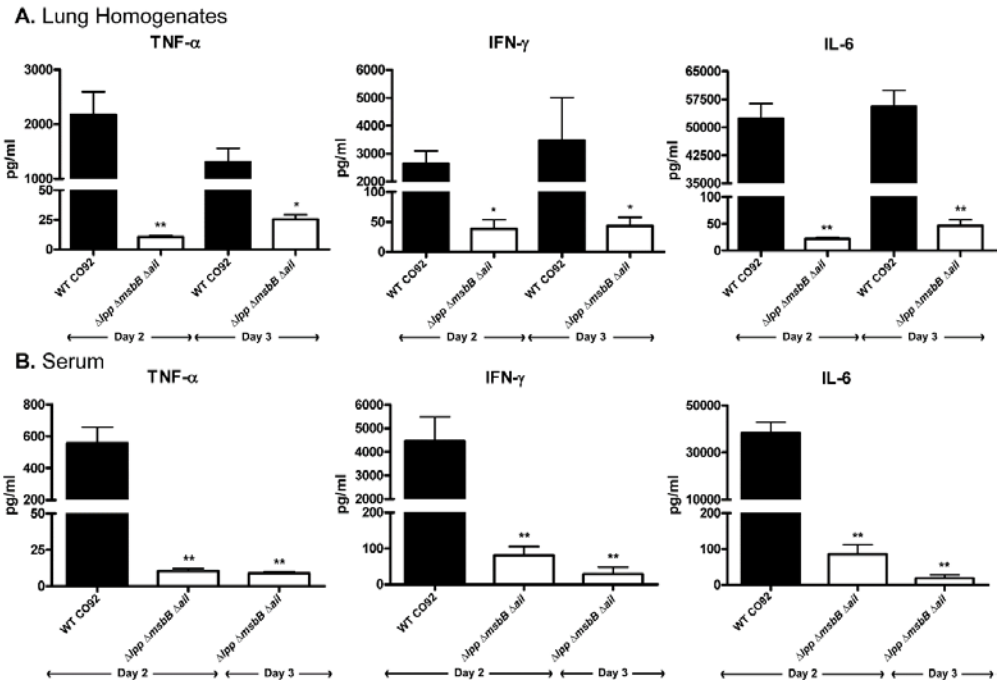

Figure 3.10. Cytokine/chemokine analysis on the sera and lung homogenates of mice in a pneumonic plague mouse model.

Mice were challenged by the i.n. route with 2.5 x 10^6 CFU of the WT *Y. pestis* CO92 or its Δ*lpp* Δ*msbB* Δ*ail* triple mutant. At 2 and 3 days p.i., 5 mice from each group (at each time point) were euthanized. The lungs were harvested and homogenized and the blood collected via cardiac puncture. Production of various cytokines/chemokines was measured by using a multiplex assay. Only the cytokines/chemokines showing statistically significant differences in the mutant compared to WT CO92-infected mice are plotted with the arithmetic means ± standard deviations. "*" and "**" indicate statistical significance with $p<0.01$ and $p<0.001$, respectively, as compared to WT CO92 on each day.

The Δ*ail* mutants of *Y. pestis* CO92 have host-dependent serum sensitivities.

Ail has been reported to function in providing serum resistance to *Y. pestis* (75-78). Consequently, the WT CO92 and its Δ*ail* single, Δ*lpp* Δ*msbB* double, and the Δ*lpp* Δ*msbB* Δ*ail* triple mutant were tested for their ability to be killed by the complement cascade. As shown in **Fig. 3.11A**, both the WT CO92 and its Δ*lpp* Δ*msbB* double mutant strain had 100% or greater survival upon exposure to normal unheated mouse, non-human primate (NHP), or human serum. Thus, the deletion of *lpp* and *msbB* genes did not affect the serum resistance of *Y. pestis*. In contrast, the Δ*ail* single- and the Δ*lpp* Δ*msbB* Δ*ail* triple- mutant strains had 100% or greater bacterial survival in normal (unheated) mouse serum, while ~0% survival in NHP and human sera, indicating Ail's role in serum resistance in NHP and humans. This serum resistance phenotype of the Δ*ail* mutants in NHP and human sera was lost when the complement was inactivated, with 100% or greater survival.

To confirm that Ail is responsible for this phenotype, the complemented strains (Δ*ail*:pBR322-*ail* and Δ*lpp* Δ*msbB* Δ*ail*:pBR322-*ail*) were exposed to normal (unheated) NHP and human sera. Both of these strains exhibited 100% or greater survival (**Fig. 3.11A**), which provided further evidence that this phenotype was indeed due to the expression of the *ail* gene. The bacterial survival over 100% indicated their ability to replicate in the sera. Essentially, a similar level of Ail was detected in the tested strains except for those from which the *ail* gene was deleted as judged by Western blot analysis (**Fig. 3.11B**).

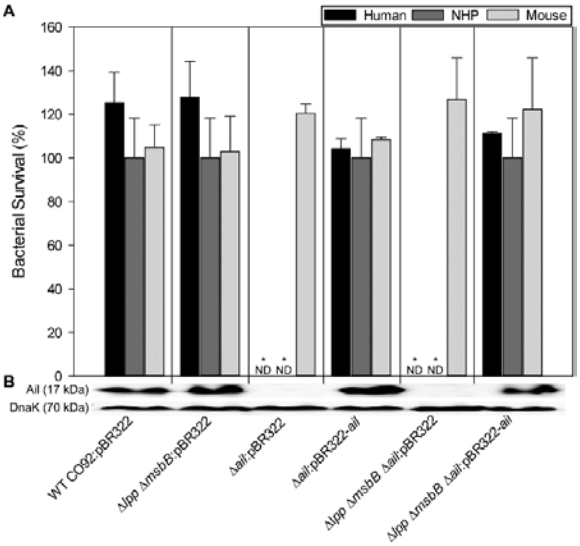

Figure 3.11. Serum resistance and Ail production by various *Y. pestis* CO92 strains. Various overnight grown *Y. pestis* strains (~5 x 10^6 CFU) was mixed with either unheated or heated sera from human, nonhuman primate (NHP) and mouse. After incubation for 2 h at 37ºC, the number of surviving bacteria (CFU) in each sample was determined. ND=not detectable. "*"indicates statistical significance with $p<0.01$ as compared to WT CO92 for each type of serum (**A**). The levels of Ail protein and DnaK were analyzed in these strains by immunoblotting by using specific antibodies to Ail and DnaK (**B**).

Decreased adherence and invasion of *Y. pestis* CO92 Δ*ail* mutants in the epithelial cells.

Since Ail functions in adherence and subsequent invasion of bacteria in the host cells, these virulence phenotypes of WT CO92 and its various mutants were first examined in HeLa cells at an MOI of 100 (**Fig. 3.12A-Panels I & II**). Both the Δ*ail* single and the Δ*lpp* Δ*msbB* Δ*ail* triple mutant had similar, significantly decreased adherence (~28%) (**Panel I**) and invasion (~1.1-1.5%) (**Panel II**) compared to those of the WT CO92 and its Δ*lpp* Δ*msbB* double mutant (which had comparable levels; ~60-75% adherence and ~3-4% invasion) (**Fig. 3.12A-Panels I & II**). Upon complementation with the *ail* gene, both Δ*ail*:pBR322-*ail* and Δ*lpp* Δ*msbB* Δ*ail*:pBR322-*ail* strains became adherent (~60%) (**Fig. 3.12A-Panel I**) and invasive (~3-4%) (**Fig. 3.12A-Panel II**), which were comparable to that seen with the WT CO92 and its Δ*lpp* Δ*msbB* double-mutant strain. In addition to depicting percentage adherence and invasion, the actual CFU associated with adherence and invasion of various tested cultures in HeLa cells were also shown (**Fig. 3.13A**). As a gentamicin protection assay was used during the experiment, the sensitivities of various *Y. pestis* strains to this antibiotic were assessed. Our data indicated that the WT CO92 and its

various mutant strains exhibited similar gentamicin sensitivities, with the MIC values of 0.125 µg/mL at 28ºC.

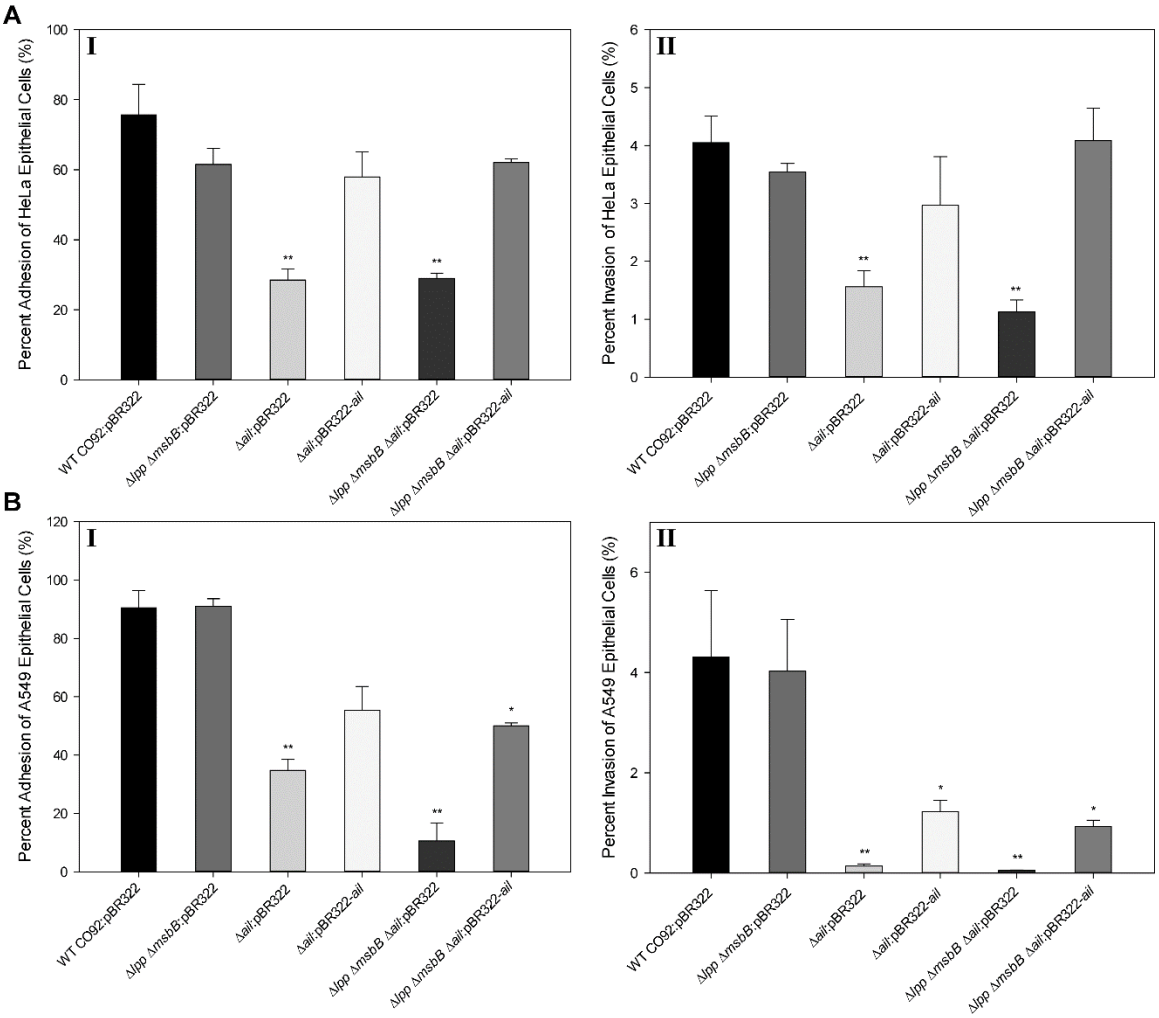

Figure 3.12. Adherence and invasion of WT *Y. pestis* CO92 and its mutant strains.
HeLa cells (**A**) and A549 (**B**) were infected at an MOI of 100 with various *Y. pestis* CO92 strains at 37°C for 2 h. The percentage of adherent (**Panel I**) and invaded (**Panel II**) bacteria compared to the total number of bacteria used to infect epithelial cells were calculated. The arithmetic means ± standard deviations are plotted. "*" and "**" indicate statistical significance with $p<0.05$ and $p<0.001$, respectively, compared to both WT CO92 and the Δ*lpp* Δ*msbB* mutant.

Since *Y. pestis* infects the lungs during the pneumonic plague, bacterial adherence and invasion of A549 human alveolar epithelial cells were then examined to mimic a natural infection scenario. As with the HeLa cell infection model, both the Δ*ail* single and the Δ*lpp* Δ*msbB* Δ*ail* triple mutants had similar significantly decreased adherence (34% and 10%, respectively) (**Fig. 3.12B-Panel I**) and minimal invasion (~0.01%) (**Fig. 3.12B-Panel II**)

compared to the WT CO92 and its Δ*lpp* Δ*msbB* double mutant (which had comparable levels: ~90% adherence and ~4% invasion). Upon complementation with the *ail* gene, both Δ*ail*:pBR322-*ail* and Δ*lpp* Δ*msbB* Δ*ail*:pBR322-*ail* strains had increased adherence (~50-55%) and invasion (~1%) (**Fig. 3.12B, Panels I&II**). Like for the HeLa cells, the actual CFU associated with adherence and invasion of various tested cultures in A549 cells were also shown (**Fig. 3.13B**). Thus, the decreased adherence and invasive properties of the Δ*ail* mutants were most likely due to the lack of Ail protein.

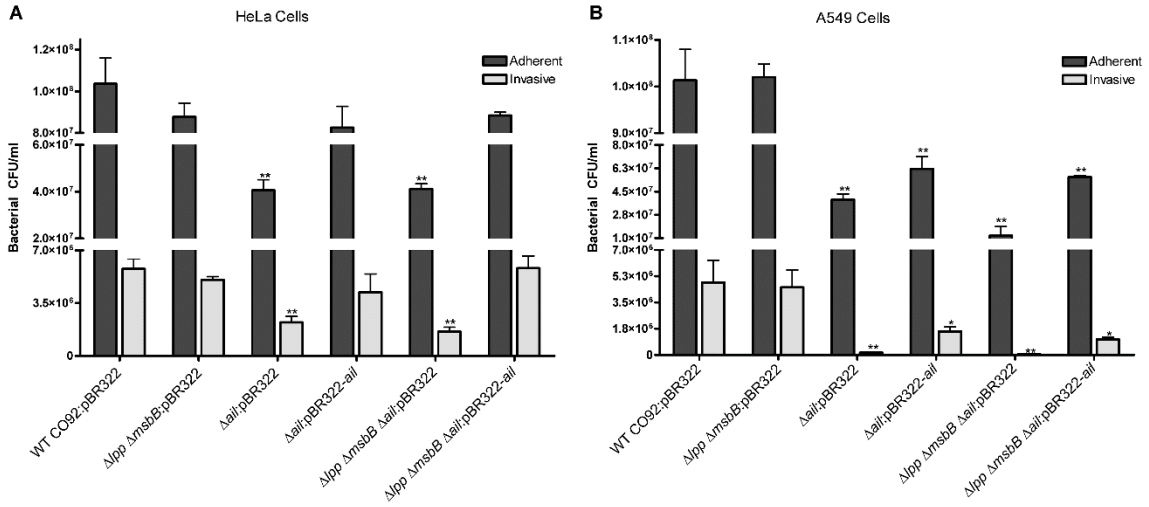

Figure 3.13. Adherence and invasion of WT *Y. pestis* CO92 and its mutant strains.
HeLa cells (**A**) and A549 (**B**) were infected at an MOI of 100 with various *Y. pestis* CO92 strains at 37°C for 2 h. The total CFU of adherent and invasive bacteria is presented. The arithmetic means ± standard deviations are plotted. "*" and "**" indicate statistical significance with $p<0.05$ and $p<0.001$, respectively, compared to both WT CO92 and the Δ*lpp* Δ*msbB* double mutant.

Host-dependent survivability of *Y. pestis* CO92 Δ*ail* mutants in murine and human macrophages and epithelial cells.

To determine the role of Ail in intracellular survival within macrophages, MH-S murine alveolar macrophages were infected with the WT, Δ*ail* single-, Δ*lpp* Δ*msbB* double-, or the Δ*lpp* Δ*msbB* Δ*ail* triple- mutant of CO92 at an MOI of 10. The macrophages had increased uptake of the Δ*lpp* Δ*msbB* Δ*ail* triple mutant (29%) compared to WT CO92 and Δ*ail* single mutant strains (12% and 13%, respectively) (data not shown). At 2 h p.i., 46%

of the Δ*lpp* Δ*msbB* double mutant and 39% of the Δ*lpp* Δ*msbB* Δ*ail* triple mutant survived in MH-S cells as compared to 77% of the WT CO92 (**Fig. 3.14A**), correlating with our previous data that Lpp contributes to intracellular survival of *Y. pestis* in macrophages (40, 42, 51, 74). The Δ*ail* single mutant strain had comparable intracellular survival rate (74%) to the WT CO92 (**Fig. 3.14A**). This trend was similar at 4 h p.i., although the percent survival of bacteria decreased further. Thus, these data suggested that Ail did not contribute to intracellular survival in murine alveolar macrophages (**Fig. 3.14A**).

To further investigate intracellular survivability of mutant bacteria, the human monocyte-derived macrophages (HMDM) were used. The Δ*lpp* Δ*msbB* Δ*ail* triple mutant strain was most impaired in surviving intracellularly (18%) in HMDM when compared to the Δ*lpp* Δ*msbB* double mutant (25%) and WT CO92 (38%) at 2 h p.i. (**Fig. 3.14B**). However, no statistical difference was noted when Δ*lpp* Δ*msbB* double- and the Δ*lpp* Δ*msbB* Δ*ail* triple- mutant were compared. This trend was similar at 4 h p.i., although percent survival of bacteria decreased further (**Fig. 3.14B**).

We then infected HeLa epithelial cells with various CO92 mutants in two independent experiments (**Fig. 3.14C&D**). In the first set of experiment, the Δ*lpp* single mutant and its complemented strain were also tested. As shown in **Fig. 3.14C**, the WT CO92 and its Δ*ail* single mutant strain had comparable intracellular survival rates (63% and 68%, respectively), whereas the Δ*lpp* single and Δ*lpp* Δ*msbB* double mutants had a decreased survival rates (31-32%) at 12 h p.i. On the contrary, the Δ*lpp* Δ*msbB* Δ*ail* triple mutant strain survived minimally (5%). We could fully complement the Δ*lpp* single mutant *in cis* with the corresponding gene (**Fig. 3.14C**), indicating a major role of Lpp in bacterial

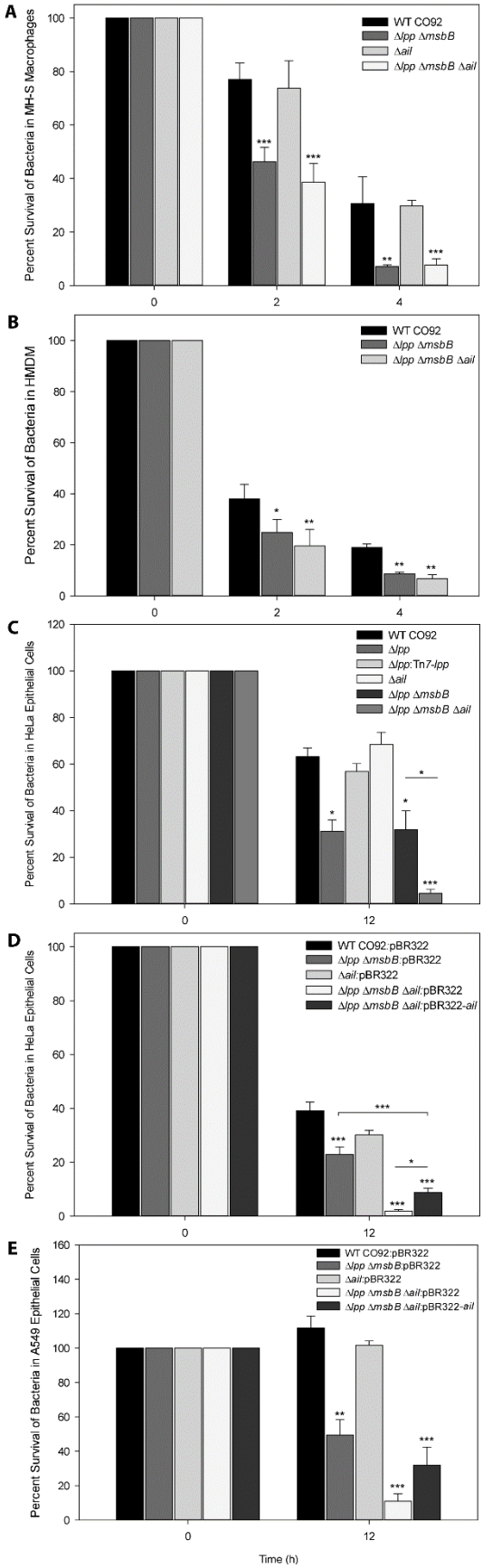

Figure 3.14. Intracellular survival of various *Y. pestis* CO92 mutant strains in epithelial cells and macrophages.
Murine MH-S macrophages (**A**), human monocyte-derived macrophages (HMDM) (**B**), HeLa epithelial cells (**C&D**), and human A549 alveolar epithelial cells (**E**) were infected with various *Y. pestis* CO 92 strains at an MOI of 10, 1, 100 and 100, respectively. After 45 to 60 min of incubation at 37ºC and following an hour of gentamicin treatment, the cells were harvested at 2 and 4 h post gentamicin treatment for macrophages, and 12 h for the epithelial cells. The number of bacteria surviving intracellularly was assessed and the percent survival was calculated. "*", "**"and "***" indicate statistical significance with $p<0.05$, $p<0.005$ and $p<0.001$, respectively, compared to the WT CO92 at each time point or between the two tested strains as indicated by the horizontal bar.

intracellular survival. In a second HeLa cell experiment (**Fig. 3.14D**), we showed a similar pattern of the Δ*lpp* Δ*msbB* Δ*ail* triple mutant surviving minimally while the Δ*ail* single mutant exhibited a survival pattern mimicking that of the WT CO92. Further, as expected, the Δ*lpp* Δ*msbB* double mutant was significantly impaired in its survival in HeLa cells compared to WT CO92 (**Fig. 3.14D**). Interestingly, we could partially restore the intracellular survival phenotype of the Δ*lpp* Δ*msbB* Δ*ail* triple mutant with the *ail* gene when provided *in trans* (**Fig. 3.14D**) but did not reach the level of intracellular survival noted for the Δ*lpp* Δ*msbB* double mutant.

Finally, we infected A549 human lung epithelial cells with the WT CO92 and its Δ*ail* single-, Δ*lpp* Δ*msbB* double-, or the Δ*lpp* Δ*msbB* Δ*ail* triple- mutant strain. Both the Δ*lpp* Δ*msbB* double- and the Δ*lpp* Δ*msbB* Δ*ail* triple- mutant strains had decreased survival rates (49% and 11%, respectively) at 12 p.i. (**Fig. 3.14E**), a pattern similar to that seen in HeLa cells. Partial complementation of the Δ*lpp* Δ*msbB* Δ*ail* triple mutant in terms of intracellular survival was noted with the *ail* gene (**Fig. 3.14E**), although the data did not reach statistical significance unlike that in the HeLa cells (**Fig. 3.14D**), but did reach to a level comparable to the Δ*lpp* Δ*msbB* double mutant.

Host-dependent inflammatory cytokine secretion by *Y. pestis* CO92 Δ*ail* mutants in infected macrophages.

Supernatants from the above-mentioned infected macrophages were collected and assessed for cytokine production by using either a Bio-Rad mouse 6-plex assay kit for MH-S cells or a Bio-Rad human 8-plex assay kit for HMDM. The Δ*lpp* Δ*msbB* double mutant-infected MH-S macrophages maintained TNF-α and IL-6 secretion comparable to that of the WT-infected cells at 2 h p.i., both of which were significantly decreased compared to

that in WT-infected MH-S macrophages at 4 h p.i. (**Fig. 3.15A**). The Δ*lpp* Δ*msbB* Δ*ail* triple mutant-infected mouse macrophages had significantly increased TNF-α and IL-6 secretion at 2 h and 4 h p.i. compared to that of WT CO92 and the Δ*lpp* Δ*msbB* double mutant-infected MH-S cells (**Fig. 3.15A**).

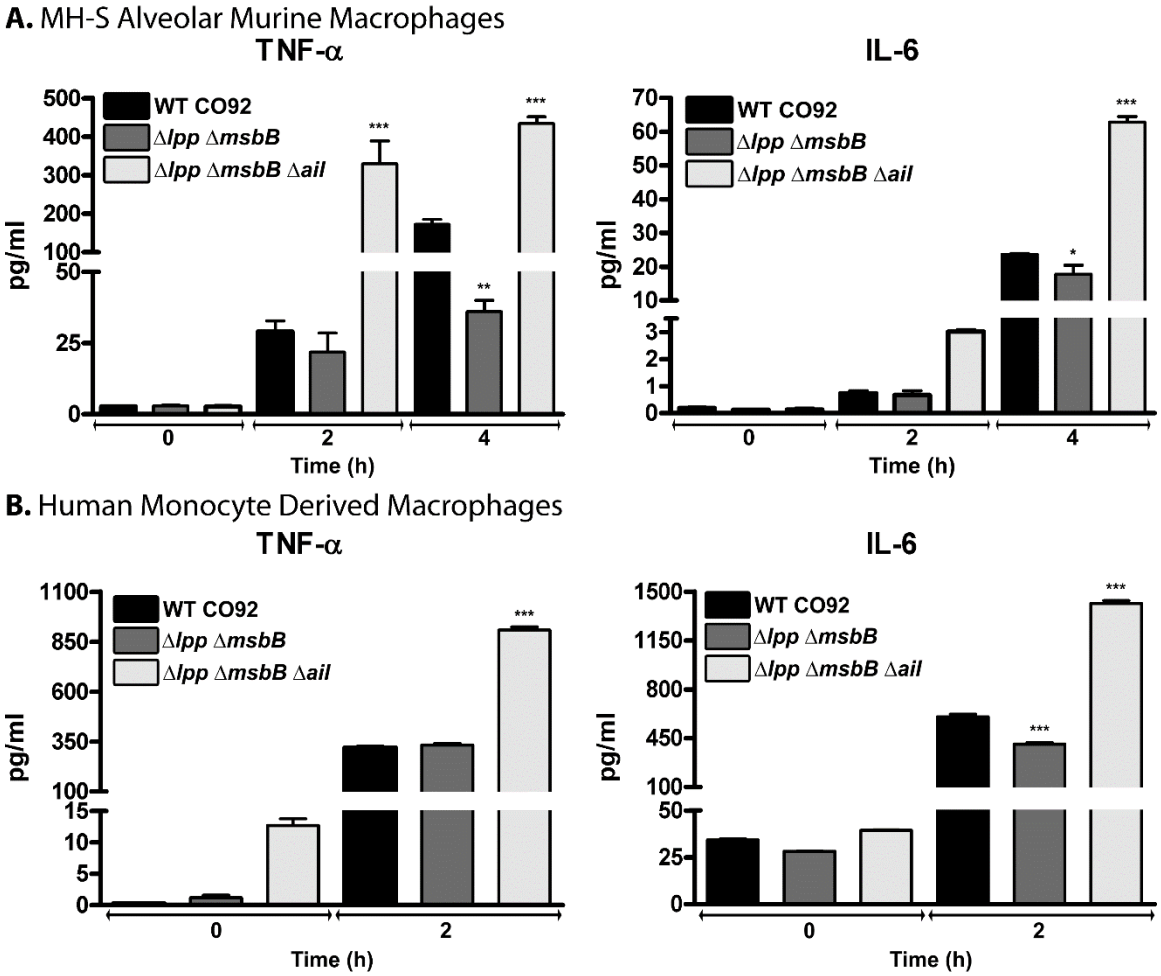

Figure 3.15. Inflammatory cytokine production by macrophages infected with various *Y. pestis* CO92 strains.

Murine alveolar macrophages (**A**) and human monocyte derived macrophages (HMDM) (**B**) were infected with various *Y. pestis* strains**.** Supernatants from infected macrophages were collected at 0, 2, or 4 h after gentamicin treatment. The levels of various cytokines in the supernatants were measured by using a multiplex assay. Only the cytokines/chemokines showing statistically significant differences compared to WT CO92-infected macrophages are plotted with arithmetic means ± standard deviations. "*", "**" and "***" indicate statistical significance with $p<0.05$, $p<0.01$ and $p<0.0001$, respectively, as compared to the WT CO92 on each day.

The Δ*lpp* Δ*msbB* Δ*ail* triple mutant-infected HMDM had statistically significant increases in TNF-α and IL-6 at 2 h p.i. compared to those in both the WT CO92 and its Δ*lpp* Δ*msbB* double mutant- infected macrophages (**Fig. 3.15B**). The Δ*lpp* Δ*msbB* double mutant-infected HMDM secreted comparable levels of TNF-α to WT CO92-infected HMDM, but exhibited a significant decrease in IL-6 secretion at 2 h p.i. (**Fig. 3.15B**). Finally, while the infected MH-S cells had extremely low levels of IFN-γ, the Δ*lpp* Δ*msbB* Δ*ail* triple mutant-infected HMDM secreted increased amounts of IFN-γ (63 pg/ml) at 2 h p.i. compared to those in both the WT CO92 and Δ*lpp* Δ*msbB* double mutant (41 and 39 pg/ml, respectively). However, the data did not reach statistical significance. Other cytokines included in the bioplex were below the detection limit for the samples obtained after infection of macrophages with either the WT CO92 or its mutant derivatives.

Discussion

We made an in-frame deletion of the *ail* gene from an already existing Δ*lpp* Δ*msbB* double mutant of WT CO92. The Δ*lpp* Δ*msbB* double mutant was attenuated in evoking both bubonic and pneumonic plague in mouse and rat models (42). This double mutant retained immunogenicity to partially protect rodents against pneumonic plague upon subsequent infection with lethal doses (8-10 LD_{50}) of WT CO92 (42). Our goal was to discern whether deletion of the *ail* gene from the Δ*lpp* Δ*msbB* double mutant of WT CO92 would further attenuate the bacterium *in vivo* while retaining immunogenicity, to serve as a possible background strain from which additional genes could be deleted for future live-attenuated vaccine development against plague. Indeed, the triple mutant was so highly attenuated that it did not kill any mice, even at a dose as high as 3.4 x 10^6 CFU (corresponding to 6800 LD_{50}s) of WT CO92 (Fig. 3.7A), and the animals did not exhibit

any clinical symptoms of the disease. Based on our data (Fig. 4), it was apparent that the Δ*lpp* Δ*msbB* Δ*ail* triple mutant was synergistically attenuated in a mouse model of pneumonic plague when compared to the Δ*ail* single and the Δ*lpp* Δ*msbB* double mutant.

In earlier studies, the Δ*lpp* Δ*msbB* double mutant of *Y. pestis* CO92 and the Δ*ail* mutant of *Y. pestis* KIM5 were reported to have a decreased ability to disseminate to peripheral organs of mice compared to their respective parental strains; however, both of these mutant strains persisted for 3-7 days p.i. in mouse organs (42, 88). On the contrary, the Δ*lpp* Δ*msbB* Δ*ail* triple mutant was more rapidly cleared from animals (by day 2-3 p.i.) (Fig. 3.8), resulting in minimal histopathological changes in the lungs, liver, and the spleen (Fig. 3.9).

The Δ*lpp* Δ*msbB* Δ*ail* triple mutant produced essentially similar levels of F1, Pla, and LcrV when compared to WT CO92 (Figs. 3.3 & 3.4). Therefore, the lower total IgG titers to F1-V antigen in the triple-mutant infected mice compared to those in animals that were challenged with either the Δ*lpp* Δ*msbB* or the Δ*lpp* Δ*ail* double mutant (Fig. 3.5B) could most likely be due to their rapid clearance by the immune system and not by the triple mutant's inability to stimulate an IgG response. This observation was substantiated by our findings that the IgG responses increased significantly when the animals were immunized with higher doses of the Δ*lpp* Δ*msbB* Δ*ail* triple mutant (Figs. 3.6B & 3.7B).

Brown Norway rats infected with the Δ*ail* mutant of *Y. pestis* CO92 were recently found to not only survive pneumonic infection (76), but also to have an influx of neutrophils in the draining lymph nodes when challenged by the intradermal route, leading to the development of large purulent abscesses (76). In addition, Ail seemed necessary in specifically targeting neutrophils for T3SS translocation of effectors in the lungs when

animals were infected intranasally with either the WT or the Δ*ail* mutant of *Y. pseudotuberculosis* (112). In our study, the lungs of the triple mutant-infected animals had minimal-to-mild neutrophilic inflammation on day 2 p.i. The lifespan of neutrophils in mice is estimated to be up to 12.5 h (113), and, therefore, the influx of neutrophils and other inflammatory cells in mice at the infection site by the Δ*lpp* Δ*msbB* Δ*ail* triple mutant at earlier time points clearly represents a possibility that will be investigated in the future.

In addition to neutrophils, *Y. pestis* preferentially infects host macrophages, probably via recognition of specific surface-associated CCR5 molecules, and survives within these phagocytic cells during early stages of infection (114). The intracellular survival and growth of *Y. pestis* in macrophages seem to play a role in the pathogenesis of the plague bacterium, as the organism acquires the ability to evade subsequent phagocytosis (e.g., by synthesizing capsule) and is protected from contact with other immune components (115). Thus, the impaired survival of the Δ*lpp* Δ*msbB* Δ*ail* triple mutant in macrophages (both murine and human) (Fig. 3.14) seemed to contribute to its significant attenuation.

Although *Y. pestis* is a facultative intracellular pathogen (2), its ability to invade epithelial cells has only been reported recently (77, 88, 101, 116). Ail is a major mediator responsible for adherence and invasion of *Y. pestis* KIM strains or when the *ail* gene is overexpressed in non-adherent and non-invasive *E. coli* strains to human epithelial cells of cervical origin (HeLa and Hep-2) (77, 78, 88, 89). Likewise, the mutated versions of the *ail* gene from *Y. pestis* when expressed and produced in *E. coli*, exhibited decreased adherence and invasion phenotypes in HeLa cells, when compared to *E. coli* strains expressing the non-mutated *ail* gene (116). We provided the first evidence that Ail of *Y.*

pestis has a role in adherence and invasion of the human alveolar A549 epithelial cell line (Fig. 3.12B), thus showing Ail's role in pneumonic plague.

Pla and pH 6 antigen (Psa), in addition to Ail, also mediate binding of *Y. pestis* KIM5 to Hep-2 cells (92). However, Ail is the most critical adhesion molecule followed by Pla, and then Psa (116). We have shown that the levels of Pla and F1 as well as the enzymatic activity of Pla were not affected in the Δ*lpp* Δ*msbB* Δ*ail* triple mutant (Fig. 3.3D&E and Fig. 3.4). The role of Psa in epithelial cell adherence and invasion at best is minimal under normal physical conditions (92, 101). Since we could restore adherence and invasion phenotypes of the triple mutant in HeLa and A549 cells after complementation with the *ail* gene (Fig. 3.12), this finding confirmed the role of Ail as a major adhesion molecule in *Y. pestis*.

Our earlier studies have shown that both Lpp and Pla, but not MsbB, contributed to WT CO92 survival in murine RAW 264.7 macrophages (40, 42, 51, 74). In various cell types we studied (e.g., murine MH-S alveolar macrophages, HeLa and A549 epithelial cells), the single *ail* gene deletion did not affect the intracellular survival of *Y. pestis* (Fig. 3.14). In contrast, deletion of the *ail* gene from the Δ*lpp* Δ*msbB* double mutant further decreased the survival of the triple mutant in HeLa and A549 epithelial cell lines, but not in the macrophages (Fig. 3.14A-E). This decreased survivability of the triple mutant could be fully or partially complemented in HeLa or in A549 cells, respectively, when the *ail* gene was supplied *in trans* (Fig. 3.14D&E), suggesting that Ail may play a role in bacterial intracellular survival. Since Ail's biological activity could possibly be masked by Lpp and LPS (77), deletion of both *lpp* and *msbB* genes from *Y. pestis* might have allowed us to glean the role of Ail in intracellular survival in epithelial cells. In addition, the differential

killing mechanism(s) employed by various host cell types could also play a crucial role in the survivability of the mutant bacteria and needs to be further investigated. This decreased survival phenotype of the triple mutant in epithelial cells was not due to the lack of production and activity of Pla (Fig. 3.3D&E), and correlated with mutant's decreased ability to disseminate and to rapidly clear from mouse organs (Fig. 3.8), compared to that of Δ*lpp* Δ*msbB* double mutant (42). These data emphasized the role of epithelial barrier in the host innate immunity.

We have consistently detected an increased amount of YopH in the culture supernatants of *ail* deletion mutants compared to that in WT CO92 supernatants (Fig. 3.3A&B). The presence of these Yops in the bacterial supernatants was not due to the leakage of bacterial cell membrane or the T3SS needle itself, as these Yops were detected in the culture medium only after induction of a low calcium response by EGTA (Fig. 3.3B). As a key adhesion molecule, Ail docks onto the host cells to help Yops delivery, and translocation of Yops (e.g. YopE) into the host cells has been found to decrease in *ail*-deficient mutants of *Y. pestis* KIM5 (88, 89, 91, 92) as well as in *Y. pestis* CO92 (Fig. 3.3C). Therefore, the decreased translocation of Yops seen in the Δ*ail* mutant strains of *Y. pestis* could possibly be due to their disregulated release into the medium (Fig. 3.3A&B) prior to docking of the T3SS onto the host cells and prior to the translocation of YopE (Fig. 3.3C).

Yops have been reported to be quickly degraded by proteases in the extracellular milieu, which could possibly explain marginally higher levels of YopE detection in the supernatant of the Δ*ail* single mutant when compared to WT CO92 (Fig. 3.3A) (92). Although the production of serine protease Pla was similar in the Δ*ail* mutant strains when compared to that in the WT CO92 (Fig. 3.3D&E), the possibility of alteration of other

proteases in the Δ*ail* mutant strains cannot be ruled out. Interestingly, the level of LcrV in the culture medium of the Δ*lpp* Δ*msbB* Δ*ail* triple mutant was unaffected compared to its levels in WT CO92 (Fig. 3.3A), correlating with reports that LcrV is secreted prior to host cell contact (117-120). Further, its extracellular location (component of the T3SS translocon) may render LcrV more resistant to *Y. pestis* proteases such as Pla (92, 121).

A recent study showed that the presence of outer membrane vesicles (OMVs) containing membrane and periplasmic components were increased in the Δ*lpp* mutant of *Y. pestis* under specific conditions (122). While our electron microscopy studies revealed no OMVs in the Δ*lpp* Δ*msbB* Δ*ail* triple mutant, an increase in the release of OMVs would not explain increased levels of some Yops in the supernatant of the Δ*lpp* Δ*msbB* Δ*ail* triple mutant (Fig. 3.3A), since increased amounts of YopE and –H were not detected in the supernatant of the Δ*lpp* Δ*msbB* double mutant.

YopE and -H act as deterrents to bacterial phagocytosis while YopP/YopJ inhibits inflammatory cytokine responses when injected into the host cells (123). Although, the translocation of all the Yops by the Δ*lpp* Δ*msbB* Δ*ail* triple mutant in host cells was not assessed in this study, we did observe an increased uptake of the triple mutant by the MH-S murine macrophages compared to that in WT CO92 (data not shown). Importantly, this increased uptake of the triple mutant correlated with an early burst of inflammatory cytokine secretion in the triple mutant- infected murine and human macrophages compared to those in the WT CO92 and the Δ*lpp* Δ*msbB* double mutant (Fig. 3.15). The increased level of TNF-α and IL-6 would help macrophages to combat the invading bacteria. In addition, IL-6 has been reported to enhance polarization of alternatively activated M2 macrophages, and, thus would promote resolution of inflammation and wound healing

(124) correlating with minimal histopathology lesions in the organs of the Δ*lpp* Δ*msbB* Δ*ail* triple mutant-infected mice (Fig. 3.9).

The mutant strains of CO92 deficient in Ail production were highly sensitive to both human and NHP sera but remained resistant to mouse serum. Thus, serum sensitivity did not seem to play a role in attenuation of these mutants in a mouse model of pneumonic plague. Differences in serum resistance of bacteria are most likely due to differences in the immune systems of the host. One obvious difference among various hosts is within the amino acid sequences of the complement proteins. For example, FH consists of 20 short consensus repeat (SCR) domains (28), and Ail is predicted to bind FH near SCR7 (12-14). Mouse SCR6-8 has 55% identity and 70% homology with human SCR6-8 (29), indicating that differences in this region of FH may influence interaction with Ail. Further, other outer membrane proteins of *Y. pestis* may bind and recognize the mouse SCR binding region, allowing Δ*ail* mutants to remain resistant to murine serum.

Despite the fact that the Δ*lpp* Δ*msbB* Δ*ail* triple mutant was highly attenuated and rapidly cleared from mouse tissues, animals infected with this triple mutant were still able to mount balanced T_H1 and T_H2 responses (Fig. 3.7B) to significantly protect them (70%) against subsequent exposure to a high challenge dose of WT CO92 in a pneumonic plague model (Fig. 3.7A).

Interestingly, in our early study, Ail was also identified by mass-spectrometric analysis along with several other outer membrane antigens, to which antibodies were generated when rats were exposed to the WT CO92 by the intranasal route to mimic pneumonic plague and then rescued by an antibiotic levofloxacin given 24 h post infection for 6 days (93). Importantly, immunization of rats with recombinant Ail protein provided partial

protection to animals from the lethal challenge dose of WT CO92 in a pneumonic plague model, indicating that Ail also has some immunogenic potential (93). Therefore, further manipulation of the *ail* gene to reduce its virulence potential while retaining immunogenicity in the Δ*lpp* Δ*msbB* background strain would provide a promising strategy in our future study.

In summary, we were able to determine the mechanistic basis of attenuation of the Δ*lpp* Δ*msbB* Δ*ail* triple mutant of *Y. pestis* CO92. The Δ*lpp* Δ*msbB* Δ*ail* triple mutant of *Y. pestis* CO92 was severely attenuated with minimal damage to the host while retaining immunogenicity. The possibility that this mutant may provide a platform for deleting additional genes to develop a viable live-attenuated plague vaccine for immuno-competent military and healthcare workers is encouraging and will be pursued in future studies. Overall, our goal is to develop several highly attenuated *Y. pestis* mutant strains (40, 42, 51, 74) as candidate vaccines which possibly could also be effective in an immuno-compromised population.

Chapter 4

Intramuscular immunization of mice with a live-attenuated triple mutant of *Yersinia pestis* CO92 induces robust humoral and cell-mediated immunity to completely protect animals against pneumonic plague[3][4]

Introduction

In an effort to search for a new live-attenuated plague vaccine, we recently constructed Δ*lpp* Δ*msbB* Δ*ail* triple mutant which was deleted for genes encoding Braun lipoprotein (Lpp), an acetyltransferase (MsbB), and the Attachment Invasion Locus (Ail) (39). Lpp activates Toll-like receptor-2, which leads to the production of pro-inflammatory cytokines and septic shock (43-46). On the other hand, MsbB modifies lipopolysaccharide (LPS) by adding lauric acid to the lipid A moiety, thus, resulting in increased biological potency of LPS (42, 55, 56, 59, 62, 125). Ail is a ~17 kDa outer membrane protein with four extracellular loops, and the loop 2 (L2) has been reported to be mainly responsible for Ail-mediated bacterial serum resistance and adherence/invasion of the host cells (39, 75-78, 88-92).

In this study, to further characterize the vaccine potential of the Δ*lpp* Δ*msbB* Δ*ail* triple mutant, we evaluated its effectiveness when administered by the most common subcutaneous (s.c) or the intramuscular (i.m.) route (126). Since Ail also has immunogenic

---

[3] Reproduced with permission from the following source: Clinical Vaccine Immunology (http://www.cvi.asm.org); **Tiner BL**, Sha J, Ponnusamy D, Baze WB, Fitts EC, Popov VL, van Lier CJ, Erova TE, Chopra AK**.** 2015. Intramuscular Immunization of Mice with a Live-Attenuated Triple Mutant of Yersinia pestis CO92 Induces Robust Humoral and Cell-Mediated Immunity To Completely Protect Animals against Pneumonic Plague. Clin Vaccine Immunol **22:**1255-1268.

[4] **Author Contributions:** Bethany Tiner was involved in the creation of all mutants, in microscopic analysis and western blot analysis of the mutants, in virulence determination assays (adherence, invasion, and serum resistance), in all *in vivo* studies, and in the T cell proliferation and cytokine secretion assays. Dr. Jian Sha (Assistant Professor) was involved in all *in vivo* studies as well as in the T cell proliferation and cytokine secretion assays. Christina van Lier and Dr. Duraisamy Ponnusamy (McLaughlin postdoctoral fellow) were involved in *in vivo* studies. Dr. Wallace Baze was involved in histopathological analysis while Dr. Vsevolod Popov assisted in transmission electron microscopy. Eric Fitts was involved in the creation of the *lux* strains as well as *in vivo* imaging dissemination experiment. Dr. Tatiana Erova was involved in preparing the *ailL2* mutant.

potential in addition to its role as a virulence factor (93), we aimed at mutating the corresponding nucleotides in the *ail* gene that encodes essential amino acid (aa) residues required for virulence of L2 instead of deleting the whole *ail* gene from the Δ*lpp* Δ*msbB* mutant of CO92 (91, 127). Indeed, the generated Δ*lpp* Δ*msbB::ailL2* mutant was severely impaired in Ail-associated virulence traits, e.g., serum resistance, host cell adhesion and invasion. Most importantly, immunization of mice with either the Δ*lpp* Δ*msbB* Δ*ail* or the Δ*lpp* Δ*msbB::ailL2* mutant *via* either the i.m. or the s.c. route, elicited robust humoral and cellular immune responses, which conferred up to 100% protection in animals at high pneumonic challenge doses of 70-92 LD_{50} with WT CO92. Therefore, Δ*lpp* Δ*msbB* Δ*ail* and Δ*lpp* Δ*msbB::ailL2* mutants represent excellent plague vaccine candidates. In addition, such vaccines could be effectively administrated *via* different routes, providing flexibility during immunization.

Results

Evaluation of protection provided by intramuscular immunization of mice with the Δ*lpp* Δ*msbB* Δ*ail* triple mutant in a pneumonic plague model.

Mice were i.m. vaccinated with one or two doses of the Δ*lpp* Δ*msbB* Δ*ail* triple mutant at 2 x 10^6 CFU/dose. As shown in **Fig. 4.1A**, similar levels of total IgG antibody titers (1:15,625) to F1-V were noted when animals were vaccinated with either one or two doses. In addition, mice developed balanced Th1- and Th2-responses based on IgG1, IgG2a, and IgG2b antibody titers to F1-V (1:15,625) despite the number of vaccine doses administered (**Fig. 4.1A**).

No disease symptoms were observed in mice during above immunizations. All of the mice immunized with two doses of the triple mutant survived the i.n. challenge with 92

LD_{50} of WT CO92 *luc2* strain when administered on day 21 after vaccination (**Fig. 4.1B**). While slightly lower, but still impressive level of protection (78%) was achieved when animals were vaccinated with only one dose of the triple mutant, and this protection was not statistically different when compared to the group of animals receiving two doses of the vaccine (**Fig. 4.1B**). In contrast, all naïve mice succumbed to infection by day 4 p.i. and exhibited clinical signs such as ruffled fur, hunched back, lethargy and they were unable to groom and tended to hurdle together.

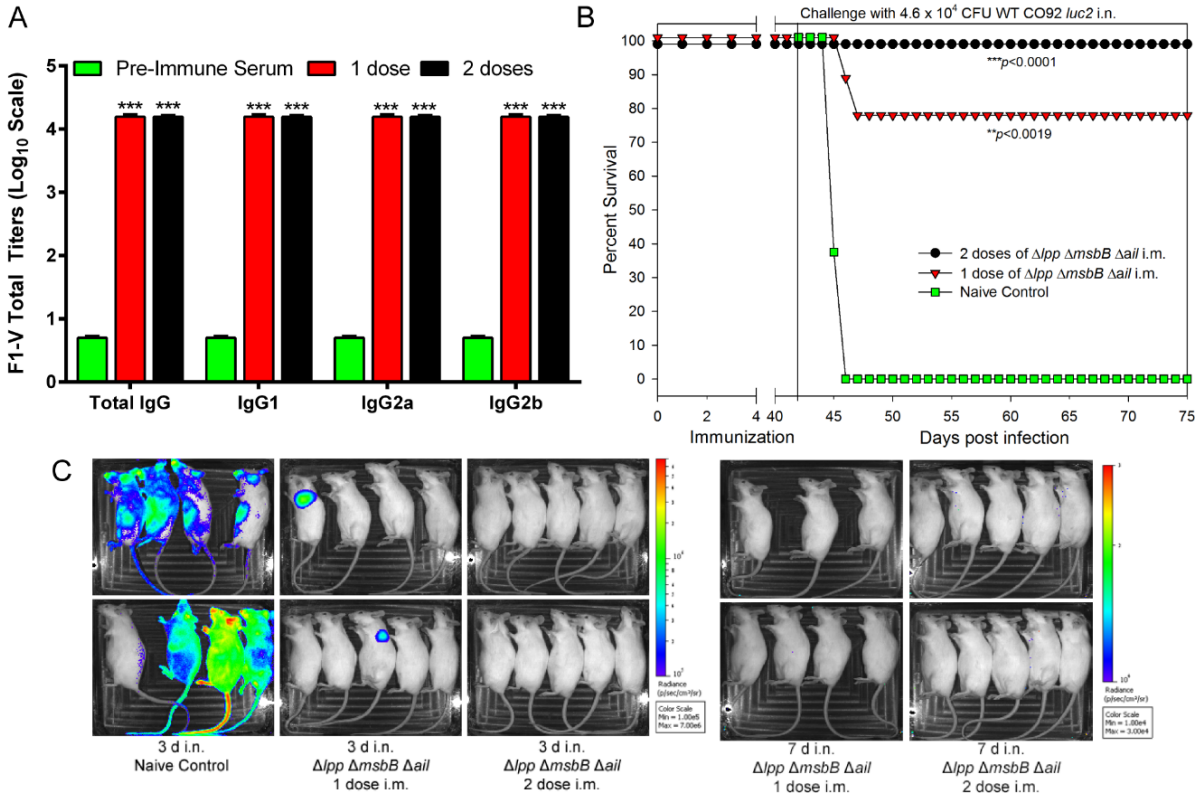

Figure 4.1. Immunity conferred by the Δ*lpp* Δ*msbB* Δ*ail* triple mutant to mice *via* intramuscular immunization.

(A) Mice (n=8-10 per group) were i.m. immunized with 1 or 2 doses of 2 x 10^6 CFU/100 µL of the Δ*lpp* Δ*msbB* Δ*ail* triple mutant on day 0 and/or on day 21. Mice were bled 14 days post-last immunization and an ELISA was performed to examine the antibody IgG titers and their isotypes to the F1-V antigen. *P* values shown are based on one-way ANOVA with a Bonferroni correction. ***$p<0.0001$ compared to their corresponding pre-immune sera. **(B)** The above immunized mice were challenged intranasally on day 42 with 4.6 x 10^4 CFU (92 $LD_{50;}$ 1 LD_{50} = ~500 CFU) of the WT *Y. pestis* CO92 *luc2* strain. Naive control: infected naïve mice. The *P* values are in comparison to naïve control and are based on Kaplan-Meier Curve Analysis. **(C).** The exposed mice were imaged on days 3 and 7 post challenge for bioluminescence and the scale within the figure ranged from most intense (red) to least intense (violet).

The above infected mice were also imaged on day 3 p.i. to monitor progression of infection. As shown in **Fig. 4.1C**, the WT CO92 *luc2* disseminated from the lungs to the whole body in 7 out of 8 naïve animals, and they all eventually succumbed to infection. On the contrary, animals receiving one immunization dose of the Δ*lpp* Δ*msbB* Δ*ail* triple mutant, only 2/9 mice were positive for bioluminescence on day 3 post challenge (**Fig. 4.1C**). These two animals succumbed to infection resulting in an overall 78% survival rate (**Fig. 4.1B**). It was also noted that the bioluminescent strain was confined at the initial infection site (lungs) in those two bioluminescent-positive animals when compared to that of the naïve but infected controls (**Fig. 4.1C**).

In the immunized group of mice receiving two doses of the vaccine, none of the animals were positive for bioluminescence after pneumonic challenge (**Fig. 4.1C**), with 100% of the animals surviving (**Fig. 4.1B**). No clinical symptoms of the disease were apparent in mice receiving two doses of the vaccine and then subsequently challenged. Since none of the surviving animals became bioluminescent positive by day 7 (0/10), these data indicated clearing of the WT CO92 *luc2* strain by day 7 (**Fig. 4.1C**). To confirm, no bacilli were detected in organs (lungs, liver, and the spleen) of the survivors on day 54 after WT CO92 *luc2* challenge based on bacterial enumeration by plating (data not shown).

In vitro characterization of the Δ*lpp* Δ*msbB::ailL2* mutant of *Y. pestis* CO92.

The replacement of native *ail* with the *ailL2* gene in the Δ*lpp* Δ*msbB* double mutant of *Y. pestis* CO92 was confirmed by PCR analysis. Further genomic DNA sequencing revealed no unexpected alterations in the *ailL2* gene as well as in its adjacent regions on the chromosome when compared to that of its parental strain (data not shown). In addition, we examined expression of the *ailL2* gene by Western blot analysis. As shown in **Fig. 4.2A**,

Ail-specific antibodies detected the correct size protein with essentially similar intensity in all of the examined strains except for the Δ*lpp* Δ*msbB* Δ*ail* triple mutant. Importantly, the expression level of the *pla* gene was also similar across all strains examined, indicating that neither deletion of the native *ail* gene nor replacing it with the *ailL2* gene in the Δ*lpp* Δ*msbB* double mutant affected production of the other tested bacterial membrane protein, i.e., Pla (**Fig. 4.2A**).

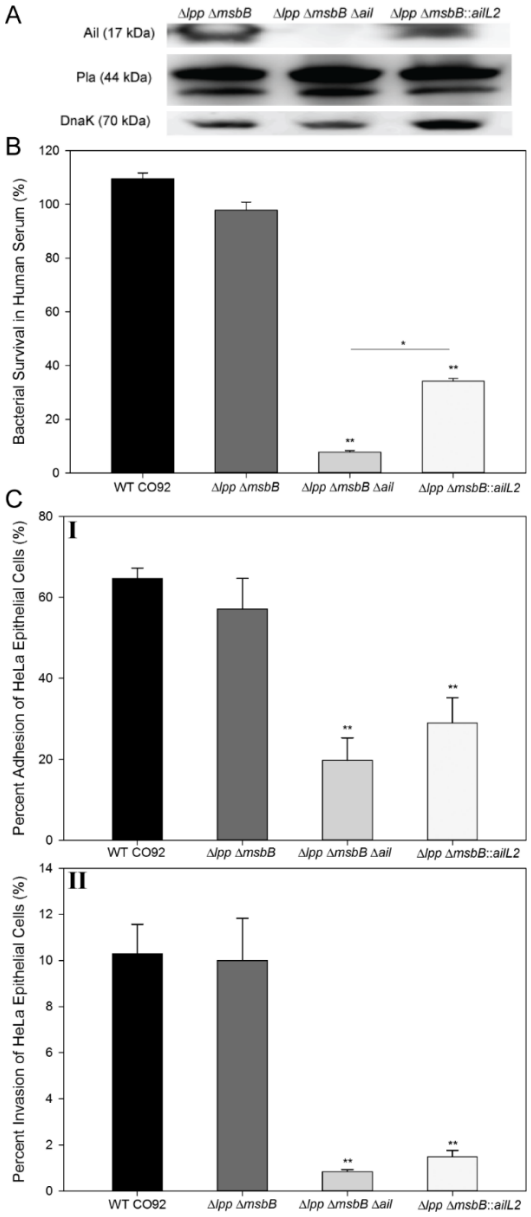

Figure 4.2. Ail associated virulence activities in the Δ*lpp* Δ*msbB::ailL2* mutant.
(A) Overnight 28ºC grown *Y. pestis* cultures were collected and analyzed by immunoblotting using antibodies to Ail and Pla, respectively. Anti-DnaK antibodies were used as a loading control for the Western blots. **(B)** Various *Y. pestis* strains were incubated separately with the normal and heat-inactivated human sera at 37ºC for 2 h. The percent bacterial survival in normal serum over the heat-inactivated serum was plotted. *P* values shown are based on one-way ANOVA. ***p* <0.005 as compared to WT CO92 and the Δ*lpp* Δ*msbB* double mutant. Horizontal line with "*" indicates statistical significance (*p* <0.05) between the two indicated groups. **(C).** HeLa cells were infected at an MOI of 100 with various *Y. pestis* strains. After 2 h of incubation, the host cells were gently washed and the adherent bacteria were collected, and percent adhesion (**I**) was calculated. In another set of wells, gentamicin protection assay was followed and the percent of invasive bacteria (**II**) was calculated. *P* values shown are based on one-way ANOVA. ***p*<0.001 compared to both WT CO92 and the Δ*lpp* Δ*msbB* mutant. The arithmetic means ± standard deviations are plotted.

Due to Ail's ability to impart serum resistance to *Y. pestis* (39, 75-78), the WT CO92 and its Δ*lpp* Δ*msbB* double, Δ*lpp* Δ*msbB* Δ*ail* triple, and Δ*lpp* Δ*msbB::ailL2* mutants were evaluated for their ability to be killed by the complement cascade. Although all tested strains survived similarly in heat-inactivated sera after 2 h incubation with CFU in the range of 1.6 to 2.0 x 10^4/ml; less than 10% of the Δ*lpp* Δ*msbB* Δ*ail* triple mutant survived when exposed to the normal sera (**Fig. 4.2B**). On the other hand, both WT CO92 and its Δ*lpp* Δ*msbB* double mutant strain exhibited slightly better or similar survival rates in the normal sera when compared to that of the heat-inactivated sera. The survival rate of the Δ*lpp* Δ*msbB::ailL2* mutant strain was ~35% in the normal sera; and as expected, it did not reach the level of the Δ*lpp* Δ*msbB* double mutant (**Fig. 4.2B**).

Since Ail also functions in adherence and subsequent invasion of bacteria in the host cells, these virulence phenotypes of WT CO92 and its various mutants were examined in HeLa cells. Both the adherence (**Fig. 4.2C-Panel I**) and invasive ability (**Fig. 4.2C-Panel II**) of the Δ*lpp* Δ*msbB* Δ*ail* triple mutant were significantly decreased when compared to those of the WT CO92 and its Δ*lpp* Δ*msbB* double mutant. The Δ*lpp* Δ*msbB::ailL2* mutant behaved very similar to that of the Δ*lpp* Δ*msbB* Δ*ail* triple mutant in terms of its ability to adhere and invade HeLa cells.

Evaluation of protection provided by intramuscular or subcutaneous immunization of mice with the Δ*lpp* Δ*msbB* Δ*ail* triple or the Δ*lpp* Δ*msbB::ailL2* mutant in a pneumonic plague model.

Since our data presented in **Fig. 4.1B** indicated that two doses of immunization in mice provided optimal protection against WT CO92 challenge, we used the same vaccination regimen for both i.m and s.c. routes of immunization and compared protection conferred

by the Δ*lpp* Δ*msbB::ailL2* mutant with that of the Δ*lpp* Δ*msbB* Δ*ail* triple mutant. Irrespective of the routes of immunization with either of the two mutant strains, 100% survivability of animals was noted with no clinical signs. All of the mice immunized intramuscularly were protected against the lethal pneumonic challenge at the dose of 3.5 x 10^4 CFU (70 LD_{50}) with WT CO92 *luc2* strain (**Fig. 4.3A**), while 67 to 88% protection was achieved in mice subcutaneously immunized with either the Δ*lpp* Δ*msbB::ailL2* or the Δ*lpp* Δ*msbB* Δ*ail* mutant, respectively (**Fig. 4.3B**). Although the level of protection provided by the s.c. route of vaccination did not reach the same level as noted for the i.m. route of immunization (**Fig. 4.3A**), the difference in protection afforded by the two mutants was statistically insignificant. All naïve and unimmunized mice succumbed to infection by 4 day post WT CO92 *luc2* challenge (**Fig. 4.3A and B**).

The bioluminescence images further showed that the organism disseminated from the lungs to the whole body of all naïve but infected control mice (10/10) by day 3 p.i. (**Fig. 4.3C-I**). Only one animal from the Δ*lpp* Δ*msbB* Δ*ail* i.m-immunized group was positive for bioluminescence and the infection was confined to the throat region (**Fig. 4.3C-II**). However, the infection cleared from this animal by day 7 p.i. and hence was not fatal. In the s.c.-immunized group of mice post challenge, one animal from each of mutants'-immunized groups was positive for bioluminescence on day 3 p.i. (**Fig. 4.3C-III**), albeit only at the original infection site of lungs, and these two mice eventually succumbed to infection by day 4-5 p.i. (**Fig. 4.3B**). Surprisingly, 2 additional mice initially negative for bioluminescence on day 3 p.i. in the Δ*lpp* Δ*msbB::ailL2* mutant s.c.-immunized group also died by day 5-6 p.i. Upon necropsy, the death of these two mice was confirmed to be due to *Y. pestis* infection, suggesting that the level of bioluminescence in these animals was

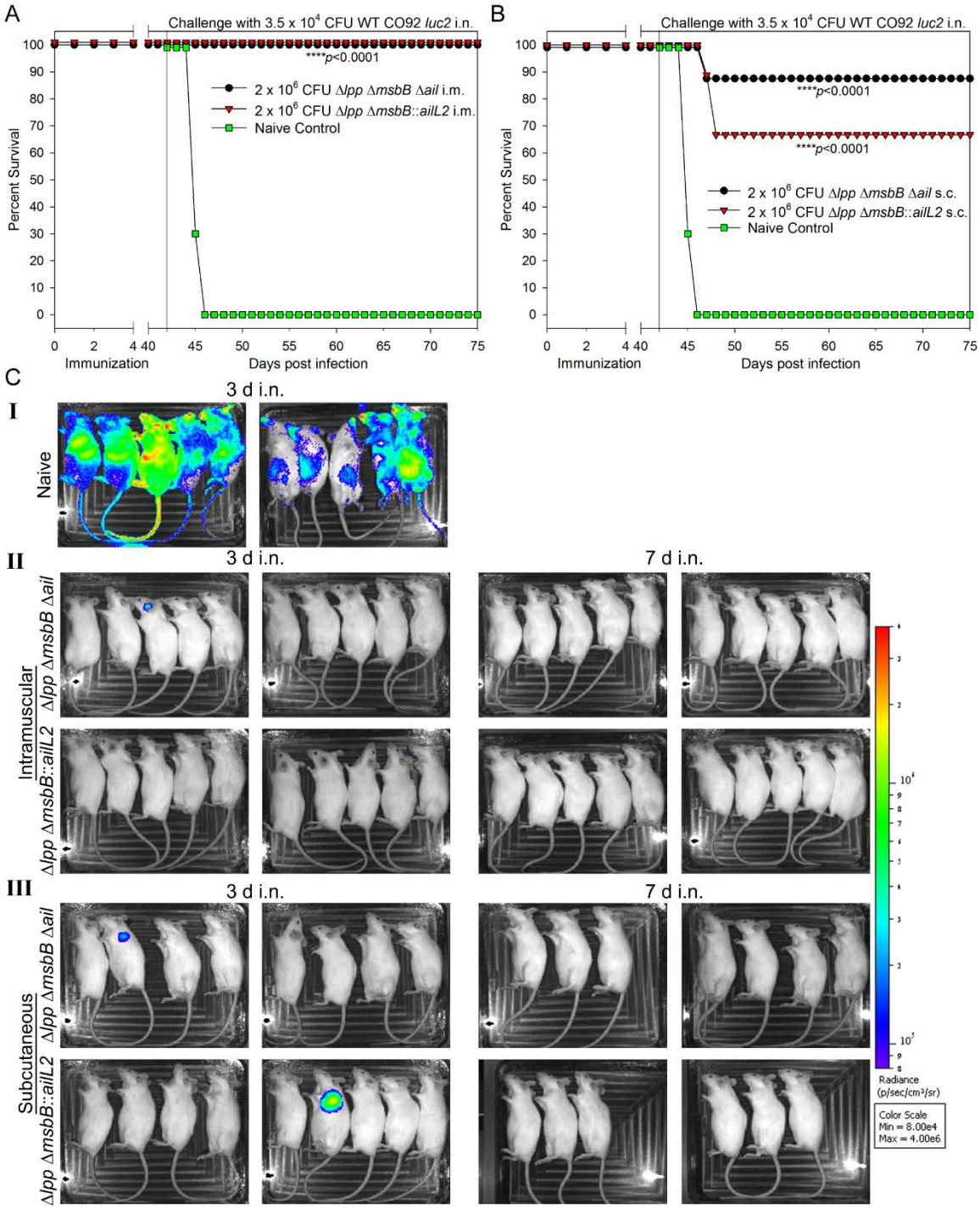

Figure 4.3. Immunity conferred by the Δ*lpp* Δ*msbB* Δ*ail* and Δ*lpp* Δ*msbB::ailL2* mutants to mice *via* intramuscular and subcutaneous routes of immunization.

Mice (n=8-10 per group) were immunized intramuscularly **(A)** or subcutaneously **(B)** with 2 doses of 2 x 10^6 CFU/100 µL of the Δ*lpp* Δ*msbB* Δ*ail* triple mutant or the Δ*lpp* Δ*msbB::ailL2* mutant on day 0 and 21. Mice were challenged intranasally on day 42 with 3.5 x 10^4 CFU (70 $LD_{50;}$ 1 LD_{50} = ~500 CFU) of the WT *Y. pestis* CO92 *luc2* strain. Naive control: infected naïve mice. The *P* values were in comparison to naïve control and were based on Kaplan-Meier Curve Analysis. **(C).** The infected mice (**I**: naïve, **II**: i.m-immunized and **III**: s.c-immunized) were imaged on days 3 and 7 post challenge for bioluminescence and the scale within the figure ranged from most intense (red) to least intense (violet).

below the threshold of detection when imaged on day 3 (97). However, by day 7 p.i., none of the remaining mice, regardless of the mutant and route used for immunization, were positive for bioluminescence, and they were healthy throughout the experiment. Importantly, 54 days after WT CO92 *luc2* challenge, organs (lungs, liver, and the spleen) harvested from randomly selected three survivors of each group (immunized via either the i.m. or the s.c. route) were free of the bacilli as evaluated by plate counting (data not shown).

To gauge immunogenicity of the vaccine strains *via* different routes of immunization, sera were collected from all mice 14 days after each immunization. We noted a boost in antibody titers between the first and the second dose when vaccination was performed *via* the s.c. route. However, this phenomenon was not observed *via* the i.m. route of immunization, as the peak antibody titers were achieved after only one vaccine dose (data not shown). Both of the above-mentioned mutants triggered higher level of antibody responses (IgG titers of 1:46,875) to F1-V antigen when vaccination occurred *via* the i.m. route over the s.c. route of immunization, which showed IgG titers of 1:18,000 (**Fig. 4.4A**). Balanced Th1- and Th2- based IgG1, IgG2a, and IgG2b antibody responses to F1-V were observed irrespective of the mutant strains used for vaccination and the route of immunization employed (e.g., i.m vs s.c.) (**Fig. 4.4B**). Only exception was that the Δ*lpp* Δ*msbB::ailL2* mutant-immunized animals by the s.c. route had significantly higher IgG1 titers over IgG2a titers, favoring a Th2 response (**Fig. 4.4B**).

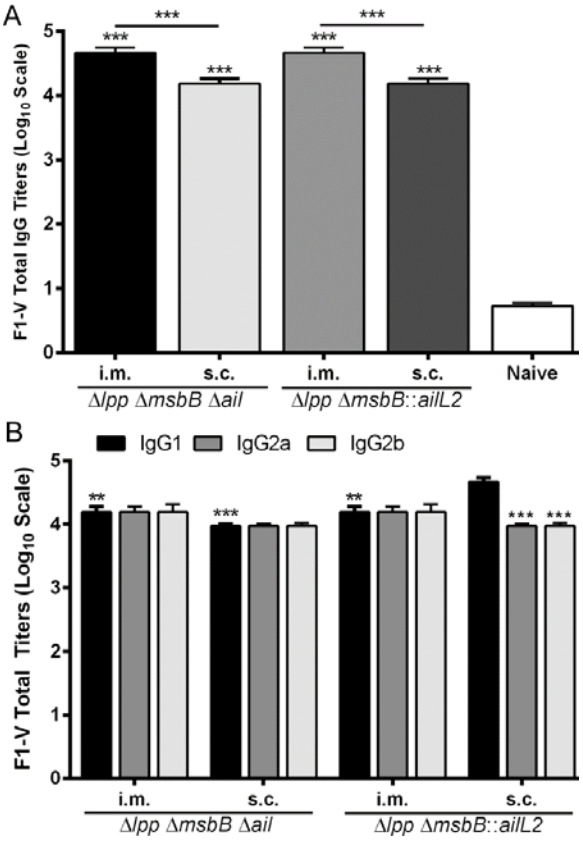

Figure 4.4. Antibody responses in mice elicited by the Δ*lpp* Δ*msbB* Δ*ail* or the Δ*lpp* Δ*msbB::ailL2* mutant *via* intramuscular or subcutaneous route of immunization.
Mice (n=8-10 per group) were immunized intramuscularly or subcutaneously with 2 doses of 2 x 10^6 CFU/100 µL of the Δ*lpp* Δ*msbB* Δ*ail* triple mutant or the Δ*lpp* Δ*msbB::ailL2* mutant on days 0 and 21. Mice were bled 14 days post-last immunization and an ELISA was performed to examine the total IgG responses **(A)** and its isotypes **(B)** to the F1-V antigen. The arithmetic means ± standard deviations are plotted and analyzed by one-way ANOVA with the Bonferroni correction. In **(A)**, ***p <0.001 as compared to the naïve sera. The horizontal lines with "***" indicate statistical significance within the two indicated groups. In **(B)**, **p<0.001 and ***p<0.0001 as compared to that of IgG1 of subcutaneously Δ*lpp* Δ*msbB::ailL2* mutant-immunized mice.

Histopathological analysis of mouse tissues after intramuscular immunization with the Δ*lpp* Δ*msbB* Δ*ail* triple and the Δ*lpp* Δ*msbB::ailL2* mutant and post exposure to WT *Y. pestis* CO92 in a pneumonic plague model.

Prior to WT CO92 challenge and after two doses of vaccination, organs (muscles, lungs, liver, and the spleen) were harvested from mice (n=2) in each group for histopathological analysis. Muscles from mice immunized with the Δ*lpp* Δ*msbB::ailL2* mutant were within the normal limits histopathologically, similar to that for muscles obtained from naïve, unimmunized mice (**Fig. 4.5**). Muscles from mice immunized with the Δ*lpp* Δ*msbB* Δ*ail* triple mutant were also within the normal limits except for mild focal inflammation (**Fig. 4.5**). Irrespective of the above two-mentioned mutants used for

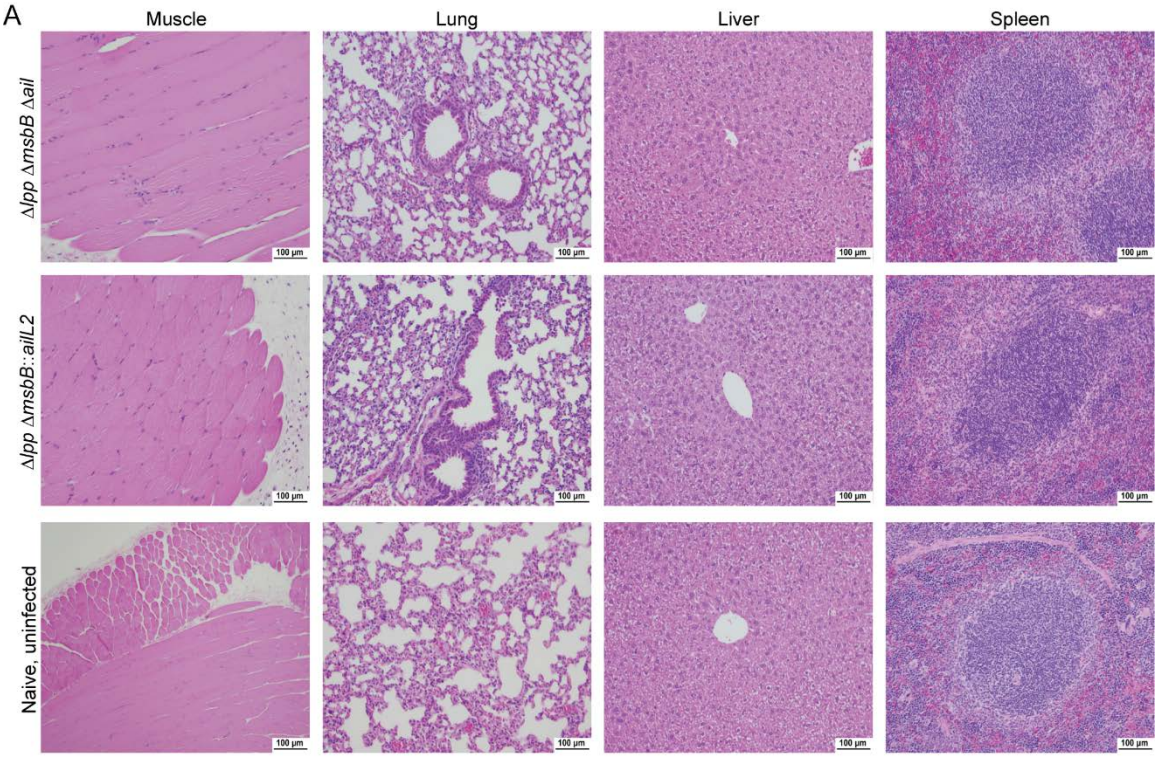

Figure 4.5. Histopathological analysis of mouse organs after immunization.
Mice were i.m. immunized with 2 doses of 2 x 10^6 CFU/100 µL of the Δ*lpp* Δ*msbB* Δ*ail* triple mutant or the Δ*lpp* Δ*msbB::ailL2* mutant on days 0 and 21. Muscles, lungs, liver, and spleen were harvested from the immunized mice (n=2 per group) on day 21 after last immunization or naïve control mice for H&E staining and evaluated by light microscopy in a blinded fashion. The scale for each panel is indicated.

immunization, the lungs, livers, and spleens of animals did not exhibit any abnormal histopathology and were comparable to the organs of naïve, unimmunized mice (**Fig. 4.5**).

As all i.m.-immunized animals survived exposure to 70 LD_{50} of WT CO92 *luc2* strain (**Fig. 4.3A**), organs (lungs, liver, and the spleen) from 3 of these immunized mice were excised on day 54 p.i., to examine histopathological lesions and bacterial clearance. All of the naïve mice succumbed to infection and organs from three of them were harvested at time of death. In the lungs, all of the WT CO92-infected, unimmunized control mice had mild-to-moderate neutrophilic inflammation (arrow), bacteria present (arrowhead), and mild and diffused congestion. Also, the alveoli of these mice had a moderate level of hemorrhage with few alveolar spaces observed (**Fig. 4.6**). All of the livers from WT CO92-infected, unimmunized mice had bacteria, some necrosis, and neutrophilic infiltration

(arrow). All of the spleens of WT CO92-infected, unimmunized mice had bacteria (arrowhead), mild lymphoid depletion of the marginal zone in the white pulp (asterisk), and mild-to-marked diffuse rarefaction or loss of normal cell population of the red pulp with fibrin present (**Fig. 4.6**). On the contrary, all of the tissues from mice immunized with either of the two mutants (Δ*lpp* Δ*msbB* Δ*ail* triple or the Δ*lpp* Δ*msbB::ailL2*) and then challenged with WT CO92 exhibited histopathology within the normal limits (**Fig. 4.6**), similar to tissues from uninfected naïve animals (**Fig. 4.5**).

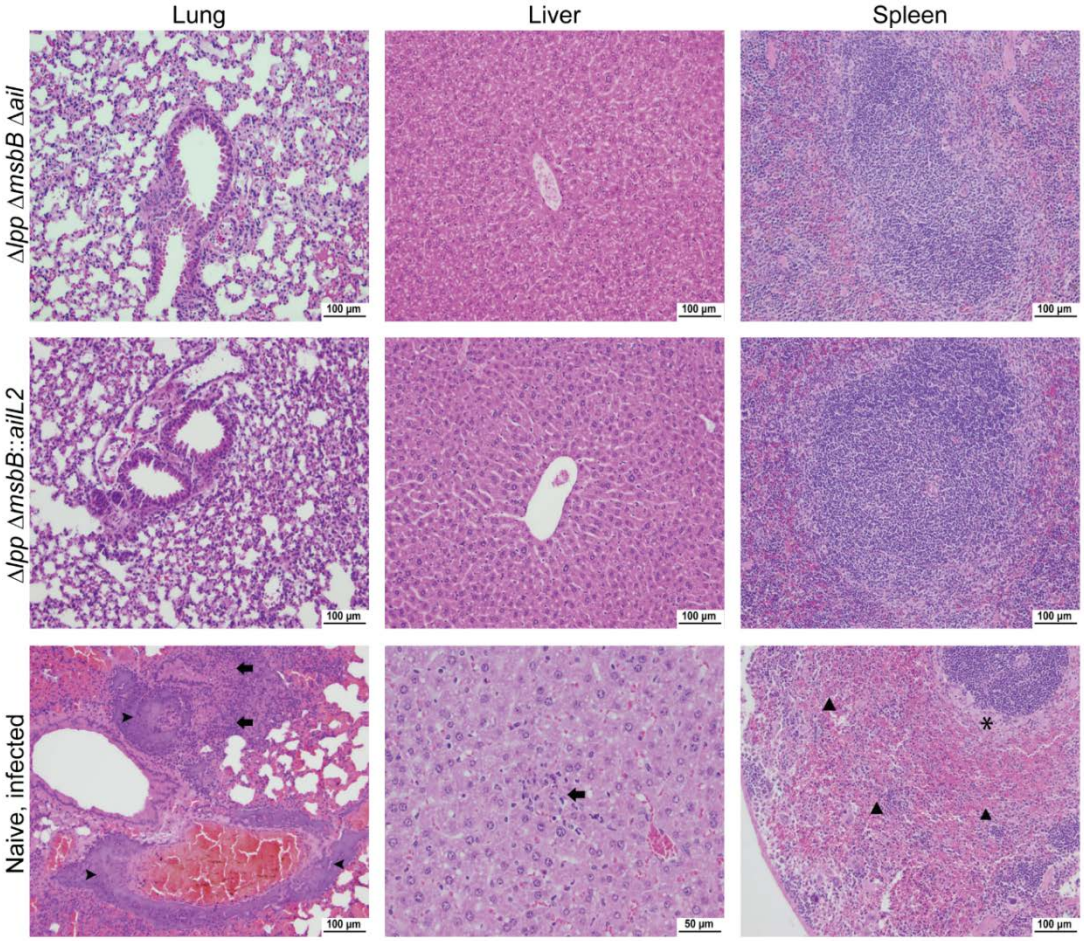

Figure 4.6. Histopathological analysis of immunized mouse organs after WT CO92 challenge. Mice were immunized by the intramuscular (i.m.) route with 2 doses of 2 x 10^6 CFU of the Δ*lpp* Δ*msbB* Δ*ail* triple mutant or the Δ*lpp* Δ*msbB*::*ailL2* mutant on days 0 and 21. Mice were exposed intranasally (i.n.) on day 42 with 3.5 x 10^4 CFU (70 LD_{50}; 1 LD_{50} = ~500 CFU) of the WT *Y. pestis* CO92 *luc2* strain. Lungs, liver, and spleen were harvested from mice (n=3 per group) upon death or 54 days post-infection. Portions of each organ were stained with H&E and evaluated by light microscopy in a blinded fashion. Bacteria (arrowhead), neutrophilic inflitration (arrow), depletion of the white pulp (asterisks). The scale for each panel is indicated.

When comparing histopathological changes, essentially similar data were obtained when immunization occurred via the s.c. route with either of the two mutants, and after challenge of the immunized mice by the pneumonic route with WT CO92 (data not shown).

Progression of infection and histopathological lesions in mice intramuscularly infected with the Δ*lpp* Δ*msbB* Δ*ail* triple and the Δ*lpp* Δ*msbB::ailL2* mutant of *Y. pestis* CO92.

Mice (n=3) were either challenged with 2 x 10^6 CFU of WT CO92-*lux*, the Δ*lpp* Δ*msbB* Δ*ail-lux*, or the Δ*lpp* Δ*msbB::ailL2-lux* strain. Using IVIS, animals were imaged at 0, 12, 24, 36, and 48 h p.i. At 0 h, all mice were positive for bioluminescence that was localized to the injection site in the muscle (**Fig. 4.7A-panel I**). By 12 h p.i. in the muscle, all mice infected with the Δ*lpp* Δ*msbB* Δ*ail-lux* or the Δ*lpp* Δ*msbB::ailL2-lux* strain were positive but the intensity of bioluminescence had decreased compared to 0 h (**Fig. 4.7A-panel II**). From 24 to 48 h p.i., none of the mice infected with the Δ*lpp* Δ*msbB* Δ*ail-lux* or the Δ*lpp* Δ*msbB::ailL2-lux* strain were positive for bioluminescence (**Fig. 4.7A-panels III-V)**.

However, mice infected with the WT CO92-*lux* strain had increased bioluminescence localized to the muscle at 12 h (**Fig. 4.7A-panel II**), and further dissemination of bacteria was observed in 1/3 mice at 24 h p.i. (**Fig. 4.7A-panel III**). This dissemination pattern became more prominent and was noted in the other two animals at 36 h p.i. (**Fig. 4.7A-panel IV**). At 48 h p.i., the level of bioluminescence was reduced in 1/3 mice **(Fig. 4.7A-panels III-V)**. This is attributed to a death of this animal which causes bioluminescence to decrease due to diminished oxygen levels and temperature (46).

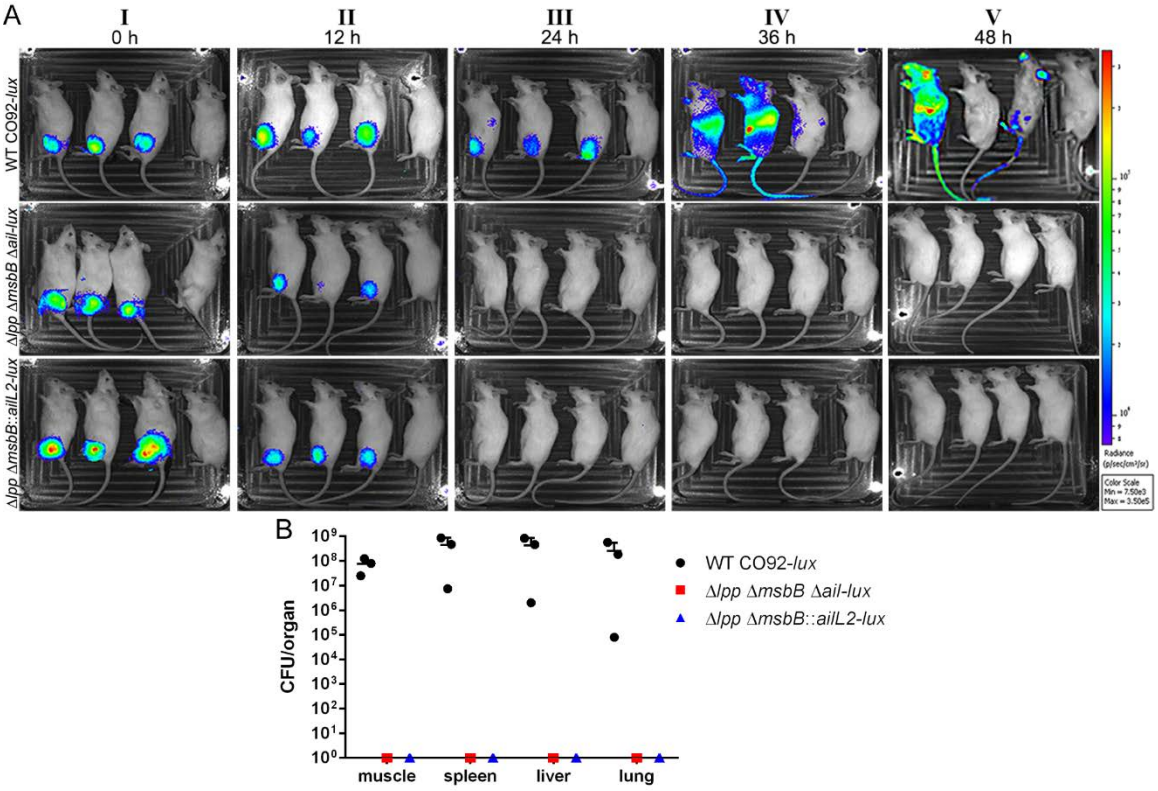

Figure 4.7. Progression of infection in mice intramuscularly infected with various *Y. pestis* CO92 strains.
Mice (n=3 per group) were challenged by the i.m. route with 2 x 10^6 CFU of the various Tn*7*-based bioluminescent *Y. pestis* strains (e.g., WT CO92-*lux*, Δ*lpp* Δ*msbB* Δ*ail-lux* and Δ*lpp* Δ*msbB::ailL2-lux*). Mice were imaged at 12 h intervals for bioluminescence **(A)** and mouse organs (muscles, lungs, liver, and spleen) were harvested to determine bacterial loads at 48 h p.i. **(B)**. The bioluminescence within the figure ranged from most intense (red) to least intense (violet). The animal on the very right side of each panel represents a naïve, unchallenged control.

To further examine bacterial load in mice, after *in vivo* imaging at 48 h p.i., all of the animals were sacrificed, and the organs (muscles, lungs, liver, and the spleen) were harvested and subjected to bacterial count determination. As shown in **Fig. 4.7B**, mice infected with the WT CO92 had a high bacterial load in each of these organs (ranged from 8 x 10^4 to 8.7 x 10^7 CFU per organ or per gram of muscle) (**Fig. 4.7B**). The animal with a relatively lower bacterial load in various organs correspondingly exhibited weak bioluminescence at 36 and 48 h p.i. (**Fig. 4.7A, panels IV-V**), indicating bacterial counts to be below the threshold of bioluminescence detection for the WT CO92-*lux* strain during *in vivo* imaging.

All of the animals infected with the WT CO92-*lux* strain had severe plague symptoms and were at the verge of death. In contrast, mice infected with either the Δ*lpp* Δ*msbB* Δ*ail-lux* triple or the Δ*lpp* Δ*msbB::ailL2-lux* mutant had minimal- to-no detectable bacterial load in any of the organs examined at 48 h p.i. (**Fig. 4.7B**). All of the tissues (muscle, liver, spleen, and lung) of WT CO92-infected animals had the presence of necrosis, hemorrhage, inflammation, edema, and bacteria (**Fig. 4.8**). However, all the tissues from mice infected with the Δ*lpp* Δ*msbB* Δ*ail-lux* triple or the Δ*lpp* Δ*msbB::ailL2-lux* mutant were within normal limits histopathologically (**Fig. 4.8**).

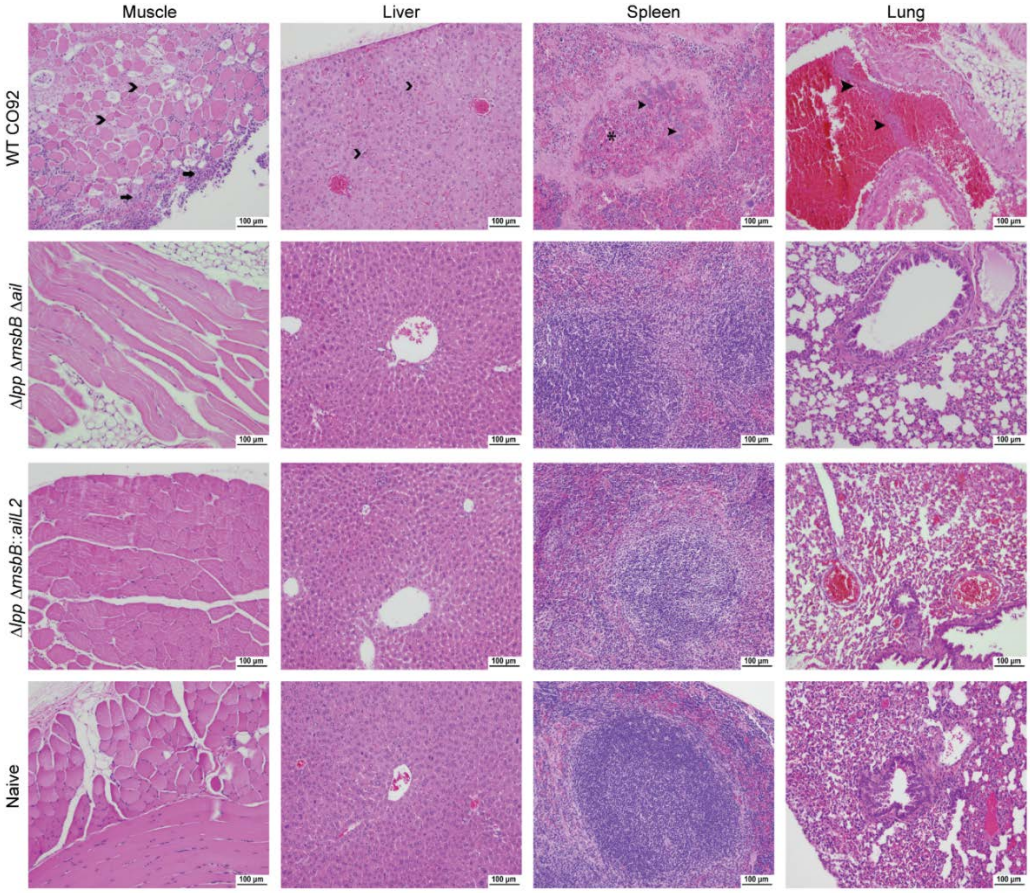

Figure 4.8. Histopathological alterations in mice intramuscularly infected with various Y. pestis CO92 strains.
Mice (n=3 per group) were challenged by the i.m. route with 2 x 10^6 CFU of the various Tn*7*-based bioluminescent strains (e.g., WT CO92-*lux*, Δ*lpp* Δ*msbB* Δ*ail-lux* and Δ*lpp* Δ*msbB::ailL2-lux*. At 48 h p.i., muscles, lungs, liver, and the spleen were harvested from mice. Portions of each organ were stained with H&E and evaluated by light microscopy in a blinded fashion. Bacteria (arrowhead), neutrophilic infiltration (arrow), depletion of the white pulp (asterisks), necrosis (open arrowhead). The scale for each panel is indicated.

Activation of T cells by the Δ*lpp* Δ*msbB* Δ*ail* triple and the Δ*lpp* Δ*msbB::ailL2* mutant of *Y. pestis* CO92 after intramuscular or subcutaneous immunization of mice.

To investigate T-cell responses, mice were i.m. or s.c. infected/immunized with 1 x 10^3 CFU dose of either KIM/D27, the Δ*lpp* Δ*msbB* Δ*ail* triple, or the Δ*lpp* Δ*msbB::ailL2* mutant strain. *Y. pestis* KIM/D27 is a *pgm*-locus minus mutant with similar characteristics as the live-attenuated *Y. pestis* EV76 vaccine strain (128), and, thus, served as an appropriate control. No clinical signs were observed in mice immunized with either the Δ*lpp* Δ*msbB* Δ*ail* triple or the Δ*lpp* Δ*msbB::ailL2* mutant strain. Although none of KIM/D27-infected mice succumbed to infection at this low dose (1 x 10^3 CFU), they all had ruffled fur and were lethargic up to 7 days post-immunization. On day 21 p.i., T-cells isolated from these mice were re-stimulated with the heat-killed WT *Y. pestis* CO92 *ex-vivo*, and T-cell proliferation (in terms of cpm) as well as cytokine production were evaluated.

As shown in **Fig 4.9**, all pulsed T-cells (black bars) proliferated robustly compared to their corresponding unpulsed controls (gray bars) except for the naïve group. In addition, T-cells from mice immunized by either the i.m. or the s.c. route significantly proliferated compared to T-cells isolated from naïve mice. These data indicated successful priming and re-stimulation during the experiment. Importantly, T-cells isolated from mice immunized intramuscularly by either the Δ*lpp* Δ*msbB* Δ*ail* triple or the Δ*lpp* Δ*msbB::ailL2* mutant robustly proliferated at comparable levels which were significantly higher than T-cells isolated from the KIM/D27-immunized mice (**Fig 4.9A**). During s.c. immunization, the T-cells from the KIM/D27-infected mice proliferated similar to that of T-cells isolated from

the Δ*lpp* Δ*msbB* Δ*ail* triple or the Δ*lpp* Δ*msbB::ailL2* mutant-infected mice (**Fig. 4.9B**). Interestingly, the T-cell proliferation was significantly higher in mice immunized (by the s.c route) with the Δ*lpp* Δ*msbB* Δ*ail* triple mutant when compared to animals vaccinated with the Δ*lpp* Δ*msbB::ailL2* mutant strain (**Fig. 4.9B**).

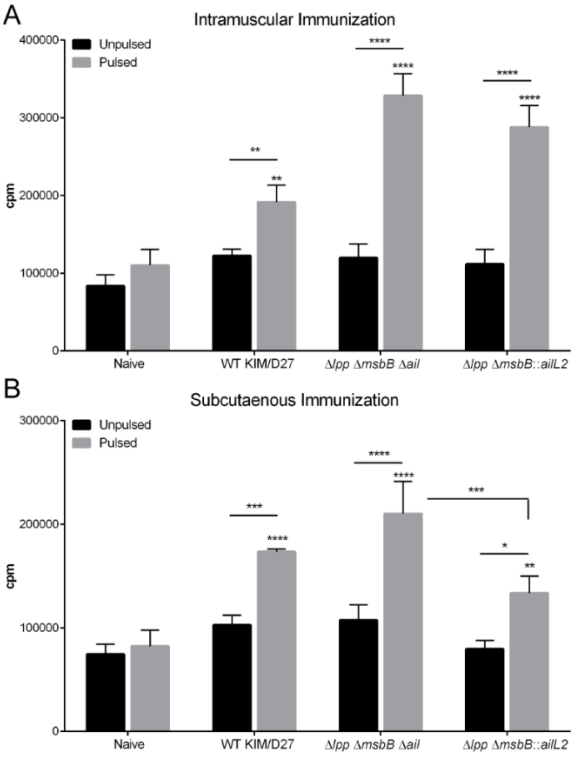

Figure 4.9. T-cell proliferation.
Mice were immunized by the i.m. (**A**) or s.c. route (**B**) with 1 x 10^3 CFU of *Y. pestis* KIM/D27, Δ*lpp* Δ*msbB* Δ*ail* triple mutant or the Δ*lpp* Δ*msbB::ailL2* mutant. On day 21 p.i., T-cells were isolated separately from the spleens of 5 mice in each immunized group or 3 mice from naïve control. The isolated T-cells were co-cultured with γ-irradiated splenocytes from naïve mice (severed as antigen-presenting cells: APCs) pulsed or un-pulsed with heat-killed WT CO92. T-cell proliferation was assessed by measuring incorporation of [^{3}H] thymidine at day 3 of co-culturing with APCs. The arithmetic means ± standard deviations are plotted. Data were analyzed by using the Bonferroni correction with a one-way ANOVA. The comparisons were made between the naive pulsed groups with the immunized pulsed groups or between the groups indicated by a horizontal line. *p<0.01, **p<0.005, ***p<0.001 and ****p<0.0001.

Supernatants collected from the above-mentioned T-cells were then assessed for cytokine production by using a Bio-Rad mouse 6-plex assay kit. Robust cytokine/chemokine production (i.e., IFN-γ TNF-α, IL-6, IL-1β, IL-10, and IL-17A) was observed in T-cells obtained from mice immunized intramuscularly across all the above-mentioned *Y. pestis* mutant strains tested in response to re-stimulation with the heat-killed *Y. pestis* CO92 (**Fig. 4.10**). A similar trend was noted for the production of IFN-γ, TNF-α, IL-1β, IL-6, and IL-10 in T-cells isolated from mice vaccinated subcutaneously with the above-mentioned mutant strains, except for the IL-17A production which was similar in

pulsed versus un-pulsed T-cells (data not shown). Overall, cytokines were either very low or undetectable from T-cells isolated from unimmunized, naïve mice (data not shown).

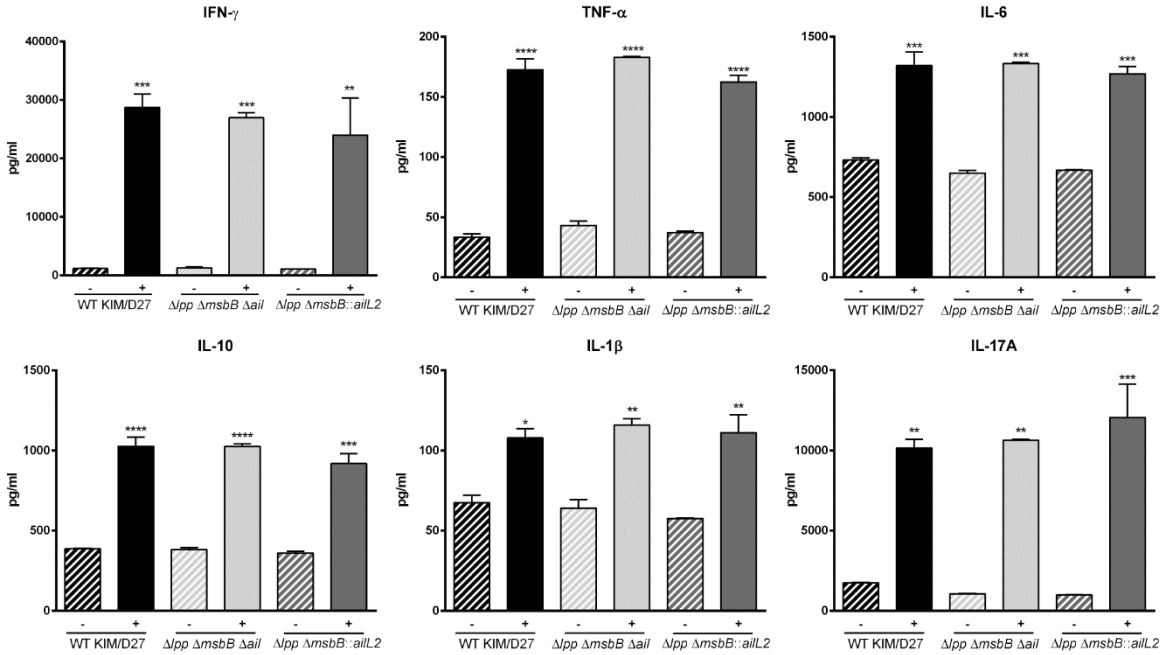

Figure 4.10. T-cell cytokine production.
Mice were immunized by the i.m. route with 1 x 10^3 CFU of *Y. pestis* KIM/D27, Δ*lpp* Δ*msbB* Δ*ail* triple mutant or Δ*lpp* Δ*msbB::ailL2* mutant. On day 21 p.i., T-cells were isolated separately from the spleens of 5 mice in each immunized group or 3 mice from naïve control. The isolated T-cells were co-cultured with the γ-irradiated APCs pulsed or un-pulsed with heat-killed WT CO92. Culture supernatants were harvested at day 2 of the co-culturing and the production of various cytokines/chemokines was measured by using a mouse 6-plex assay kit. Data were analyzed by using the Bonferroni correction with a one-way ANOVA. The comparisons were made between the un-pulsed (-) and pulsed (+) cells within each immunization group. ****$p \leq 0.0001$, ***$p<0.001$, **$p<0.01$ and *$p<0.05$.

Discussion

The resurgence of plague in many parts of the world, the existence of antibiotic-resistant strains naturally or generated intentionally, and the lack of a current FDA-approved plague vaccine in the United States necessitate the development of an effective vaccine.

Currently, the most promising and undergoing clinical trials are recombinant subunit vaccines consisting of F1 and LcrV antigens. These F1-V-based vaccines are efficacious against pneumonic plague in rodents and macaques (7, 20, 23, 24, 26); however, protection

was variable in African green monkeys (7, 16, 19, 22, 25). Further, F1 capsular antigen is dispensable for virulence (28, 29) and the LcrV amino acid (aa) sequence has diverged among *Y. pestis* strains (2, 27). Therefore, the F1-V-based subunit vaccines most likely will not provide optimal protection across all plague-causing strains in humans, specifically those that have been intentionally modified for possible use in terrorist attacks (30, 31).

The live-attenuated vaccines which promote both humoral- and cell- mediated immune responses may represent a better option to overcome the above-mentioned shortcomings of the subunit vaccines (16, 19). Recently, others and our laboratory reported development of mutant strains of *Y. pestis* that have shown vaccine potential (39, 40, 42). For example, a single dose of our Δ*lpp* Δ*msbB* Δ*ail* triple mutant conferred dose-dependent protection in mice against developing subsequent pneumonic plague when immunization occurred by the intranasal route (39). Our data showed that up to 3.4 x 10^6 CFU dose of this vaccine strain was unable to kill mice, and the animals developed balanced Th1- and Th2- antibody responses which provided subsequent protection (70%) to mice when challenged with 28 LD_{50} of WT CO92 (39). Although the experiments were not performed in parallel, our intramuscular immunization data with a single dose of this mutant (Fig. 4.1) provided comparable protection (78%) in mice but under a much stringent challenge dose of WT CO92 (92 LD_{50}). These data suggested that vaccination by the i.m. route might be superior to the i.n. route of immunization with this triple mutant in a mouse model.

It is generally believed that intranasal immunization has an advantage as it results in the development of both mucosal immunity and the systemic immune response. However, during mucosal immunization, the vaccine must be able to penetrate the epithelial barrier and to survive luminal host innate defenses. On the contrary, intramuscular immunization

enables the vaccine to easily access blood vessels to reach blood circulation to directly stimulate the immune system (129). However, irrespective of the vaccination route, the Δ*lpp* Δ*msbB* Δ*ail* triple mutant (at doses of 2 x 10^6-3.4 x 10^6 CFU) was unable to confer 100% protection to immunized mice in a single dose against developing subsequent pneumonic plague (39) (Fig. 4.1). Since Ail also has an immunogenic potential in addition to its role as a virulence factor (93), we generated the Δ*lpp* Δ*msbB::ailL2* mutant strain with the intention of further improving its immunogenicity.

Ail protein has eight transmembrane domains with four extracellular loops, and 8 aa residues in loops 2 and 3 of *Y. enterocolitica* being responsible for imparting serum resistance and microbe's ability to adhere/invade host cells (127). Likewise, 3 aa residues within loop 1 have been predicted to play an important role in bacterial adherence (91). Loop 2 of Ail in *Y. enterocolitica* and *Y. pestis* share 70% homology, and mutations in 4 aa residues resulted in drastically altering Δ*lpp* Δ*msbB::ailL2* mutant's ability to adhere, invade, and or to exhibit serum resistance when compared to WT CO92 and other tested mutants (Fig. 4.2).

A slight increase in serum resistance of the Δ*lpp* Δ*msbB::ailL2* mutant when compared to that of the Δ*lpp* Δ*msbB* Δ*ail* triple mutant was possibly related to the contribution of other Ail loops in serum resistance that were intact in the Δ*lpp* Δ*msbB::ailL2* mutant. Indeed loops 1 and 3 of Ail in *Y. pestis* are important for adherence and invasion, with up to 50% reduction in the above-mentioned phenotypes when these two loops were mutated (116). However, a similar adherence and invasion of Δ*lpp* Δ*msbB::ailL2* and Δ*lpp* Δ*msbB* Δ*ail* triple mutants in HeLa cells signified an important role of loop 2 in Ail-associated virulence phenotypes and also suggested that a conformational association between various

loops of Ail might be necessary for efficient adherence and invasion of bacteria to the host cells.

A comparable level of AilL2 production in the Δ*lpp* Δ*msbB::ailL2* mutant and its parental Δ*lpp* Δ*msbB* strain (Fig. 4.2A), as well as diminished virulence of Ail in the Δ*lpp* Δ*msbB::ailL2* mutant (Fig. 4.2B&C) indicated successful creation of a potentially better vaccine candidate than the Δ*lpp* Δ*msbB* Δ*ail* triple mutant. In addition, a partial restoration of serum resistance of this Δ*lpp* Δ*msbB::ailL2* mutant (Fig. 4.2B) might lead to a better recognition by the host immune system. However, our data indicated that both of the Δ*lpp* Δ*msbB* Δ*ail* triple and Δ*lpp* Δ*msbB::ailL2* mutants triggered similar humoral and cell-mediated immune responses in mice immunized *via* the i.m. route (Figs. 4.4 and 4.9A) and provided 100% protection to vaccinated animals when exposed to a high challenge dose of WT CO92 in a pneumonic plague model (Fig. 4.3).

A biased Th2 antibody response was observed in mice when vaccinated with the Δ*lpp* Δ*msbB::ailL2* mutant by the s.c. route which provided a slightly lower protection rate in immunized mice (67%) during subsequent pneumonic challenge. In comparison, 88% protection rate with a balanced Th1 and Th2 antibody response and a higher T-cell proliferation were noticed in mice when vaccinated by the s.c. route with the Δ*lpp* Δ*msbB* Δ*ail* triple (Figs. 4.3B, 4.4B and 4.9B).

The reason for this phenomenon is not clear; however, additional animal models, such as rat or nonhuman primate (NHP), may be needed to fully evaluate immunogenic potential of the Δ*lpp* Δ*msbB::ailL2* mutant. Indeed studies have shown that Ail plays even a more important role in the pathogenesis of *Y. pestis* infection in a rat model of pneumonic plague

when compared to the mouse model (75-78). In addition, a correlation between distinct IgG antibody subclasses and the Th1/Th2 profile seen in mice may differ in humans (129).

Of the two vaccination routes examined, and based on the protection rates, antibody and T-cell responses generated by the Δ*lpp* Δ*msbB* Δ*ail* triple and Δ*lpp* Δ*msbB::ailL2* mutants in the mouse model, i.m. route was certainly optimal when compared to the s.c. route (Figs. 4.3, 4.4, 4.9 and 4.10). Important was our observation that a robust IL-17A recall response was only observed in T-cells from mice that were immunized intramuscularly but not subcutaneously with the above-mentioned mutants (Fig. 4.10). A study has shown that injection of a vaccine into the layer of subcutaneous fat, where vascularization is poor, may result in slow mobilization and processing of the antigen (130). Compared to intramuscular administration, subcutaneous injection of hepatitis B vaccine leads to significantly lower sero-conversion rates and more rapid decay of antibody response (130, 131). A similar phenomenon was reported with the rabies and influenza vaccines (132).

Recently, it was reported that intradermal inoculation of *Y. pestis* in C57BL/6J mice resulted in faster kinetics of infection when compared to subcutaneous route of inoculation due to organisms' greater ability to access the vascular and lymphatic vessels in the dermis (133). Studies have shown that dermis of the skin is enriched in terminal lymphatic vessels which facilitate antigen uptake as well as infiltration of immune cells to mount a stronger immune response as compared to the subcutaneous layer (134-136). Therefore, future studies examining intradermal route of immunization with our mutants will be undertaken.

IL-17A is a signature cytokine of Th17 cells which has recently been shown to provide an antibody-independent heterogonous protection and has also been implicated in

protecting the host against many pathogenic bacterial infections, including *Y. pestis* (21, 137). Interestingly, production of IL-17A from T-cells was also observed in our previous study with the Δ*lpp* Δ*msbB* double mutant of WT CO92 when mice were intranasally immunized (42). Similarly, IL-17A was induced by the intranasal immunization of mice with the *Y. pestis* strain D27-pLpxL KIM/D27 engineered to express *E. coli* LpxL (138), which contributed significantly to the cell-mediated defense against pulmonary *Y. pestis* Infection (21). Therefore, the induction of Th17 response in addition to the Th1 and Th2 responses provided by the Δ*lpp* Δ*msbB* Δ*ail* triple and Δ*lpp* Δ*msbB::ailL2* mutants might be beneficial in live-attenuated plague vaccines, and need to be further studied.

The vaccine dose we used for both of our mutants (2 x 10^6 CFU/dose) was considerably lower compared to 8 x 10^8 CFU/dose of the live-attenuated EV76 vaccine strain given to humans by the i.m. route in some countries, and 1 x 10^7 CFU/dose that has been used in murine studies (139-141). In addition, up to 3 x10^9 CFU/dose of EV76 has been used to immunize humans by the cutaneous route (142). EV76 vaccine strain causes severe local and systemic reactions in both animals and human (143-146), and more seriously, deaths have been reported in NHPs (145). In addition, a similar *pgm*-minus strain of *Y. pestis* retains virulence in mice and NHPs when administered by the intranasal (i.n.) and intravenous (i.v.) routes (22, 145, 147), raising serious questions about their suitability as a human vaccine (148). Indeed, a fatal laboratory-acquired infection with the *pgm*-minus KIM/D27 strain in an individual with hemochromatosis was reported recently (37), and mice infected intramuscularly with 10^3 CFU of KIM/D27 in our study also showed ruffled fur and lethargy up to 7 days post infection. However, mice immunized with up to 2-3.4 x10^6 of either the Δ*lpp* Δ*msbB* Δ*ail* triple or Δ*lpp* Δ*msbB::ailL2* mutant *via* various

immunization routes (i.n., i.m. and s.c.) did not display any local or systemic reactions as well as any adverse histopathological lesions (Figs. 4.5 and 4.8) (39).

In summary, both of our Δ*lpp* Δ*msbB* Δ*ail* triple and Δ*lpp* Δ*msbB::ailL2* mutants have rationally designed in-frame deletions, and, therefore, trigger minimal inflammatory response. Most importantly, T-cells isolated from mice immunized with either the Δ*lpp* Δ*msbB* Δ*ail* triple or the Δ*lpp* Δ*msbB::ailL2* mutant *via* the i.m route displayed stronger proliferative responses than the KIM/D27-vaccinated mice (Fig. 4.10A). Therefore, the above-mentioned mutants might represent better plague vaccine candidates than the *pgm*-minus mutants for further development and testing in higher animal models.

Chapter 5

Immunization of mice with new live-attenuated mutants of *Yersinia pestis* CO92 induces protective long-term humoral- and cell-mediated immunity against pneumonic plague [5][6]

Introduction

Recently, our laboratory generated three live-attenuated mutant strains of *Y. pestis* CO92. The Δ*lpp* Δ*msbB* Δ*ail* triple mutant was shown to be safe and highly immunogenic (39, 41). However, since Ail also has immunogenic potential (93), the corresponding virulence-associated amino acid residues in L2 of the *ail* gene were mutated generating the Δ*lpp* Δ*msbB::ailL2* mutant of CO92 (41). Immunization of mice with two doses of either Δ*lpp* Δ*msbB* Δ*ail* or the Δ*lpp* Δ*msbB::ailL2* mutant *via* the intramuscular (i.m.) route triggered robust humoral and cellular immune responses. Such vaccinated animals were 100% protected when challenged 21 days after the second immunization with high pneumonic challenge doses (70-92 LD_{50}) of WT CO92, indicating these vaccines were capable of providing short-term protection (41). We also developed a Δ*lpp* Δ*pla* double mutant of CO92, and mice immunized with this double mutant developed protective immunity against subsequent pneumonic challenge (40). Studies have shown that deletion of the *msbB* gene from *Y. pestis* EV76 strain modulated major immunoreactive antigens (149), and that the Δ*lpp* Δ*msbB* double mutant was significantly more attenuated compared

---

[5] Publication is currently under review in NPJ Vaccines.

[6] **Author Contributions:** Bethany L. Tiner and Jian Sha planned as well as executed all experiments described above. Bethany L. Tiner analyzed all collected data and wrote the manuscript. Yingzi Cong and Ashok Chopra helped in the planning of all experiments and in discussion of the acquired results. All authors contributed to the editing of the manuscript. Ashok Chopra is the guarantor.

to the single mutants (42). Therefore, we deleted *msbB* gene from the Δ*lpp* Δ*pla* double mutant to improve immunogenicity and safety of the Δ*lpp* Δ*msbB* Δ*pla* triple mutant.

It is imperative that a successful plague vaccine should generate long-term immunity in immunized animals. Thus, it is essential to examine if the newly created Δ*lpp* Δ*msbB* Δ*pla* mutant as well as the Δ*lpp* Δ*msbB* Δ*ail* and Δ*lpp* Δ*msbB::ailL2* mutants have the ability to elicit protective long-term humoral- and cell-mediated immune responses, which formed the basis of this study.

Results

Attenuation in virulence of the Δ*lpp* Δ*msbB* Δ*pla* mutant of *Y. pestis* CO92.

To gauge the extent of attenuation, mice (n=5/group) were infected by the intranasal (i.n.) route with 2.5 x 10^6 colony forming units [CFU] or 5.0 x 10^6 CFU doses of the WT CO92 or the Δ*lpp* Δ*msbB* Δ*pla* mutant *(*representing 5000 and 10000 LD_{50} of the WT bacterium) (40). While animals inoculated with the WT CO92 died by day 3 post infection (p.i.), all mice infected with the Δ*lpp* Δ*msbB* Δ*pla* mutant survived with no clinical signs of the disease such as ruffled fur, hunch back, and lethargy (**Fig. 5.1**). On day 22, the surviving animals as well as the age-matched naïve controls were exposed i.n. to 1.8 x 10^4 CFU dose of WT CO92 (36 LD_{50}). All of the naïve mice succumbed to infection by day 27 (5 days p.i.). Animals receiving the higher immunization dose of the Δ*lpp* Δ*msbB* Δ*pla* mutant had 80% survival after WT CO92 infection; while dropping to 70% at the lower vaccination dose (**Fig. 5.1**).

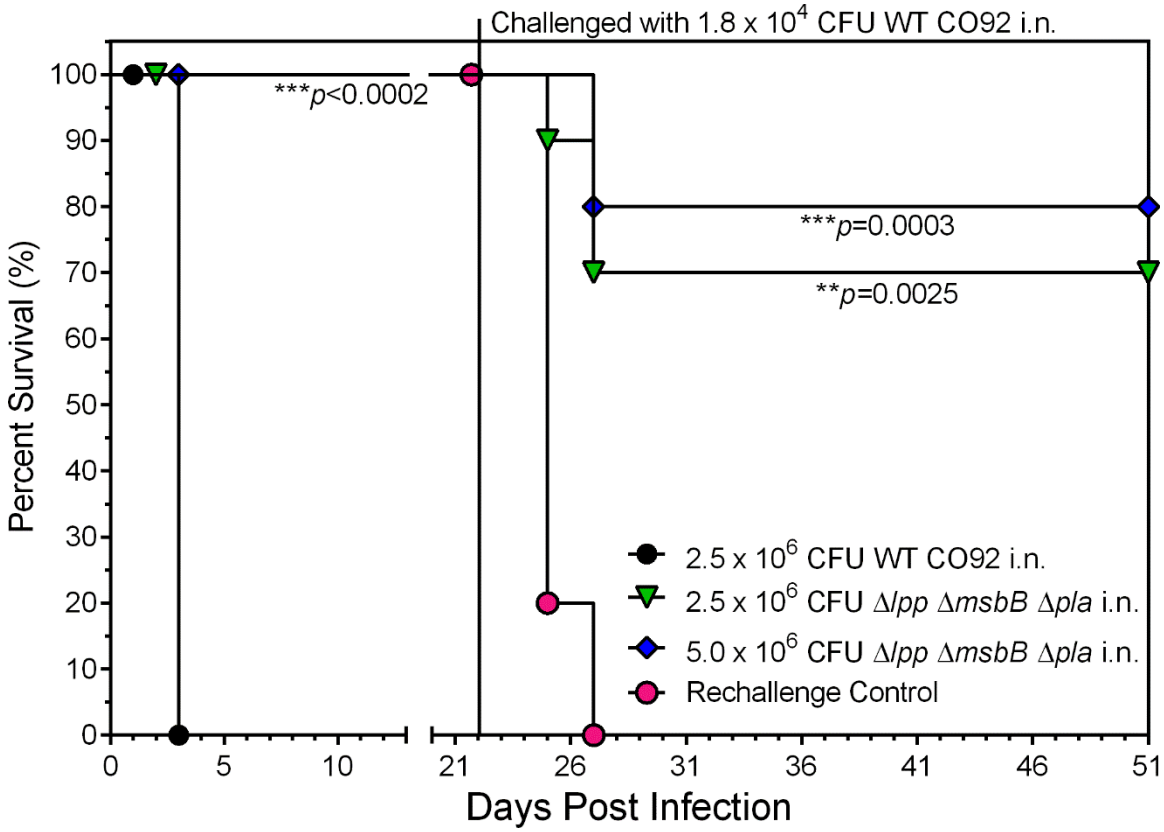

Figure 5.1. Survival analysis and protection conferred by vaccination of mice with high doses of the Δ*lpp* Δ*msbB* Δ*pla* mutant of *Y. pestis* CO92 in a pneumonic plague mouse model.
Female Swiss Webster mice (n=5 per group) were exposed by the intranasal (i.n.) route with one dose of 2.5 x 10^6 CFU or 5.0 x 10^6 CFU of the WT CO92 or the Δ*lpp* Δ*msbB* Δ*pla* mutant on day 0. Surviving mice were exposed i.n. on day 22 with 1.8 x 10^4 CFU (36 $LD_{50;}$ 1 LD_{50} = ~500 CFU) of WT CO92 strain(40). Age-matched mice were used as infection controls (Rechallenge Control). The *p* values were calculated using Kaplan Meier analysis with Log-rank (Mantel-Cox) test and were in comparison to naïve control.

Evaluation of long-term humoral immunity in mice after immunization with live-attenuated mutants of *Y. pestis* CO92.

To gauge vaccine potential of these three mutants (i.e., Δ*lpp* Δ*msbB* Δ*ail*, Δ*lpp* Δ*msbB::ailL2*, and Δ*lpp* Δ*msbB* Δ*pla*), we used the optimal vaccination regimen (41), which utilized two i.m. doses (2.5 x 10^6 CFU/dose, 21 days apart). A recently study also indicated that parental immunization can lead to protective mucosal immunity, by yet unidentified mechanism(s) (150). Based on this study, 100% survivability was observed

with no clinical signs of disease in immunized mice, irrespective of the mutant used, up to 120 days after the initial immunization.

To determine long-term humoral immune response generated by the three live-attenuated vaccine strains, splenocytes were harvested from mice (n=3-5 per group per time point) on days 42, 63, and 84 after the first immunization. The total $CD19^+$ B cell population was similar across all groups of mice on all days examined (~30% of the live cell population) based on flow cytometry. On day 42, animals immunized with Δ*lpp* Δ*msbB::ailL2*, Δ*lpp* Δ*msbB* Δ*pla*, or the Δ*lpp* Δ*msbB* Δ*ail* mutant exhibited significantly increased $CD19^+$ $CD38^+$ IgG^+ memory B cell populations (10.5%, 7.3%, and 4.2%, respectively) in the spleen compared to animals injected with PBS (1.6%) (**Fig. 5.2A**). By day 63, this population decreased in mice immunized with the Δ*lpp* Δ*msbB::ailL2* mutant (3.2%) which was comparable to the population observed in control (PBS) animals (**Fig. 5.2A**). In comparison, mice immunized with Δ*lpp* Δ*msbB* Δ*ail* or Δ*lpp* Δ*msbB* Δ*pla* mutants continued to show increased or similar population of $CD19^+$ $CD38^+$ IgG^+ memory B cells (7.6% and 6.4%, respectively) on day 63. By day 84, these populations decreased in all of the immunized groups of animals, which were similar to those in the PBS-injected mice (~0.7-1.0%) (**Fig. 5.2A**).

Sera were collected from all mice on days 14, 35, 56, 81, and 112 after the first vaccination for measuring antigen-specific antibody responses (**Fig. 5.2B**). On day 14, mice immunized with Δ*lpp* Δ*msbB* Δ*ail* or Δ*lpp* Δ*msbB* Δ*pla* mutants exhibited increased IgG antibody titers (Geometric Mean IgG titers of 15,625) against *Y. pestis* F1-V fusion antigen, representing capsular (F1) and low calcium response V (LcrV) antigens, compared to animals vaccinated with the Δ*lpp* Δ*msbB::ailL2* mutant (titer of 9,365). By day 35, a

boost in the IgG antibody titers (46,875) occurred after the second immunization (given on day 21) when mice were immunized with Δ*lpp* Δ*msbB* Δ*ail* or Δ*lpp* Δ*msbB* Δ*pla* mutants. On the contrary, a boost to the peak IgG antibody titers (46,875) in the Δ*lpp* Δ*msbB::ailL2* mutant-vaccinated mice was attained by day 56. These antibody titers remained at similar high levels until day 112 in all of the immunized groups of mice.

A significantly higher IgG1 over IgG2a/b antibody titers were noted in all of the immunized mice on day 14 (**Fig. 5.2C-I**). After the second vaccine dose, and on days 35 and 56, animals immunized with the Δ*lpp* Δ*msbB* Δ*ail* and Δ*lpp* Δ*msbB* Δ*pla* mutants had balanced Th1-based IgG2a and Th2-based IgG1 antibody responses, whereas mice vaccinated with the Δ*lpp* Δ*msbB::ailL2* mutant continued to have higher IgG1 over IgG2a titers (**Fig. 5.2C-II;** data not shown for day 56). By day 81, balanced Th1-based IgG2a and Th2-based IgG1 antibody titers were observed in mice immunized with the Δ*lpp* Δ*msbB* Δ*ail* or the Δ*lpp* Δ*msbB::ailL2* mutant, whereas the Δ*lpp* Δ*msbB* Δ*pla* mutant-vaccinated animals exhibited significantly higher IgG1 titers compared to IgG2a/b titers (**Fig. 5.2C-III**). By day 112, mice immunized with the Δ*lpp* Δ*msbB* Δ*ail* or the Δ*lpp* Δ*msbB::ailL2* mutant maintained balanced Th1-based IgG2a and Th2-based IgG1 antibody titers. However, Δ*lpp* Δ*msbB* Δ*pla* mutant-vaccinated animals possessed significantly higher IgG2a titers compared to IgG1 antibody titers (**Fig. 5.2C-IV**). Overall, all immunized mice maintained high levels of IgG1, IgG2a, and IgG2b antibody titers over the duration of the experiment, albeit some skewing of Th1- and Th2-based immune responses occurred.

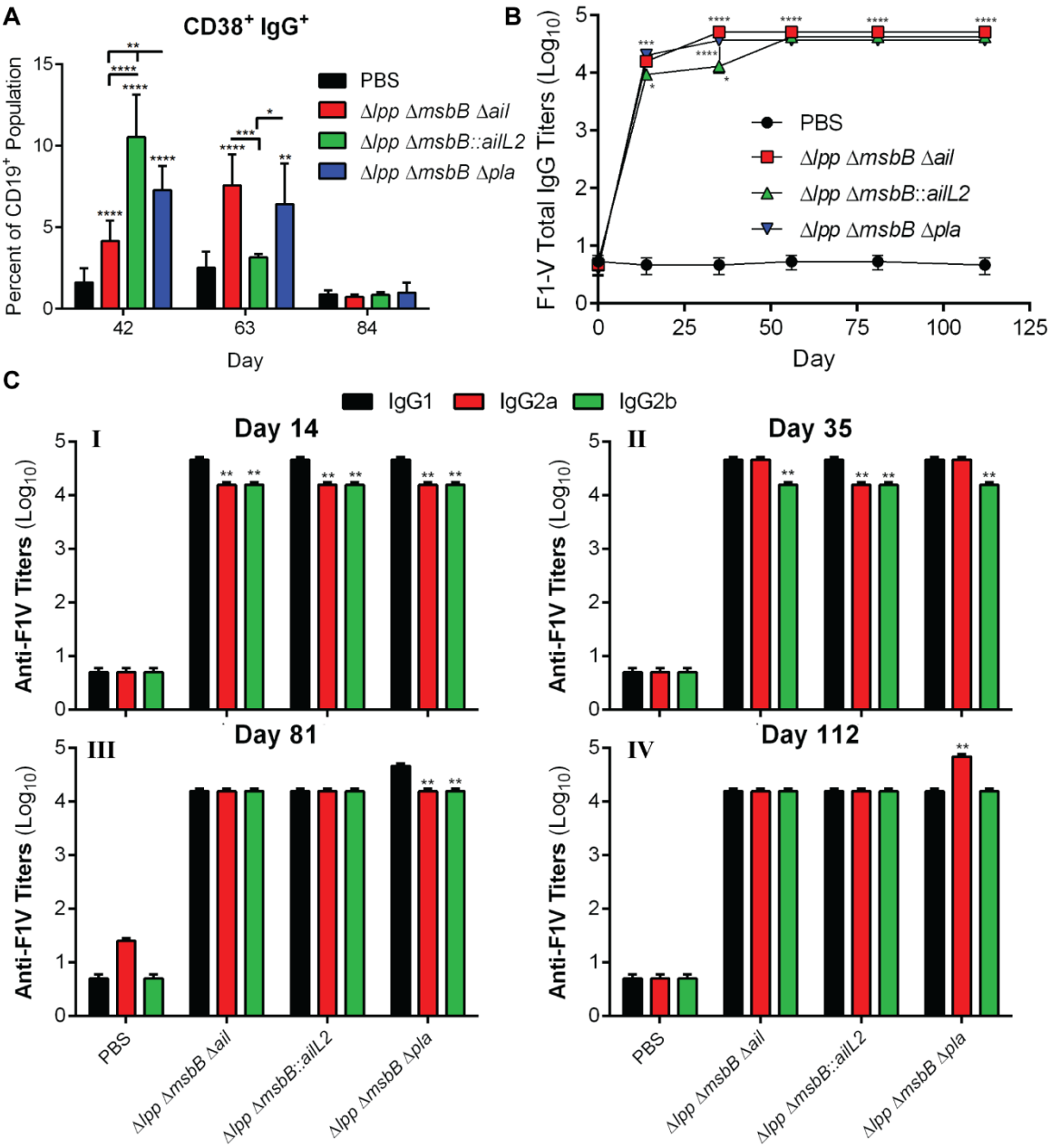

Figure 5.2. Long-term humoral immune responses in mice immunized with live-attenuated mutants of *Y. pestis* CO92.

Female Swiss Webster mice (n=5 per group/time point) were immunized by the i.m. route with two doses (2 x 10^6 CFU/dose) of Δ*lpp* Δ*msbB* Δ*ail*, Δ*lpp* Δ*msbB::ailL2*, or the Δ*lpp* Δ*msbB* Δ*pla* mutants on days 0 and 21. Mice were injected i.m. with PBS to serve as controls (n=3 per time point). **(A)** Spleens were harvested from mice on days 42, 63, and 84. Splenocytes were stained and analyzed by Flow cytometry. Percent $CD38^+$ IgG^+ (memory B cell markers) expressing $CD19^+$ B cells were calculated using FlowJo. Two-way ANOVA with Tukey post *hoc* was utilized for statistical analysis. **(B)** Sera were collected from mice on days 0, 14, 35, 56, 84, and 112 after first immunization. Specific *Y. pestis* IgG was measured using ELISA against the F1-V antigen. Each time point was statistically analyzed using a One-way ANOVA with Tukey post *hoc*. **(C)** Specific *Y. pestis* IgG isotypes to F1-V antigen in sera collected on day 14 **(Panel I)**, 35 **(Panel II)**, 81 **(Panel III)**, and 112 **(Panel IV)** were measured by ELISA using isotyping specific secondary antibodies. Each time point was analyzed using a Two-way ANOVA with Tukey post *hoc*. *$p<0.05$, **$p<0.01$, ***$p<0.001$, and ****$p<0.0001$ as compared to PBS-injected controls. Horizontal and vertical bars represented differences between groups.

Long-term cell-mediated immunity after immunization of mice with live-attenuated mutants of *Y. pestis* CO92.

To examine T cell-mediated immune responses after immunization, splenocytes were isolated from mice and stained for T cell specific markers on days 42 and 84. By day 42, all immunized animals had statistically significant increased population of $CD4^+$ cells in the spleen (**Fig. 5.3A**). However, on day 84, only mice vaccinated with the Δ*lpp* Δ*msbB* Δ*ail* or the Δ*lpp* Δ*msbB* Δ*pla* mutant had significantly higher $CD4^+$ population (29.7 and 28.4%, respectively) compared to mice injected with PBS (20.5%) (**Fig. 5.3A**). The $CD4^+$ population was increased (26.5%), albeit not significantly, in Δ*lpp* Δ*msbB::ailL2* mutant immunized mice compared to the PBS-injected mice (**Fig. 5.3A**).

To further evaluate T cell-mediated immune responses in vaccinated mice, T cells were stained for selected cytokines or transcription factors. On day 42, interferon (IFN)-γ^+ $CD4^+$ cell population was significantly increased in mice immunized with the Δ*lpp* Δ*msbB* Δ*ail* mutant (2.7%) or Δ*lpp* Δ*msbB* Δ*pla* mutant (3.2%) compared to PBS-injected animals (1.7%) (**Fig. 5.3B-I**). On day 84, while the IFN-γ^+ $CD4^+$ cell population remained significantly high in mice immunized with the Δ*lpp* Δ*msbB* Δ*ail* mutant (2.7%), this cell population decreased in Δ*lpp* Δ*msbB* Δ*pla* mutant-immunized animals (0.7%) (**Fig. 5.3B-I**). The IFN-γ^+ $CD4^+$ cell population remained unaltered in mice vaccinated with the Δ*lpp* Δ*msbB::ailL2* mutant on both days 42 and 84 (1.7%) similar to that in PBS-injected animals.

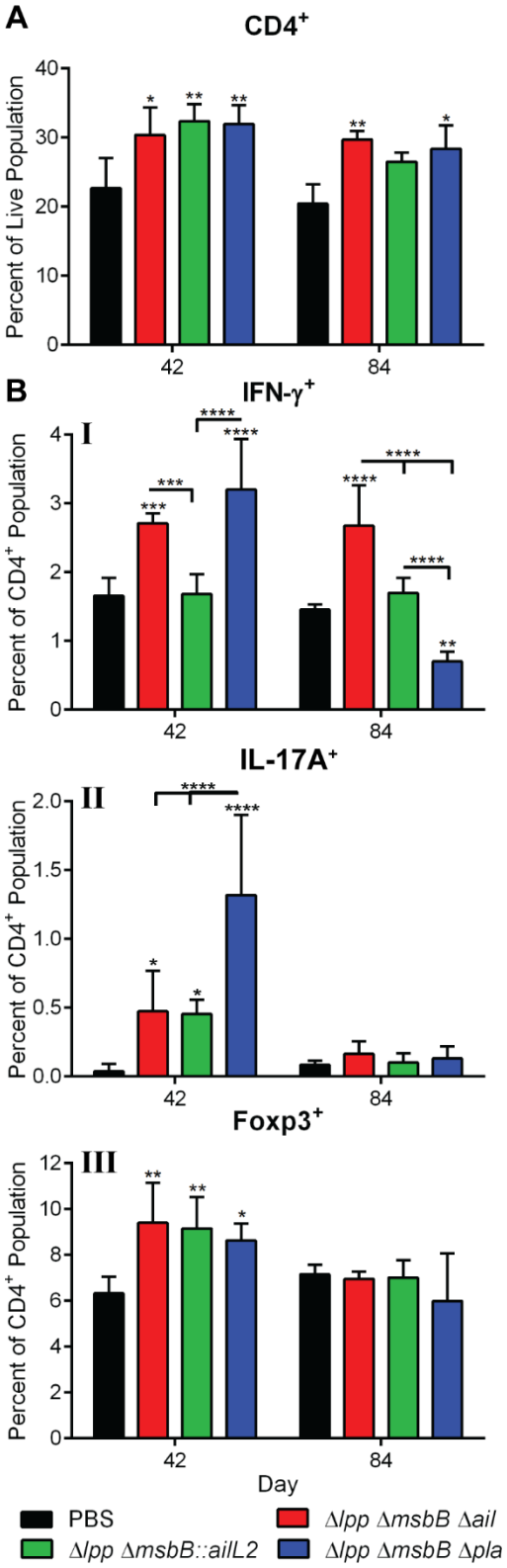

Figure 5.3. Long-term cell-mediated immune responses in mice immunized with live-attenuated mutants of *Y. pestis* CO92.
Female Swiss Webster mice (n=5 per group/time point) were immunized by the i.m. route with two doses (2 x 10^6 CFU/dose) of Δ*lpp* Δ*msbB* Δ*ail*, Δ*lpp* Δ*msbB::ailL2*, or the Δ*lpp* Δ*msbB* Δ*pla* mutants on days 0 and 21. Mice were injected i.m. with PBS to serve as controls (n=3 per time point). Spleens were harvested from mice on days 42 and 84. Splenocytes were stained and analyzed by Flow cytometry. **(A)** Total percent of $CD4^+$ (T helper cell marker) expressing cells was calculated using FlowJo. **(B)** Percent of IFN-γ (**Panel I**; Th1 marker), IL-17A (**Panel II**; Th17 marker), and Foxp3 (**Panel III**; T_{reg} marker) expressing $CD4^+$ cells was calculated. Two-way ANOVA with Tukey post *hoc* was utilized for determining statistical significance. *$p<0.05$, **$p<0.01$, ***$p<0.001$, and ****$p<0.0001$ as compared to PBS-injected controls. Horizontal bars represent differences between the indicated groups.

IL-17A$^+$ CD4$^+$ cell population significantly increased in all immunized mice on day 42 (~0.5-1.3%) compared to PBS-injected animals (0.003%) (**Fig. 5.3B-II**). Importantly, mice immunized with the Δ*lpp* Δ*msbB* Δ*pla* mutant had the highest IL-17A$^+$ CD4$^+$ population compared to all other groups. By day 84, this subset of population in the immunized mice returned to that of the PBS-injected animals. Interestingly, Foxp3$^+$ CD4$^+$ cell population increased significantly in all immunized mice on day 42 (~8.6-9.4%) compared to PBS-injected animals (6.3%) (**Fig. 5.3B-III**). By day 84, this subset of cell population in vaccinated mice returned to that of PBS-injected animals.

Evaluation of long-term protection against pneumonic plague provided by immunization of mice with live-attenuated mutants of *Y. pestis* CO92.

On day 120, mice were challenged *via* the i.n. route with 1.2 x 10^4 CFU dose (24 LD_{50}) of the WT CO92 *luc2* strain (with the luciferase gene). The PBS-injected animals succumbed to infection by day 125 (5 days p.i.) (**Fig. 5.4A**). Two of these five mice died prior to imaging for bioluminescence. The image in **Fig. 5.4B-I** (PBS) showed that two of the remaining control animals were positive for bioluminescence on day 123 (3 days p.i.). The mouse on the extreme right side in the panel PBS represented an uninfected control for imaging. One animal from each of the Δ*lpp* Δ*msbB* Δ*ail* and Δ*lpp* Δ*msbB::ailL2* mutant-immunized groups were positive for bioluminescence, and the infection was confined to the lungs (**Fig. 5.4B-II&III**). These two mice succumbed to infection on day 125 (5 days p.i.), resulting in 80% animal survival (**Fig. 5.4A**). The remaining mice in these groups survived and were negative for bioluminescence on day 10 after challenge with the WT CO92 *luc2* strain. All of the mice immunized with the Δ*lpp* Δ*msbB* Δ*pla* mutant

survived exposure to WT CO92, and they were negative for bioluminescence on both days 3 and 10 p.i. (**Fig. 5.4A&B-IV**).

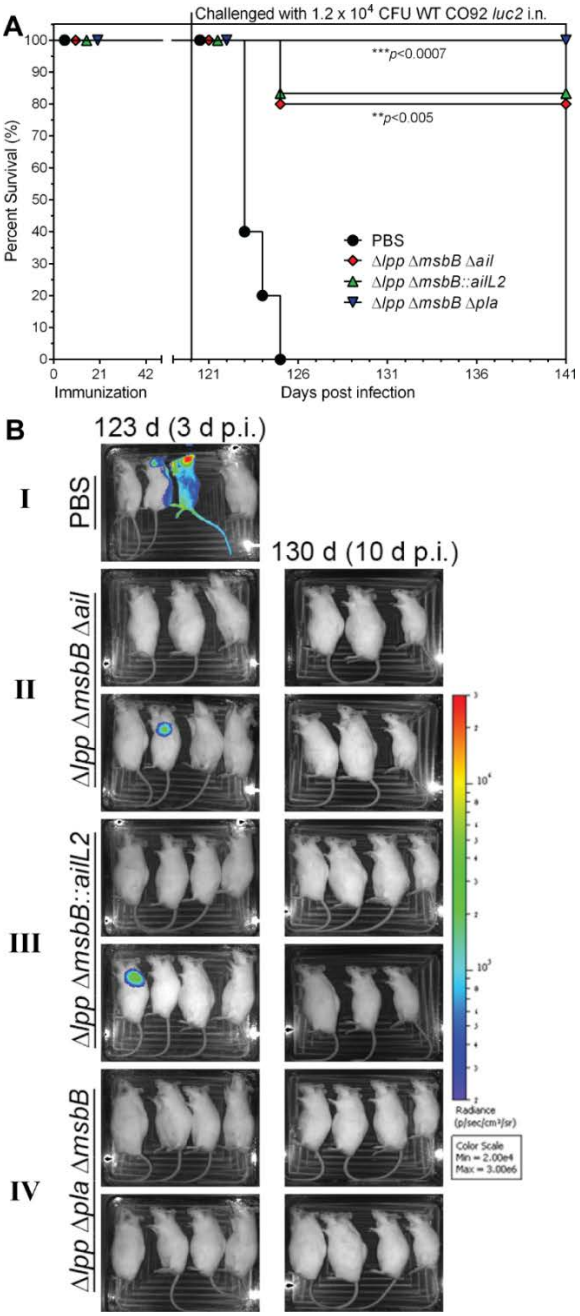

Figure 5.4. Survival analysis of immunized mice after exposure to WT *Y. pestis* CO92 in a pneumonic plague model.
Female Swiss Webster mice (n=5-6 per group) were immunized by the i.m. route with two doses (2 x 10^6 CFU/dose) of Δ*lpp* Δ*msbB* Δ*ail*, Δ*lpp* Δ*msbB::ailL2*, or the Δ*lpp* Δ*msbB* Δ*pla* mutants on days 0 and 21. Mice were injected i.m. with PBS to serve as controls (n=5 per group). **(A)** Mice were exposed i.n. on day 120 with 1.2 x 10^4 CFU (24 $LD_{50;}$ 1 LD_{50} = ~500 CFU)(40) of the WT *Y. pestis luc2* CO92 strain (with luciferase gene). The *p* values were calculated using Kaplan Meier analysis with Log-rank (Mantel-Cox) test and were in comparison to the naïve control. **(B)** Bioluminescence imaging of mice. Surviving mice were exposed i.n. with 1.2 x 10^4 CFU of *Y. pestis-luc2* strain and all animals were imaged on days 123 and 130 (days 3 and 10 p.i.). The bioluminescent scale is within the figures and ranges from most intense (red) to least intense (violet).

Evaluation of the immediate innate immune response of vaccinated mice after exposure to WT *Y. pestis* CO92 in a pneumonic plague model.

On day 124 (4 days p.i.), spleens were harvested from a subset of the challenged mice (n=3 to 4 per group) to determine innate immune cell response subsequent to WT *Y. pestis* CO92 challenge. The total number of CD11c$^+$ CD11b$^-$ resident dendritic cells (DCs) was maximally increased in mice immunized with the Δ*lpp* Δ*msbB::ailL2* mutant and exposed to WT CO92 (6.3%) compared to the other two groups of vaccinated (with Δ*lpp* Δ*msbB* Δ*ail* [4.3%] or Δ*lpp* Δ*msbB* Δ*pla* [4.7%] mutant) animals (**Fig. 5.5A**). These DC numbers were in comparison to animals injected with PBS and then exposed to WT CO92 (2.5%) (**Fig. 5.5A**).

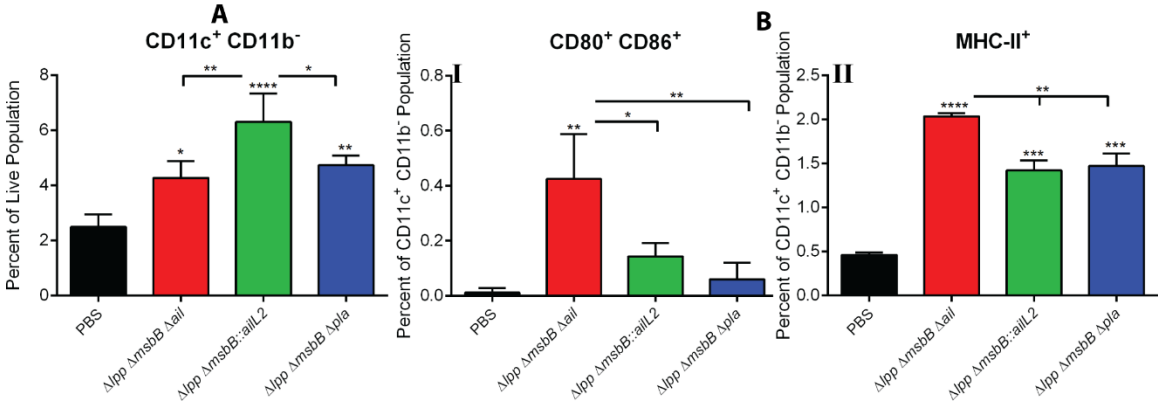

Figure 5.5. Innate immune responses in immunized mice after exposure to WT *Y. pestis* CO92 in a pneumonic plague model.
Female Swiss Webster mice were immunized by the i.m. route with two doses (2 x 10^6 CFU/dose) of Δ*lpp* Δ*msbB* Δ*ail*, Δ*lpp* Δ*msbB::ailL2*, or the Δ*lpp* Δ*msbB* Δ*pla* mutants on days 0 and 21. On day 120, mice were exposed i.n. to 1.7 x 10^3 CFU (3.4 $LD_{50;}$ 1 LD_{50} = ~500 CFU)(40) of the WT *Y. pestis luc2* CO92 strain (with luciferase gene). Mice which were injected i.m. with PBS and then either exposed or not exposed to WT CO92 served as controls. Spleens were harvested from mice (n=3-4 per group) on day 124 (days 4 p.i.). Splenocytes were stained and analyzed by Flow cytometry. **(A)** Total percent of CD11c$^+$ CD11b$^-$ (resident dendritic cell markers) expressing cells was calculated using FlowJo. **(B)** Percent of CD80$^+$ CD86$^+$ (**Panel I**; activation markers) and MHC-II$^+$ (**Panel II**) expressing dendritic cells were also calculated. Two-way ANOVA analysis with Tukey post *hoc* was utilized for determining statistical significance. *p<0.05, **p<0.01, ***p<0.001, and ****p<0.0001 as compared to PBS-injected controls. Horizontal bars represent differences between the indicated groups.

The total number of $CD80^+$ $CD86^+$ cells, which represented activated $CD11c^+$ $CD11b^-$ DC populations, was maximally increased in mice immunized with the Δ*lpp* Δ*msbB* Δ*ail* mutant followed by the Δ*lpp* Δ*msbB::ailL2* and Δ*lpp* Δ*msbB* Δ*pla* mutants subsequent to the WT CO92 exposure (**Fig. 5.5B-I**). These activated DC cell numbers were in comparison to animals injected with PBS and exposed to WT CO92. Likewise, MHC-II expression was highest in the $CD11c^+$ $CD11b^-$ cell population isolated from mice vaccinated with the Δ*lpp* Δ*msbB* Δ*ail* mutant followed by that of Δ*lpp* Δ*msbB::ailL2* or Δ*lpp* Δ*msbB* Δ*pla* mutants when compared to mice injected with PBS and exposed to WT CO92 (**Fig. 5.5B-II**).

Evaluation of cytokine producing $CD4^+$ T cells in immunized mice after exposure to WT *Y. pestis* CO92 in a pneumonic plague model.

Spleens were isolated from a subset of the challenged mice (n=3 to 4 per group) on day 124 (4 days p.i.) and from all surviving (vaccinated) animals on day 141 (21 days p.i.) to determine immune recall response of T cells after exposure to WT CO92. For the 124-day time point, spleens from PBS-injected animals with and without exposure to WT CO92 were used as a controls. Since all PBS-injected mice, exposed to WT CO92 succumbed to infection by day 141 (21 days p.i.), we only used PBS-injected animals not exposed to WT CO92 as controls for this time point.

On day 124 (4 days p.i.), there were no differences in the total number of $CD4^+$ cell population in any groups of the immunized mice after challenge with WT CO92 (**Fig. 5.6A**). By day 141 (21 days p.i.), mice immunized with Δ*lpp* Δ*msbB::ailL2* or Δ*lpp* Δ*msbB* Δ*pla* mutants and exposed to WT CO92 had increased number of total $CD4^+$ population

(~26.0-27.5%) compared to Δ*lpp* Δ*msbB* Δ*ail* mutant-immunized animals, or those which served as controls (**Fig. 5.6A**).

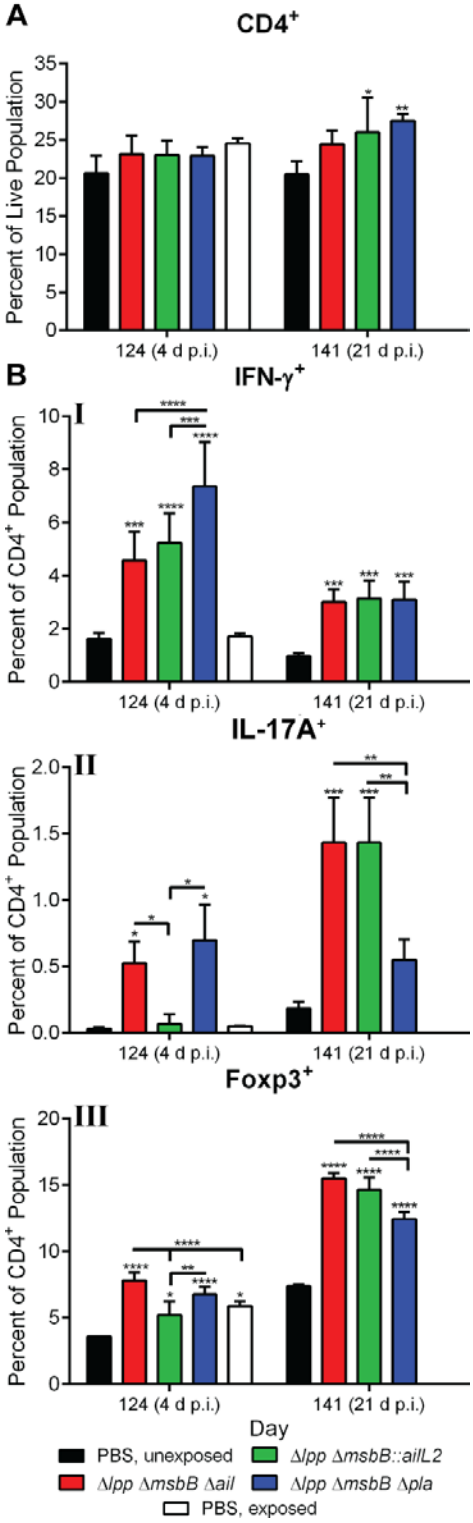

Figure 5.6. Cell-mediated immune responses in immunized mice after exposure to WT *Y. pestis* CO92 in a pneumonic plague model.
Female Swiss Webster mice were immunized by the i.m. route with two doses (2 x 10^6 CFU/dose) of Δ*lpp* Δ*msbB* Δ*ail*, Δ*lpp* Δ*msbB::ailL2*, or the Δ*lpp* Δ*msbB* Δ*pla* mutants on days 0 and 21. Mice were injected i.m. with PBS to serve as controls. Mice were exposed i.n. on day 120 with 1.2 x 10^4 CFU (24 $LD_{50;}$ 1 LD_{50} = ~500 CFU)(40) of the WT *Y. pestis luc2* CO92 strain (with luciferase gene). Spleens were harvested from surviving, immunized mice on days 124 (4 days p.i.; n=4 per group) and 141 (21 days p.i.; n=4-6 per group). Spleens were harvested from PBS-injected, WT CO92 exposed or non-exposed mice as controls (n=3 per group/time point). Splenocytes were stained and analyzed by Flow cytometry. **(A)** Total percent of $CD4^+$ (T helper cell marker) expressing cells was calculated using FlowJo. **(B)** Percent of IFN-γ (**Panel I**; Th1 marker), IL-17A (**Panel II**; Th17 marker), and Foxp3 (**Panel III**; T_{reg} marker) expressing $CD4^+$ cells was calculated. Two-way ANOVA analysis with Tukey post *hoc* was utilized for determining statistical significance. *p<0.05, **p<0.01, ***p<0.001, and ****p<0.0001 as compared to PBS-injected controls. Horizontal bars represent differences between the indicated groups.

Early after exposure to WT CO92, the spleens of all immunized animals, e.g., with Δ*lpp* Δ*msbB* Δ*ail*, Δ*lpp* Δ*msbB::ailL2* or the Δ*lpp* Δ*msbB* Δ*pla* mutants possessed increased percentage of IFN-γ^+ $CD4^+$ cells (4.6%, 5.2%, and 7.4%), respectively. This was in comparison to mice injected with PBS but not exposed to WT CO92 (1.6%) as well as to those animals which were injected with PBS and exposed to WT CO92 (1.7%) (**Fig. 5.6B-I**). By day 141, the percentage of IFN-γ^+ $CD4^+$ cells decreased in all surviving mice immunized with Δ*lpp* Δ*msbB* Δ*ail*, Δ*lpp* Δ*msbB::ailL2*, or Δ*lpp* Δ*msbB* Δ*pla* mutants and exposed to WT CO92 (3.0%, 3.2%, and 3.4%, respectively) (**Fig. 5.6B-I**). However, this cell population was still significantly higher when compared to the control animals (1.0%).

IL-$17A^+$ $CD4^+$ cells were increased in spleens of mice immunized with the Δ*lpp* Δ*msbB* Δ*ail* and Δ*lpp* Δ*msbB* Δ*pla* mutants and exposed to WT CO92 compared to animals vaccinated with the Δ*lpp* Δ*msbB::ailL2* mutant or injected with PBS (**Fig. 5.6B-II**). On day 141 (21 days p.i.), the percentage of IL-$17A^+$ $CD4^+$ cells was further increased in spleens of mice immunized with the Δ*lpp* Δ*msbB* Δ*ail* mutant, while maintaining a similar level in mice vaccinated with the Δ*lpp* Δ*msbB* Δ*pla* mutant. On the contrary, a robust increase in the population of IL-$17A^+$ $CD4^+$ cells was noted in animals vaccinated with the Δ*lpp* Δ*msbB::ailL2* mutant followed by exposure to WT CO92 on day 141 (21 days p.i.) (**Fig. 5.6B-II**).

On day 124 (4 days p.i.), the $Foxp3^+$ $CD4^+$ cell population was increased in mice vaccinated with Δ*lpp* Δ*msbB* Δ*ail*, Δ*lpp* Δ*msbB::ailL2*, or the Δ*lpp* Δ*msbB* Δ*pla* mutants (7.8%, 5.2%, and 6.8%, respectively), and subsequently exposed to WT CO92 when compared to naïve (uninfected) animals injected with PBS (3.6%) (**Fig. 5.6B-III**). This difference was only significant for the Δ*lpp* Δ*msbB* Δ*ail* mutant when compared to animals

that were injected with PBS and exposed to WT CO92. By day 141 (21 days p.i.), all surviving mice immunized with Δ*lpp* Δ*msbB* Δ*ail*, Δ*lpp* Δ*msbB::ailL2,* or Δ*lpp* Δ*msbB* Δ*pla* mutants and then exposed to WT CO92 had increased Foxp3$^+$ CD4$^+$ cells (15.5%, 14.7%, and 12.5%, respectively), compared to control mice (7.4%) (**Fig. 5.6B-III**).

Discussion

It is crucial that a potential vaccine candidate(s) demonstrates long-term immune responses and protection. This is the first study to examine several components of the immune response generated after immunization of mice with the above three live-attenuated mutants over a period of four months.

The kinetics of memory B cell production in *Y. pestis* EV76 vaccine strain-immunized mice has been reported (139). Similar to our protocol, mice were immunized i.m. with two doses (8 x 10^7 CFU/dose) of EV76 (21 days apart) with splenoyctes harvested periodically after immunization (139). However, CD38 and IgD expressing CD19$^+$ CD27$^+$ population was evaluated in that study. CD27 is not considered as an appropriate marker for memory B cells in mice (151, 152), and the lack of CD27 expression on memory B cells has been previously reported (153). Since IgD and IgG are produced by activated B cells, we designated memory B cell population as CD38 and IgG producing CD19$^+$ cells. By day 7, memory B cell populations increased in EV76-immunized mice in the spleen (139). However, this population of cells sharply decreased by day fifty-six (139). Memory B cells in the Δ*lpp* Δ*msbB::ailL2* mutant-immunized mice behaved similar to those in the EV76-immunized animals with increases in the CD19$^+$ CD38$^+$ IgG$^+$ cell population on day 42 which decreased to the levels seen in naïve mice by day 63 (Fig. 5.2A). However, memory B cell population in Δ*lpp* Δ*msbB* Δ*ail* and Δ*lpp* Δ*msbB* Δ*pla* mutant-immunized mice

increased or remained high through day 63 and declined to levels seen in naïve mice only on day 84 (Fig. 5.2A).

In terms of antibody production, total IgG titers in the Δ*lpp* Δ*msbB::ailL2* mutant-immunized mice reached a maximal level on day 56 and then plateaued, whereas animals immunized with the other two mutants, Δ*lpp* Δ*msbB* Δ*ail* and Δ*lpp* Δ*msbB* Δ*pla*, showed maximum IgG titers by day 35 and then plateaued (Fig. 5.2B). In contrast, the total memory B cell population peaked at day 42 in the Δ*lpp* Δ*msbB::ailL2* mutant-immunized mice which then decreased to levels of PBS-injected, naïve animals by day 63 (Fig. 5.2A). Interestingly, mice immunized with the other two mutants were capable of sustaining memory B cell populations until day 63 (Fig. 5.2A). These differences in time to peak antibody titers versus the maximum percentage of memory B cell population in the Δ*lpp* Δ*msbB::ailL2* mutant-immunized animals (Fig. 5.2A&B) could be attributed to low avidity of the IgG antibodies to F1-V antigens of *Y. pestis* early during vaccination before switching to high affinity antibodies later during immunization. Alternatively, these memory B cells from Δ*lpp* Δ*msbB::ailL2* mutant-immunized mice might be secreting less IgG per cell compared to that of the memory B cells of Δ*lpp* Δ*msbB* Δ*ail*- and Δ*lpp* Δ*msbB* Δ*pla* mutant-immunized animals because of a high proportion of unswitched memory B cells early during immunization (154).

Mice immunized i.m. with two doses (8 x 10^7 CFU/dose) of EV76 strain (21 days apart) had lower total F1-specific IgG titers (10,000-15,000 on day 42) (141). These titers decreased below 10,000 by day 70, and further declined before attaining a steady state level (1,400) by day 322 (141). In comparison, animals vaccinated with our live-attenuated mutants at a lower dose (2 x 10^6 CFU/dose) were not only able to achieve total F1-V

specific IgG titers of 46,875 by day 35 to 56 but were able to maintain these maximum titers until day 112 (Fig. 5.2B).

Overall, all three live-attenuated mutants stimulated long-lasting T cell-mediated immune responses capable of protecting mice from developing subsequent pneumonic plague. Our data generally indicated an increase in IFN-γ–, IL-17A-, and Foxp3-expressing $CD4^+$ T cells after immunization (Fig. 5.3). A similar trend was also noted when these mutant-immunized mice were subsequently exposed to WT CO92 in a pneumonic model (Fig. 5.6). All immunized animals that survived WT CO92 *luc2* strain challenge rapidly cleared the bacteria (3 days p.i.) as measured by bioluminescence (Fig. 5.4B), possibly due to increased production of IFN-γ by $CD4^+$ cells (Fig. 5.6B-I). IFN-γ promotes macrophage activation facilitating defense against bacterial pathogens (155), and it has been shown that IFN-γ as well as tumor necrosis factor (TNF)-α are important co-determinants of antibody-mediated protection against pneumonic plague (156). Consequently, the increased presence of IFN-γ^+ $CD4^+$ cells in conjunction with F1-V specific neutralizing antibody production could augment opsonization and clearance of *Y. pestis*.

Th17 cells are potent secretors of IL-17A, and it has recently been shown that IL-17A provides an antibody-independent heterologous protection of the host against many pathogenic bacterial infections, including *Y. pestis* (21, 137). For example, IL-17A was induced by the intranasal immunization of mice with the *Y. pestis* strain D27-pLpxL KIM/D27 engineered to produce *Escherichia coli* LpxL, which increases TLR-4 activation by LPS of *Y. pestis* (138). Thus, IL-17A contributed significantly to T cell-mediated defense against pulmonary *Y. pestis* infection (21). Consistent with previous reports (21,

137), we also showed Δ*lpp* Δ*msbB* Δ*pla* mutant-immunized mice had the highest increase in IL-17A producing $CD4^+$ cells immediately after WT CO92 exposure (Fig. 5.6B-II) resulting in efficient clearance of the invading pathogen. Importantly, the IL-$17A^+$ $CD4^+$ cell population decreased in the Δ*lpp* Δ*msbB* Δ*pla* mutant-immunized mice 21 days post WT CO92 exposure (Fig. 5.6B-II) signifying a possible faster resolution of inflammation which is desirable in a potential vaccine.

In contrast, mice vaccinated with Δ*lpp* Δ*msbB* Δ*ail* or Δ*lpp* Δ*msbB::ailL2* mutants and subsequently challenged with WT CO92 had increased IL-17A producing $CD4^+$ cells 21 days p.i. (Fig. 5.6B-II). Thus, these animals would most likely had somewhat of a prolonged inflammatory response after exposure to WT CO92; however, not to an extent to cause any adverse histopathological lesions in immunized mice (41). Interestingly, production of IL-17A from T cells was also observed in our previous study when isolated T cells from Δ*lpp* Δ*msbB* Δ*ail* and Δ*lpp* Δ*msbB*::*ailL2* mutant-immunized mice were co-cultured with antigen presenting cells which had been exposed to heat-killed WT CO92 (41).

Foxp3 is a transcription factor and marker for T_{reg} cells ($Foxp3^+$ $CD4^+$), which are primarily responsible for dampening immune responses. Recent studies have revealed that T_{reg} cells can promote protective Th17-associated immune responses against bacterial infections (157, 158). Interestingly, both $Foxp3^+$ and IL-$17A^+$ $CD4^+$ cells were concurrently increased both after immunization as well as after WT CO92 challenge (Figs. 5.3B & 5.6B). However, a direct link between T_{reg} cells and Th17-based protective immune responses against *Y. pestis* still needs further investigation.

Consistent with the above-mentioned data, all mutant-immunized animals had increased DC population expressing MHC-II (Fig. 5.5B-II), which is required for antigen presentation to $CD4^+$ cells (159). An increasing trend in the activation of DCs was noted for all mutant-immunized mice, which attained statistical significance for the Δ*lpp* Δ*msbB* Δ*ail* mutant. Overall, our results indicated immunization of animals with any of these mutants could successfully induce activation of an innate immune response after exposure to WT CO92.

In summary, all three live-attenuated mutants characterized in this study would be viable vaccine candidates due to their ability to stimulate both long-term humoral- and cell-mediated immune responses, which protected mice against exposure to highly lethal pneumonic challenge (Fig. 5.4). Future studies involving immunocompromised mice as well as evolutionary higher animal models of pneumonic plague are needed to determine the efficacy and safety of these potential live-attenuated plague vaccines.

Chapter 6

Conclusions and Future Directions

The aim of this study was to examine Ail's role in virulence and immunogenicity as well as to evaluate the efficacy and safety of novel live-attenuated vaccines against pneumonic plague. Ail's role in adherence, invasion, and serum resistance was further elucidated, and it was the main mediator of these virulence abilities, as evidenced by their impairment in the Δ*lpp* Δ*msbB* Δ*ail* triple mutant. It was also determined that Δ*lpp* Δ*msbB* Δ*ail*'s decreased intracellular survival was not due to the absence of Ail, but rather to that of Lpp. We further verified that Ail affects Yop protein translocation into host cells due to the lack of Yop translocation when *ail* is deleted from *Y. pestis* CO92. This is most likely because Δ*ail* bacteria cannot attach to host cells allowing for the docking of the T3SS needle. Interestingly, secretion of Yops was increased when Ail was absent from the outer membrane of mutant plague bacteria. This suggests that Ail may interact with the T3SS and affect its activation. Future studies are needed to elucidate Ail's role in the T3SS beyond its role in cell adhesion.

In summary, the Δ*lpp* Δ*msbB* Δ*ail,* Δ*lpp* Δ*msbB::ailL2,* and Δ*lpp* Δ*msbB* Δ*pla* live-attenuated mutants are viable vaccine candidates. All three are highly attenuated in mice when administered both intranasally to mimic pneumonic plague and intramuscularly for immunization. They are all capable of stimulating both long-term humoral and cell-mediated immune responses that can protect mice against exposure to pneumonic plague. Besides immunological effectiveness, another important aspect of a good vaccine is whether it is safe and non-damaging. While the Δ*lpp* Δ*msbB* Δ*ail* and Δ*lpp* Δ*msbB::ailL2*

mutants have been shown to be extremely safe through histopathological analysis and dissemination studies, the safety of the Δ*lpp* Δ*msbB* Δ*pla* needs further analysis even though no clinical signs have been observed in immunized mice.

Also, future studies are needed to test the extent these vaccines can protect all populations. The optimal vaccine would be able to protect a diverse population without any side effects. These studies have all been performed in immune-competent, wild-type mice, but the effectiveness and safety of these live-attenuated mutants need to be examined in immunocompromised mice. Because Ail's ability to confer serum resistance is host-dependent (i.e. Δ*ail* strains remain serum resistant upon exposure to mouse sera but serum sensitive to rat, human, and NHP sera), it is necessary to evaluate the efficacy and safety of these potential live-attenuated plague vaccines in evolutionarily higher animal models of pneumonic plague, including rats and NHPs.

REFERENCES

1. **Galindo CL, Rosenzweig JA, Kirtley ML, Chopra AK.** 2011. Pathogenesis of *Y. enterocolitica* and *Y. pseudotuberculosis* in Human Yersiniosis. J Pathog **2011:**182051.
2. **Perry RD, Fetherston JD.** 1997. *Yersinia pestis*--etiologic agent of plague. Clin Microbiol Rev **10:**35-66.
3. **Prentice MB, Rahalison L.** 2007. Plague. Lancet **369:**1196-1207.
4. **Achtman M, Morelli G, Zhu P, Wirth T, Diehl I, Kusecek B, Vogler AJ, Wagner DM, Allender CJ, Easterday WR, Chenal-Francisque V, Worsham P, Thomson NR, Parkhill J, Lindler LE, Carniel E, Keim P.** 2004. Microevolution and history of the plague bacillus, *Yersinia pestis*. Proc Natl Acad Sci U S A **101:**17837-17842.
5. **Achtman M, Zurth K, Morelli G, Torrea G, Guiyoule A, Carniel E.** 1999. *Yersinia pestis*, the cause of plague, is a recently emerged clone of *Yersinia pseudotuberculosis*. Proc Natl Acad Sci U S A **96:**14043-14048.
6. **Skurnik M, Peippo A, Ervelä E.** 2000. Characterization of the O-antigen gene clusters of *Yersinia pseudotuberculosis* and the cryptic O-antigen gene cluster of *Yersinia pestis* shows that the plague bacillus is most closely related to and has evolved from *Y. pseudotuberculosis* serotype O:1b. Mol Microbiol **37:**316-330.
7. **Quenee LE, Ciletti NA, Elli D, Hermanas TM, Schneewind O.** 2011. Prevention of pneumonic plague in mice, rats, guinea pigs and non-human primates with clinical grade rV10, rV10-2 or F1-V vaccines. Vaccine **29:**6572-6583.
8. **Centers for Disease Control and Prevention.** 17 November 2008, posting date. Protecting the American public by ensuring safe and secure possession, use, and transfer of select agents and toxins that pose a threat to public health., http://www.cdc.gov/phpy/documents/DSAT_brochure_July2011.pdf ed. CDC Select Agent Program, Centers for Disease Control and Prevention, Atlanta, GA.
9. **Inglesby TV, Dennis DT, Henderson DA, Bartlett JG, Ascher MS, Eitzen E, Fine AD, Friedlander AM, Hauer J, Koerner JF, Layton M, McDade J, Osterholm MT, O'Toole T, Parker G, Perl TM, Russell PK, Schoch-Spana M, Tonat K.** 2000. Plague as a biological weapon: medical and public health management. Working Group on Civilian Biodefense. JAMA **283:**2281-2290.
10. **Evans RG, Crutcher JM, Shadel B, Clements B, Bronze MS.** 2002. Terrorism from a public health perspective. Am J Med Sci **323:**291-298.
11. **World Health Organization Media Center.** 6 August 2009, posting date. Plague: questions and answers about plague., http://www.who.int/ith/diseases/plague/en/ ed. World Health Organization, Geneva, Switzerland.
12. **Pearson G, Woollett G, Chevrier M, Tucker J, Smithson A.** 1998. Biological Weapons Proliferation: Reasons for Concern, Courses of Action. Henry L. Stimson Center, Washington DC.
13. **Rosenzweig JA, Brackman SM, Kirtley ML, Sha J, Erova TE, Yeager LA, Peterson JW, Xu ZQ, Chopra AK.** 2011. Cethromycin-mediated protection against the plague pathogen *Yersinia pestis* in a rat model of infection and comparison with levofloxacin. Antimicrob Agents Chemother **55:**5034-5042.

14. **Layton RC, Mega W, McDonald JD, Brasel TL, Barr EB, Gigliotti AP, Koster F.** 2011. Levofloxacin cures experimental pneumonic plague in African green monkeys. PLoS Negl Trop Dis **5:**e959.
15. **Peterson JW, Moen ST, Healy D, Pawlik JE, Taormina J, Hardcastle J, Thomas JM, Lawrence WS, Ponce C, Chatuev BM, Gnade BT, Foltz SM, Agar SL, Sha J, Klimpel GR, Kirtley ML, Eaves-Pyles T, Chopra AK.** 2010. Protection Afforded by Fluoroquinolones in Animal Models of Respiratory Infections with *Bacillus anthracis, Yersinia pestis*, and *Francisella tularensis*. Open Microbiol J **4:**34-46.
16. **Smiley ST.** 2008. Current challenges in the development of vaccines for pneumonic plague. Expert Rev Vaccines **7:**209-221.
17. **Centers for Disease Control and Prevention (CDC) DpoHaHSH.** 2012. Possession, use, and transfer of select agents and toxins; biennial review. Final rule. Fed Regist **77:**61083-61115.
18. **Alvarez ML, Cardineau GA.** 2010. Prevention of bubonic and pneumonic plague using plant-derived vaccines. Biotechnol Adv **28:**184-196.
19. **Rosenzweig JA, Jejelowo O, Sha J, Erova TE, Brackman SM, Kirtley ML, van Lier CJ, Chopra AK.** 2011. Progress on plague vaccine development. Appl Microbiol Biotechnol **91:**265-286.
20. **Quenee LE, Ciletti N, Berube B, Krausz T, Elli D, Hermanas T, Schneewind O.** 2011. Plague in Guinea pigs and its prevention by subunit vaccines. Am J Pathol **178:**1689-1700.
21. **Lin JS, Kummer LW, Szaba FM, Smiley ST.** 2011. IL-17 contributes to cell-mediated defense against pulmonary *Yersinia pestis* infection. J Immunol **186:**1675-1684.
22. **Smiley ST.** 2008. Immune defense against pneumonic plague. Immunol Rev **225:**256-271.
23. **Agar SL, Sha J, Foltz SM, Erova TE, Walberg KG, Baze WB, Suarez G, Peterson JW, Chopra AK.** 2009. Characterization of the rat pneumonic plague model: infection kinetics following aerosolization of *Yersinia pestis* CO92. Microbes Infect **11:**205-214.
24. **Williamson ED, Packer PJ, Waters EL, Simpson AJ, Dyer D, Hartings J, Twenhafel N, Pitt ML.** 2011. Recombinant (F1+V) vaccine protects cynomolgus macaques against pneumonic plague. Vaccine **29:**4771-4777.
25. **FDA.** 2012. African Green monkey (*Chlorocebus aethiops*) animal model development to evaluate treatment of pneumonic plague.
26. **Fellows P, Price J, Martin S, Metcalfe K, Krile R, Barnewall R, Hart MK, Lockman H.** 2015. Characterization of a Cynomolgus Macaque Model of Pneumonic Plague for Evaluation of Vaccine Efficacy. Clin Vaccine Immunol **22:**1070-1078.
27. **Huang XZ, Nikolich MP, Lindler LE.** 2006. Current trends in plague research: from genomics to virulence. Clin Med Res **4:**189-199.
28. **Sha J, Endsley JJ, Kirtley ML, Foltz SM, Huante MB, Erova TE, Kozlova EV, Popov VL, Yeager LA, Zudina IV, Motin VL, Peterson JW, DeBord KL, Chopra AK.** 2011. Characterization of an F1 deletion mutant of *Yersinia pestis* CO92, pathogenic role of F1 antigen in bubonic and pneumonic plague, and

evaluation of sensitivity and specificity of F1 antigen capture-based dipsticks. J Clin Microbiol **49:**1708-1715.

29. **Quenee LE, Cornelius CA, Ciletti NA, Elli D, Schneewind O.** 2008. *Yersinia pestis caf1* variants and the limits of plague vaccine protection. Infect Immun **76:**2025-2036.
30. **Anisimov AP, Dentovskaya SV, Panfertsev EA, Svetoch TE, Kopylov P, Segelke BW, Zemla A, Telepnev MV, Motin VL.** 2010. Amino acid and structural variability of *Yersinia pestis* LcrV protein. Infect Genet Evol **10:**137-145.
31. **Anisimov AP, Panfertsev EA, Svetoch TE, Dentovskaya SV.** 2007. Variability of the protein sequences of *lcrV* between epidemic and atypical rhamnose-positive strains of *Yersinia pestis*. Adv Exp Med Biol **603:**23-27.
32. **Williams JE, Altieri PL, Berman S, Lowenthal JP, Cavanaugh DC.** 1980. Potency of killed plague vaccines prepared from avirulent *Yersinia pestis*. Bull World Health Organ **58:**753-756.
33. **GIRARD G.** 1963. [IMMUNITY IN PLAGUE. ACQUISITIONS SUPPLIED BY 30 YEARS OF WORK ON THE "PASTEURELLA PESTIS EV" (GIRARD AND ROBIC) STRAIN]. Biol Med (Paris) **52:**631-731.
34. **Zhou D, Han Y, Dai E, Song Y, Pei D, Zhai J, Du Z, Wang J, Guo Z, Yang R.** 2004. Defining the genome content of live plague vaccines by use of whole-genome DNA microarray. Vaccine **22:**3367-3374.
35. **Cui Y, Yang X, Xiao X, Anisimov AP, Li D, Yan Y, Zhou D, Rajerison M, Carniel E, Achtman M, Yang R, Song Y.** 2014. Genetic variations of live attenuated plague vaccine strains (*Yersinia pestis* EV76 lineage) during laboratory passages in different countries. Infect Genet Evol **26:**172-179.
36. **Feodorova VA, Corbel MJ.** 2009. Prospects for new plague vaccines. Expert Rev Vaccines **8:**1721-1738.
37. **CDC.** 2011. Fatal laboratory-acquired infection with an attenuated *Yersinia pestis* Strain--Chicago, Illinois, 2009. MMWR Morb Mortal Wkly Rep **60:**201-205.
38. **Quenee LE, Hermanas TM, Ciletti N, Louvel H, Miller NC, Elli D, Blaylock B, Mitchell A, Schroeder J, Krausz T, Kanabrocki J, Schneewind O.** 2012. Hereditary hemochromatosis restores the virulence of plague vaccine strains. J Infect Dis **206:**1050-1058.
39. **Tiner BL, Sha J, Kirtley ML, Erova TE, Popov VL, Baze WB, van Lier CJ, Ponnusamy D, Andersson JA, Motin VL, Chauhan S, Chopra AK.** 2015. Combinational Deletion of Three Membrane Protein-Encoding Genes Highly Attenuates *Yersinia pestis* while Retaining Immunogenicity in a Mouse Model of Pneumonic Plague. Infect Immun **83:**1318-1338.
40. **van Lier CJ, Sha J, Kirtley ML, Cao A, Tiner BL, Erova TE, Cong Y, Kozlova EV, Popov VL, Baze WB, Chopra AK.** 2014. Deletion of Braun lipoprotein and plasminogen-activating protease-encoding genes attenuates *Yersinia pestis* in mouse models of bubonic and pneumonic plague. Infect Immun **82:**2485-2503.
41. **Tiner BL, Sha J, Ponnusamy D, Baze WB, Fitts EC, Popov VL, van Lier CJ, Erova TE, Chopra AK.** 2015. Intramuscular Immunization of Mice with a Live-Attenuated Triple Mutant of *Yersinia pestis* CO92 Induces Robust Humoral and Cell-Mediated Immunity To Completely Protect Animals against Pneumonic Plague. Clin Vaccine Immunol **22:**1255-1268.

42. **Sha J, Kirtley ML, van Lier CJ, Wang S, Erova TE, Kozlova EV, Cao A, Cong Y, Fitts EC, Rosenzweig JA, Chopra AK.** 2013. Deletion of the Braun lipoprotein-encoding gene and altering the function of lipopolysaccharide attenuate the plague bacterium. Infect Immun **81:**815-828.
43. **Glauser MP, Zanetti G, Baumgartner JD, Cohen J.** 1991. Septic shock: pathogenesis. Lancet **338:**732-736.
44. **Braun V, Hantke K.** 1974. Biochemistry of bacterial cell envelopes. Annu Rev Biochem **43:**89-121.
45. **Neilsen PO, Zimmerman GA, McIntyre TM.** 2001. *Escherichia coli* Braun lipoprotein induces a lipopolysaccharide-like endotoxic response from primary human endothelial cells. J Immunol **167:**5231-5239.
46. **Aliprantis AO, Yang RB, Mark MR, Suggett S, Devaux B, Radolf JD, Klimpel GR, Godowski P, Zychlinsky A.** 1999. Cell activation and apoptosis by bacterial lipoproteins through toll-like receptor-2. Science **285:**736-739.
47. **Pernerstorfer T, Stohlawetz P, Hollenstein U, Dzirlo L, Eichler HG, Kapiotis S, Jilma B, Speiser W.** 1999. Endotoxin-induced activation of the coagulation cascade in humans: effect of acetylsalicylic acid and acetaminophen. Arterioscler Thromb Vasc Biol **19:**2517-2523.
48. **Jacob A, Hensley LK, Safratowich BD, Quigg RJ, Alexander JJ.** 2007. The role of the complement cascade in endotoxin-induced septic encephalopathy. Lab Invest **87:**1186-1194.
49. **Bashir A, Banday MZ, Haq E.** 2011. Lipopolysaccharide, mediator of sepsis enigma: recognition and signaling. Int J Biochem Res Rev **1:**1-13.
50. **van Lier CJ, Tiner BL, Chauhan S, Motin VL, Fitts EC, Huante MB, Endsley JJ, Ponnusamy D, Sha J, Chopra AK.** 2015. Further characterization of a highly attenuated *Yersinia pestis* CO92 mutant deleted for the genes encoding Braun lipoprotein and plasminogen activator protease in murine alveolar and primary human macrophages. Microb Pathog **80C:**27-38.
51. **Sha J, Agar SL, Baze WB, Olano JP, Fadl AA, Erova TE, Wang S, Foltz SM, Suarez G, Motin VL, Chauhan S, Klimpel GR, Peterson JW, Chopra AK.** 2008. Braun lipoprotein (Lpp) contributes to virulence of yersiniae: potential role of Lpp in inducing bubonic and pneumonic plague. Infect Immun **76:**1390-1409.
52. **Liu T, Agar SL, Sha J, Chopra AK.** 2010. Deletion of Braun lipoprotein gene (*lpp*) attenuates *Yersinia pestis* KIM/D27 strain: role of Lpp in modulating host immune response, NF-kappaB activation and cell death. Microb Pathog **48:**42-52.
53. **Hantke K, Braun V.** 1973. Covalent binding of lipid to protein. Diglyceride and amide-linked fatty acid at the N-terminal end of the murein-lipoprotein of the *Escherichia coli* outer membrane. Eur J Biochem **34:**284-296.
54. **Rebeil R, Ernst RK, Jarrett CO, Adams KN, Miller SI, Hinnebusch BJ.** 2006. Characterization of late acyltransferase genes of *Yersinia pestis* and their role in temperature-dependent lipid A variation. J Bacteriol **188:**1381-1388.
55. **Clementz T, Bednarski JJ, Raetz CR.** 1996. Function of the *htrB* high temperature requirement gene of *Escherchia coli* in the acylation of lipid A: HtrB catalyzed incorporation of laurate. J Biol Chem **271:**12095-12102.
56. **Clementz T, Zhou Z, Raetz CR.** 1997. Function of the *Escherichia coli msbB* gene, a multicopy suppressor of *htrB* knockouts, in the acylation of lipid A.

Acylation by MsbB follows laurate incorporation by HtrB. J Biol Chem **272:**10353-10360.

57. **Somerville JE, Cassiano L, Bainbridge B, Cunningham MD, Darveau RP.** 1996. A novel *Escherichia coli* lipid A mutant that produces an antiinflammatory lipopolysaccharide. J Clin Invest **97:**359-365.
58. **Rebeil R, Ernst RK, Gowen BB, Miller SI, Hinnebusch BJ.** 2004. Variation in lipid A structure in the pathogenic yersiniae. Mol Microbiol **52:**1363-1373.
59. **Anisimov AP, Shaikhutdinova RZ, Pan'kina LN, Feodorova VA, Savostina EP, Bystrova OV, Lindner B, Mokrievich AN, Bakhteeva IV, Titareva GM, Dentovskaya SV, Kocharova NA, Senchenkova SN, Holst O, Devdariani ZL, Popov YA, Pier GB, Knirel YA.** 2007. Effect of deletion of the *lpxM* gene on virulence and vaccine potential of *Yersinia pestis* in mice. J Med Microbiol **56:**443-453.
60. **Knirel YA, Lindner B, Vinogradov EV, Kocharova NA, Senchenkova SN, Shaikhutdinova RZ, Dentovskaya SV, Fursova NK, Bakhteeva IV, Titareva GM, Balakhonov SV, Holst O, Gremyakova TA, Pier GB, Anisimov AP.** 2005. Temperature-dependent variations and intraspecies diversity of the structure of the lipopolysaccharide of *Yersinia pestis.* Biochemistry **44:**1731-1743.
61. **Pérez-Gutiérrez C, Llobet E, Llompart CM, Reinés M, Bengoechea JA.** 2010. Role of lipid A acylation in *Yersinia enterocolitica* virulence. Infect Immun **78:**2768-2781.
62. **Oyston PC, Prior JL, Kiljunen S, Skurnik M, Hill J, Titball RW.** 2003. Expression of heterologous O-antigen in *Yersinia pestis* KIM does not affect virulence by the intravenous route. J Med Microbiol **52:**289-294.
63. **Montminy SW, Khan N, McGrath S, Walkowicz MJ, Sharp F, Conlon JE, Fukase K, Kusumoto S, Sweet C, Miyake K, Akira S, Cotter RJ, Goguen JD, Lien E.** 2006. Virulence factors of *Yersinia pestis* are overcome by a strong lipopolysaccharide response. Nat Immunol **7:**1066-1073.
64. **Kawahara K, Tsukano H, Watanabe H, Lindner B, Matsuura M.** 2002. Modification of the structure and activity of lipid A in *Yersinia pestis* lipopolysaccharide by growth temperature. Infect Immun **70:**4092-4098.
65. **Sodeinde OA, Goguen JD.** 1988. Genetic analysis of the 9.5-kilobase virulence plasmid of *Yersinia pestis*. Infect Immun **56:**2743-2748.
66. **Lähteenmäki K, Virkola R, Sarén A, Emödy L, Korhonen TK.** 1998. Expression of plasminogen activator *pla* of *Yersinia pestis* enhances bacterial attachment to the mammalian extracellular matrix. Infect Immun **66:**5755-5762.
67. **Suomalainen M, Haiko J, Ramu P, Lobo L, Kukkonen M, Westerlund-Wikström B, Virkola R, Lähteenmäki K, Korhonen TK.** 2007. Using every trick in the book: the Pla surface protease of *Yersinia pestis.* Adv Exp Med Biol **603:**268-278.
68. **Sodeinde OA, Subrahmanyam YV, Stark K, Quan T, Bao Y, Goguen JD.** 1992. A surface protease and the invasive character of plague. Science **258:**1004-1007.
69. **Sebbane F, Jarrett CO, Gardner D, Long D, Hinnebusch BJ.** 2006. Role of the *Yersinia pestis* plasminogen activator in the incidence of distinct septicemic and bubonic forms of flea-borne plague. Proc Natl Acad Sci U S A **103:**5526-5530.

70. **Szaba FM, Smiley ST.** 2002. Roles for thrombin and fibrin(ogen) in cytokine/chemokine production and macrophage adhesion in vivo. Blood **99:**1053-1059.
71. **Caulfield AJ, Lathem WW.** 2012. Substrates of the plasminogen activator protease of *Yersinia pestis.* Adv Exp Med Biol **954:**253-260.
72. **Lathem WW, Price PA, Miller VL, Goldman WE.** 2007. A plasminogen-activating protease specifically controls the development of primary pneumonic plague. Science **315:**509-513.
73. **Luo D, Lin JS, Parent MA, Mullarky-Kanevsky I, Szaba FM, Kummer LW, Duso DK, Tighe M, Hill J, Gruber A, Mackman N, Gailani D, Smiley ST.** 2013. Fibrin facilitates both innate and T cell-mediated defense against *Yersinia pestis*. J Immunol **190:**4149-4161.
74. **Agar SL, Sha J, Baze WB, Erova TE, Foltz SM, Suarez G, Wang S, Chopra AK.** 2009. Deletion of Braun lipoprotein gene (*lpp*) and curing of plasmid pPCP1 dramatically alter the virulence of *Yersinia pestis* CO92 in a mouse model of pneumonic plague. Microbiology **155:**3247-3259.
75. **Bartra SS, Styer KL, O'Bryant DM, Nilles ML, Hinnebusch BJ, Aballay A, Plano GV.** 2008. Resistance of *Yersinia pestis* to complement-dependent killing is mediated by the Ail outer membrane protein. Infect Immun **76:**612-622.
76. **Hinnebusch BJ, Jarrett CO, Callison JA, Gardner D, Buchanan SK, Plano GV.** 2011. Role of the *Yersinia pestis* Ail protein in preventing a protective polymorphonuclear leukocyte response during bubonic plague. Infect Immun **79:**4984-4989.
77. **Kolodziejek AM, Schnider DR, Rohde HN, Wojtowicz AJ, Bohach GA, Minnich SA, Hovde CJ.** 2010. Outer membrane protein X (Ail) contributes to *Yersinia pestis* virulence in pneumonic plague and its activity is dependent on the lipopolysaccharide core length. Infect Immun **78:**5233-5243.
78. **Kolodziejek AM, Sinclair DJ, Seo KS, Schnider DR, Deobald CF, Rohde HN, Viall AK, Minnich SS, Hovde CJ, Minnich SA, Bohach GA.** 2007. Phenotypic characterization of OmpX, an Ail homologue of *Yersinia pestis* KIM. Microbiology **153:**2941-2951.
79. **Myers-Morales T, Cowan C, Gray ME, Wulff CR, Parker CE, Borchers CH, Straley SC.** 2007. A surface-focused biotinylation procedure identifies the *Yersinia pestis* catalase KatY as a membrane-associated but non-surface-located protein. Appl Environ Microbiol **73:**5750-5759.
80. **Pieper R, Huang ST, Robinson JM, Clark DJ, Alami H, Parmar PP, Perry RD, Fleischmann RD, Peterson SN.** 2009. Temperature and growth phase influence the outer-membrane proteome and the expression of a type VI secretion system in *Yersinia pestis*. Microbiology **155:**498-512.
81. **Pieper R, Huang ST, Clark DJ, Robinson JM, Alami H, Parmar PP, Suh MJ, Kuntumalla S, Bunai CL, Perry RD, Fleischmann RD, Peterson SN.** 2009. Integral and peripheral association of proteins and protein complexes with *Yersinia pestis* inner and outer membranes. Proteome Sci **7:**5.
82. **Ho DK, Riva R, Kirjavainen V, Jarva H, Ginstrom E, Blom AM, Skurnik M, Meri S.** 2012. Functional recruitment of the human complement inhibitor C4BP to

Yersinia pseudotuberculosis outer membrane protein Ail. J Immunol **188:**4450-4459.

83. **Kirjavainen V, Jarva H, Biedzka-Sarek M, Blom AM, Skurnik M, Meri S.** 2008. *Yersinia enterocolitica* serum resistance proteins YadA and Ail bind the complement regulator C4b-binding protein. PLoS Pathog **4:**e1000140.
84. **Ho DK, Skurnik M, Blom AM, Meri S.** 2014. *Yersinia pestis* Ail recruitment of C4b-binding protein leads to factor I-mediated inactivation of covalently and noncovalently bound C4b. Eur J Immunol **44:**742-751.
85. **Ho DK, Riva R, Skurnik M, Meri S.** 2012. The *Yersinia pseudotuberculosis* outer membrane protein Ail recruits the human complement regulatory protein factor H. J Immunol **189:**3593-3599.
86. **Biedzka-Sarek M, Jarva H, Hyytiainen H, Meri S, Skurnik M.** 2008. Characterization of complement factor H binding to *Yersinia enterocolitica* serotype O:3. Infect Immun **76:**4100-4109.
87. **Biedzka-Sarek M, Salmenlinna S, Gruber M, Lupas AN, Meri S, Skurnik M.** 2008. Functional mapping of YadA- and Ail-mediated binding of human factor H to *Yersinia enterocolitica* serotype O:3. Infect Immun **76:**5016-5027.
88. **Felek S, Krukonis ES.** 2009. The *Yersinia pestis* Ail protein mediates binding and Yop delivery to host cells required for plague virulence. Infect Immun **77:**825-836.
89. **Tsang TM, Felek S, Krukonis ES.** 2010. Ail binding to fibronectin facilitates *Yersinia pestis* binding to host cells and Yop delivery. Infect Immun **78:**3358-3368.
90. **Tsang TM, Annis DS, Kronshage M, Fenno JT, Usselman LD, Mosher DF, Krukonis ES.** 2012. Ail protein binds ninth type III fibronectin repeat (^{9}FNIII) within central 120-kDa region of fibronectin to facilitate cell binding by *Yersinia pestis*. J Biol Chem **287:**16759-16767.
91. **Yamashita S, Lukacik P, Barnard TJ, Noinaj N, Felek S, Tsang TM, Krukonis ES, Hinnebusch BJ, Buchanan SK.** 2011. Structural insights into Ail-mediated adhesion in *Yersinia pestis*. Structure **19:**1672-1682.
92. **Felek S, Tsang TM, Krukonis ES.** 2010. Three *Yersinia pestis* adhesins facilitate Yop delivery to eukaryotic cells and contribute to plague virulence. Infect Immun **78:**4134-4150.
93. **Erova TE, Rosenzweig JA, Sha J, Suarez G, Sierra JC, Kirtley ML, van Lier CJ, Telepnev MV, Motin VL, Chopra AK.** 2013. Evaluation of protective potential of *Yersinia pestis* outer membrane protein antigens as possible candidates for a new-generation recombinant plague vaccine. Clin Vaccine Immunol **20:**227-238.
94. **Choi KH, Schweizer HP.** 2005. An improved method for rapid generation of unmarked *Pseudomonas aeruginosa* deletion mutants. BMC Microbiol **5:**30.
95. **Datsenko KA, Wanner BL.** 2000. One-step inactivation of chromosomal genes in *Escherichia coli* K-12 using PCR products. Proc Natl Acad Sci U S A **97:**6640-6645.
96. **Edwards RA, Keller LH, Schifferli DM.** 1998. Improved allelic exchange vectors and their use to analyze 987P fimbria gene expression. Gene **207:**149-157.
97. **Sha J, Rosenzweig JA, Kirtley ML, van Lier CJ, Fitts EC, Kozlova EV, Erova TE, Tiner BL, Chopra AK.** 2013. A non-invasive in vivo imaging system to study

dissemination of bioluminescent *Yersinia pestis* CO92 in a mouse model of pneumonic plague. Microb Pathog **55:**39-50.

98. **Galindo CL, Sha J, Moen ST, Agar SL, Kirtley ML, Foltz SM, McIver LJ, Kozlova EV, Garner HR, Chopra AK.** 2010. Comparative Global Gene Expression Profiles of Wild-Type *Yersinia pestis* CO92 and Its Braun Lipoprotein Mutant at Flea and Human Body Temperatures. Comp Funct Genomics**:**342168.
99. **Choi KH, Gaynor JB, White KG, Lopez C, Bosio CM, Karkhoff-Schweizer RR, Schweizer HP.** 2005. A Tn*7*-based broad-range bacterial cloning and expression system. Nat Methods **2:**443-448.
100. **Sebbane F, Lemaitre N, Sturdevant DE, Rebeil R, Virtaneva K, Porcella SF, Hinnebusch BJ.** 2006. Adaptive response of *Yersinia pestis* to extracellular effectors of innate immunity during bubonic plague. Proc Natl Acad Sci U S A **103:**11766-11771.
101. **Cowan C, Jones HA, Kaya YH, Perry RD, Straley SC.** 2000. Invasion of epithelial cells by *Yersinia pestis*: evidence for a *Y. pestis*-specific invasin. Infect Immun **68:**4523-4530.
102. **Korhonen TK, Haiko J, Laakkonen L, Jarvinen HM, Westerlund-Wikstrom B.** 2013. Fibrinolytic and coagulative activities of *Yersinia pestis*. Front Cell Infect Microbiol **3:**35.
103. **Caulfield AJ, Walker ME, Gielda LM, Lathem WW.** 2014. The Pla protease of *Yersinia pestis* degrades fas ligand to manipulate host cell death and inflammation. Cell Host Microbe **15:**424-434.
104. **Agarkov A, Chauhan S, Lory PJ, Gilbertson SR, Motin VL.** 2008. Substrate specificity and screening of the integral membrane protease Pla. Bioorg Med Chem Lett **18:**427-431.
105. **Liu F, Chen H, Galván EM, Lasaro MA, Schifferli DM.** 2006. Effects of Psa and F1 on the adhesive and invasive interactions of *Yersinia pestis* with human respiratory tract epithelial cells. Infect Immun **74:**5636-5644.
106. **Tao P, Mahalingam M, Kirtley ML, van Lier CJ, Sha J, Yeager LA, Chopra AK, Rao VB.** 2013. Mutated and bacteriophage T4 nanoparticle arrayed F1-V immunogens from *Yersinia pestis* as next generation plague vaccines. PLoS Pathog **9:**e1003495.
107. **Craig NL.** 1996. Transposon Tn*7*. Curr Top Microbiol Immunol **204:**27-48.
108. **Peters JE, Craig NL.** 2001. Tn*7*: smarter than we thought. Nat Rev Mol Cell Biol **2:**806-814.
109. **Chromy BA, Choi MW, Murphy GA, Gonzales AD, Corzett CH, Chang BC, Fitch JP, McCutchen-Maloney SL.** 2005. Proteomic characterization of Y*ersinia pestis* virulence. J Bacteriol **187:**8172-8180.
110. **Suomalainen M, Lobo LA, Brandenburg K, Lindner B, Virkola R, Knirel YA, Anisimov AP, Holst O, Korhonen TK.** 2010. Temperature-induced changes in the lipopolysaccharide of *Yersinia pestis* affect plasminogen activation by the *pla* surface protease. Infect Immun **78:**2644-2652.
111. **Du Y, Rosqvist R, Forsberg A.** 2002. Role of fraction 1 antigen of *Yersinia pestis* in inhibition of phagocytosis. Infect Immun **70:**1453-1460.

112. **Paczosa MK, Fisher ML, Maldonado-Arocho FJ, Mecsas J.** 2014. *Yersinia pseudotuberculosis* uses Ail and YadA to circumvent neutrophils by directing Yop translocation during lung infection. Cell Microbiol **16:**247-268.
113. **Pillay J, den Braber I, Vrisekoop N, Kwast LM, de Boer RJ, Borghans JA, Tesselaar K, Koenderman L.** 2010. In vivo labeling with $^{2}H_{2}O$ reveals a human neutrophil lifespan of 5.4 days. Blood **116:**625-627.
114. **Elvin SJ, Williamson ED, Scott JC, Smith JN, Pérez De Lema G, Chilla S, Clapham P, Pfeffer K, Schlöndorff D, Luckow B.** 2004. Evolutionary genetics: Ambiguous role of CCR5 in *Y. pestis* infection. Nature **430:**417.
115. **Pujol C, Bliska JB.** 2003. The ability to replicate in macrophages is conserved between *Yersinia pestis* and *Yersinia pseudotuberculosis*. Infect Immun **71:**5892-5899.
116. **Tsang TM, Wiese JS, Felek S, Kronshage M, Krukonis ES.** 2013. Ail proteins of *Yersinia pestis* and *Y. pseudotuberculosis* have different cell binding and invasion activities. PLoS One **8:**e83621.
117. **Cheng LW, Schneewind O.** 2000. *Yersinia enterocolitica* TyeA, an intracellular regulator of the type III machinery, is required for specific targeting of YopE, YopH, YopM, and YopN into the cytosol of eukaryotic cells. J Bacteriol **182:**3183-3190.
118. **DeBord KL, Lee VT, Schneewind O.** 2001. Roles of LcrG and LcrV during type III targeting of effector Yops by *Yersinia enterocolitica*. J Bacteriol **183:**4588-4598.
119. **Houppert AS, Kwiatkowski E, Glass EM, DeBord KL, Merritt PM, Schneewind O, Marketon MM.** 2012. Identification of chromosomal genes in *Yersinia pestis* that influence type III secretion and delivery of Yops into target cells. PLoS One **7:**e34039.
120. **Lee VT, Anderson DM, Schneewind O.** 1998. Targeting of Yersinia Yop proteins into the cytosol of HeLa cells: one-step translocation of YopE across bacterial and eukaryotic membranes is dependent on SycE chaperone. Mol Microbiol **28:**593-601.
121. **Straley SC.** 1988. The plasmid-encoded outer-membrane proteins of *Yersinia pestis*. Rev Infect Dis **10 Suppl 2:**S323-326.
122. **Eddy JL, Gielda LM, Caulfield AJ, Rangel SM, Lathem WW.** 2014. Production of Outer Membrane Vesicles by the Plague Pathogen *Yersinia pestis*. PLoS One **9:**e107002.
123. **Boland A, Cornelis GR.** 1998. Role of YopP in suppression of tumor necrosis factor alpha release by macrophages during Yersinia infection. Infect Immun **66:**1878-1884.
124. **Fernando MR, Reyes JL, Iannuzzi J, Leung G, McKay DM.** 2014. The pro-inflammatory cytokine, interleukin-6, enhances the polarization of alternatively activated macrophages. PLoS One **9:**e94188.
125. **Perez-Gutierrez C, Llobet E, Llompart CM, Reines M, Bengoechea JA.** 2010. Role of lipid A acylation in *Yersinia enterocolitica* virulence. Infect Immun **78:**2768-2781.

126. **Diseases NCfIaR.** 2011. General recommendations on immunization --- recommendations of the Advisory Committee on Immunization Practices (ACIP). MMWR Recomm Rep **60:**1-64.
127. **Miller VL, Beer KB, Heusipp G, Young BM, Wachtel MR.** 2001. Identification of regions of Ail required for the invasion and serum resistance phenotypes. Mol Microbiol **41:**1053-1062.
128. **You YH, Wang P, Wang YH, Zhang MJ, Song ZZ, Hai R, Yu DZ, Wang HB, Dong XQ, Zhang JZ.** 2012. Comparative genomic analysis of gene variations of two Chinese *Yersinia pestis* isolates from vaccine strain EV76. Biomed Environ Sci **25:**440-448.
129. **Nicolas JF, Guy B.** 2008. Intradermal, epidermal and transcutaneous vaccination: from immunology to clinical practice. Expert Rev Vaccines **7:**1201-1214.
130. **Poland GA, Borrud A, Jacobson RM, McDermott K, Wollan PC, Brakke D, Charboneau JW.** 1997. Determination of deltoid fat pad thickness. Implications for needle length in adult immunization. JAMA **277:**1709-1711.
131. **Shaw FE, Jr., Guess HA, Roets JM, Mohr FE, Coleman PJ, Mandel EJ, Roehm RR, Jr., Talley WS, Hadler SC.** 1989. Effect of anatomic injection site, age and smoking on the immune response to hepatitis B vaccination. Vaccine **7:**425-430.
132. **Groswasser J, Kahn A, Bouche B, Hanquinet S, Perlmuter N, Hessel L.** 1997. Needle length and injection technique for efficient intramuscular vaccine delivery in infants and children evaluated through an ultrasonographic determination of subcutaneous and muscle layer thickness. Pediatrics **100:**400-403.
133. **Gonzalez RJ, Weening EH, Lane MC, Miller VL.** 2015. Comparison of Models for Bubonic Plague Reveals Unique Pathogen Adaptations to the Dermis. Infect Immun **83:**2855-2861.
134. **Combadiere B, Liard C.** 2011. Transcutaneous and intradermal vaccination. Hum Vaccin **7:**811-827.
135. **Shayan R, Achen MG, Stacker SA.** 2006. Lymphatic vessels in cancer metastasis: bridging the gaps. Carcinogenesis **27:**1729-1738.
136. **Teunissen MB, Haniffa M, Collin MP.** 2012. Insight into the immunobiology of human skin and functional specialization of skin dendritic cell subsets to innovate intradermal vaccination design. Curr Top Microbiol Immunol **351:**25-76.
137. **Kumar P, Chen K, Kolls JK.** 2013. Th17 cell based vaccines in mucosal immunity. Curr Opin Immunol **25:**373-380.
138. **Szaba FM, Kummer LW, Wilhelm LB, Lin JS, Parent MA, Montminy-Paquette SW, Lien E, Johnson LL, Smiley ST.** 2009. D27-pLpxL, an avirulent strain of *Yersinia pestis*, primes T cells that protect against pneumonic plague. Infect Immun **77:**4295-4304.
139. **Zhang X, Wang Q, Bi Y, Kou Z, Zhou J, Cui Y, Yan Y, Zhou L, Tan Y, Yang H, Du Z, Han Y, Song Y, Zhang P, Zhou D, Yang R, Wang X.** 2014. Kinetics of memory B cell and plasma cell responses in the mice immunized with plague vaccines. Scand J Immunol **79:**157-162.
140. **Qi Z, Zhou L, Zhang Q, Ren L, Dai R, Wu B, Wang T, Zhu Z, Yang Y, Cui B, Wang Z, Wang H, Qiu Y, Guo Z, Yang R, Wang X.** 2010. Comparison of mouse,

guinea pig and rabbit models for evaluation of plague subunit vaccine F1+rV270. Vaccine **28:**1655-1660.

141. **Wang Z, Zhou L, Qi Z, Zhang Q, Dai R, Yang Y, Cui B, Wang H, Yang R, Wang X.** 2010. Long-term observation of subunit vaccine F1-rV270 against *Yersinia pestis* in mice. Clin Vaccine Immunol **17:**199-201.
142. **Feodorova VA, Sayapina LV, Corbel MJ, Motin VL.** 2014. Russian vaccines against especially dangerous bacterial pathogens. Emerg Microbes Infect **3:**e86.
143. **Russell P, Eley SM, Hibbs SE, Manchee RJ, Stagg AJ, Titball RW.** 1995. A comparison of Plague vaccine, USP and EV76 vaccine induced protection against *Yersinia pestis* in a murine model. Vaccine **13:**1551-1556.
144. **Meyer KF, Cavanaugh DC, Bartelloni PJ, Marshall JD.** 1974. Plague immunization. I. Past and present trends. J Infect Dis **129:**Suppl:S13-18.
145. **Meyer KF, Smith G, Foster L, Brookman M, Sung M.** 1974. Live, attenuated *Yersinia pestis* vaccine: virulent in nonhuman primates, harmless to guinea pigs. J Infect Dis **129:**Suppl:S85-12.
146. **Hallett AF, Isaäcson M, Meyer KF.** 1973. Pathogenicity and immunogenic efficacy of a live attentuated plaque vaccine in vervet monkeys. Infect Immun **8:**876-881.
147. **Une T, Brubaker RR.** 1984. In vivo comparison of avirulent Vwa- and Pgm- or Pstr phenotypes of yersiniae. Infect Immun **43:**895-900.
148. **Sun W, Roland KL, Curtiss R.** 2011. Developing live vaccines against plague. J Infect Dev Ctries **5:**614-627.
149. **Feodorova VA, Pan'kina LN, Savostina EP, Kuznetsov OS, Konnov NP, Sayapina LV, Dentovskaya SV, Shaikhutdinova RZ, Ageev SA, Lindner B, Kondakova AN, Bystrova OV, Kocharova NA, Senchenkova SN, Holst O, Pier GB, Knirel YA, Anisimov AP, Motin VL.** 2009. Pleiotropic effects of the *lpxM* mutation in *Yersinia pestis* resulting in modification of the biosynthesis of major immunoreactive antigens. Vaccine **27:**2240-2250.
150. **Clements JD, Freytag LC.** 2016. Parenteral Vaccination Can Be An Effective Means of Inducing Protective Mucosal Responses. Clin Vaccine Immunol.
151. **Anderson SM, Tomayko MM, Ahuja A, Haberman AM, Shlomchik MJ.** 2007. New markers for murine memory B cells that define mutated and unmutated subsets. J Exp Med **204:**2103-2114.
152. **Xiao Y, Hendriks J, Langerak P, Jacobs H, Borst J.** 2004. CD27 is acquired by primed B cells at the centroblast stage and promotes germinal center formation. J Immunol **172:**7432-7441.
153. **Sanz I, Wei C, Lee FE, Anolik J.** 2008. Phenotypic and functional heterogeneity of human memory B cells. Semin Immunol **20:**67-82.
154. **Nduati EW, Nkumama IN, Gambo FK, Muema DM, Knight MG, Hassan AS, Jahangir MN, Etyang TJ, Berkley JA, Urban, C. B.** 2016. HIV-exposed uninfected infants show robust memory B cell responses in spite of a delayed accumulation of memory B cells: An observational study in the first two years of life. Clinical Vaccine Immunology.
155. **Hume DA.** 2015. The Many Alternative Faces of Macrophage Activation. Front Immunol **6:**370.

156. **Lin JS, Park S, Adamovicz JJ, Hill J, Bliska JB, Cote CK, Perlin DS, Amemiya K, Smiley ST.** 2010. TNFα and IFNγ contribute to F1/LcrV-targeted immune defense in mouse models of fully virulent pneumonic plague. Vaccine **29:**357-362.
157. **Moore-Connors JM, Fraser R, Halperin SA, Wang J.** 2013. $CD4^+CD25^+Foxp3^+$ regulatory T cells promote Th17 responses and genital tract inflammation upon intracellular Chlamydia muridarum infection. J Immunol **191:**3430-3439.
158. **Wang Z, Friedrich C, Hagemann SC, Korte WH, Goharani N, Cording S, Eberl G, Sparwasser T, Lochner M.** 2014. Regulatory T cells promote a protective Th17-associated immune response to intestinal bacterial infection with C. rodentium. Mucosal Immunol **7:**1290-1301.
159. **Kambayashi T, Laufer TM.** 2014. Atypical MHC class II-expressing antigen-presenting cells: can anything replace a dendritic cell? Nat Rev Immunol **14:**719-730.

VITAE

Bethany Leeann Tiner was born on June 16th, 1989 in Houston, Texas, USA to parents, Wayne and Roxane Tiner, and she is the younger sister to Charlotte Beresik. In December 2010, she obtained her Bachelor's degree in Microbiology from Texas A&M University in College Station, Texas, USA. Due to her excellence in academics and research, Bethany was recruited to the University of Texas Medical Branch in August 2011 as a McLaughlin Scholar. She was awarded the Sealy Center for Vaccine Development Predoctoral Fellowship in the Fall of 2013 as well as the Jeane B. Kemper Predoctoral Fellowship in the Fall of 2015. Bethany also received numerous scholarships and travel awards. She attended the 2014 American Society of Microbiology Biodefense and Emerging Diseases Conference, the 2014 NFID Annual Conference on Vaccine Research, and the 2014 Vaccine Development Center of San Antonio Meeting. During Summer 2015, Bethany served as an intern for the Global Influenza Programme at the World Health Organziation in Geneva, Switzerland. She also represented current graduate students on the Microbiology and Immunology admissions committee and the UTMB alumni association. In January 2016, she married her husband, Peter Kundert.

Education

B.S., December 2010, Texas A&M University, College Station, Texas, USA

Permanent address: 1330 Old Spanish Trail
Apt. 3103
Houston, Texas 77054

This dissertation was typed by Bethany Tiner.

Publications

Articles in Peer-reviewed Journals

1. **Tiner BL**, Sha J, Cong Y, Chopra AK. 2016. Immunization of mice with new live-attenuated mutants of *Yersinia pestis CO92* induces protective long-term humoral- and cell-mediated immunity against pneumonic plague. Npj Vaccine (submitted; under review).
2. Sha J, Kirtley ML, Klages C, Erova TE, Telepnev M, Ponnusamy D, Fitts EC, Baze WB, Sivasubramani SK, Lawrence WS, Patrikeev I, Peel JE, Andersson JA, Kozlova EV, **Tiner BL**, Peterson JW, McWilliams D, Patel S, Rothe E, Motin VL, Chopra AK. 2016. A replication-defective human type-5 adenovirus-based trivalent vaccine confers complete protection against plague in mice and non-human primates. Clin Vaccine Immunol.
3. Ponnusamy D, Kozlova EV, Sha J, Erova TE, Azar SR, Fitts EC, Kirtley ML, **Tiner BL**, Andersson JA, Grim CJ, Isom RP, Hasan NA, Colwell RR, Chopra AK**.** 2016. Cross-talk among flesh-eating *Aeromonas hydrophila* strains in mixed infection leading to necrotizing fasciitis. Proc Natl Acad Sci U S A **113:**722-727.
4. **Tiner BL**, Sha, J, Ponnusamy D, Baze WB, Fitts EC, Popov VL, van Lier CJ, Erova TE, Chopra AK. 2015. Intramuscular immunization of mice with a live-attenuated triple mutant of *Yersinia pestis* CO92 induces robust humoral and cell-mediated immunity to completely protect animals against pneumonic plague. Clin Vaccine Immunol **22(12):**1255-1268.
5. Ponnusamy D, Fitts EC, Sha J, Erova TE, Kozlova EV, Kirtley ML, **Tiner BL**, Andersson JA, Chopra AK. 2015. High-throughput signature-tagged mutagenic approach to identify novel virulence factors of *Yersinia pestis* CO92 in a mouse model of infection. Infect. Immun. **83(5)**:2065-81.
6. **Tiner BL,** Sha J, Kirtley ML, Erova TE, Popov VL, Baze WB, van Lier CJ, Ponnusamy D, Andersson JA Motin VL, Chauhan S, Chopra AK. 2015. Combinational deletion of three membrane protein-encoding genes highly attenuates *Yersinia pestis* while retaining immunogenicity in a mouse model of pneumonic plague. Infect Immun. 83(4):1318-38.
7. van Lier CJ*, **Tiner BL***, Chauhan S, Motin VL, Fitts EC, Huante MB, Endsley JJ, Ponnusamy D, Sha J, Chopra AK. 2015. Further characterization of a highly attenuated *Yersinia pestis* CO92 mutant deleted for the genes encoding Braun lipoprotein and plasminogen activator protease in murine alveolar and primary human macrophages. Microb Pathog **80C:**27-38. ***first authors contributed equally**
8. Grim CJ, Kozlova EV, Ponnusamy D, Fitts EC, Sha J, Kirtley ML, van Lier CJ, **Tiner BL**, Erova TE, Joseph SJ, Read TD, Shak JR, Joseph SW, Singletary E, Felland T, Baze WB, Horneman AJ, Chopra AK. 2014. Functional genomic characterization of virulence factors from necrotizing fasciitis-causing strains of *Aeromonas hydrophila*. Applied and environmental microbiology **80:**4162-4183.
9. van Lier CJ, Sha J, Kirtley ML, Cao A, **Tiner BL,** Erova TE, Cong Y, Kozlova EV, Popov VL, Baze WB, Chopra AK. 2014. Deletion of Braun lipoprotein and plasminogen-activating protease-encoding genes attenuates *Yersinia pestis* in

mouse models of bubonic and pneumonic plague. Infect Immun **82:**2485-2503.

10. Sha J, Rosenzweig JA, Kirtley ML, van Lier CJ, Fitts EC, Kozlova EV, Erova TE, **Tiner BL**, Chopra AK. 2013. A non-invasive in vivo imaging system to study dissemination of bioluminescent *Yersinia pestis* CO92 in a mouse model of pneumonic plague. Microb Pathog **55:**39-50.
11. Xie J, **Tiner BL,** Vilchez I, Mateos M. 2010 Reproductive fitness of *Spiroplasma*-infected *Drosophila* flies surviving a parasitoid wasp attack. Evolutionary Ecology. DOI: 10.1007/s10682-010-9453-7

Abstracts

1. **Tiner BL**, Sha J, Cong Y, Chopra AK. 2016. Immunization of mice with new live-attenuated mutants of *Yersinia pestis CO92* induces protective long-term humoral- and cell-mediated immunity against pneumonic plague. (Poster; 2016 Institute of for Human Infections & Immunity McLaughlin Colloquium on Infection & Immunity)
2. **Tiner BL**, Sha J, Ponnuamy D, Fitts EC, Baze WB, Kirtley ML, Erova TE, Chopra AK. (2015). Triple Deletion of Membrane Protein-Encoding Genes Highly Attenuates *Yersinia pestis* CO92: Development of a Potential Live-Attenuated Plague Vaccine. (Poster; 2015 American Society for Microbiology General Meeting, New Orleans, LA, May 2015)
3. **Tiner BL**, Sha J, Ponnuamy D, Fitts EC, Baze WB, Kirtley ML, Erova TE, Chopra AK. (2015). Triple Deletion of Membrane Protein-Encoding Genes Highly Attenuates *Yersinia pestis* CO92: Development of a Potential Live-Attenuated Plague Vaccine. (Poster; 2015 Institute of for Human Infections & Immunity McLaughlin Colloquium on Infection & Immunity)
4. **Tiner BL**, Sha J, Kirtley ML, Ponnuamy D, van Lier C, Chopra AK. (2014). Construction and Testing of a Novel Live-Attenuated Plague Vaccine Deleted for Three Virulence Determinants. (Poster; 17th National Foundation for Infectious Diseases Annual Conference on Vaccine Research in Bethesda, Maryland, April 2014)
5. **Tiner BL**, Sha J, Kirtley ML, Ponnuamy D, van Lier C, Chopra AK. (2014). Construction and Testing of a Novel Live-Attenuated Plague Vaccine Deleted for Three Virulence Determinants. (Poster; 2014 Institute of for Human Infections & Immunity McLaughlin Colloquium on Infection & Immunity)
6. **Tiner BL**, Sha J, Kirtley ML, Erova TE, Popov VL, Baze WB, van Lier CJ, Ponnusamy D, Andersson JA, Motin VL, Chauhan S, and Chopra AK. (2014). Combinational deletion of three membrane protein-encoding genes highly attenuates *Yersinia pestis* while retaining immunogenicity in a mouse model of pneumonic plague. (Oral and Poster Presentation; 2014 Vaccine Development Center of San Antonio Conference in San Antonio, TX, Novermber 2014).
7. **Tiner BL**, Sha J, Kirtley ML, Ponnuamy D, van Lier C, Chopra AK. (2014). Construction and Testing of a Novel Live-Attenuated Plague Vaccine Deleted for Three Virulence Determinants. (Poster; 17th National Foundation for Infectious Diseases Annual Conference on Vaccine Research in Bethesda, Maryland, April 2014)

8. **Tiner BL**, Sha J, Kirtley ML, Ponnuamy D, van Lier C, Chopra AK. (2014). Construction and Testing of a Novel Live-Attenuated Plague Vaccine Deleted for Three Virulence Determinants. (Poster; 2014 Institute of for Human Infections & Immunity McLaughlin Colloquium on Infection & Immunity)
9. **Tiner BL**, Sha J, Kirtley ML, Ponnuamy D, van Lier C, Chopra AK. (2014). Construction and Testing of a Novel Live-Attenuated Plague Vaccine Deleted for Three Virulence Determinants. (Oral Presentation; 2014 ASM Biodefense and Emerging Diseases Research Meeting in Washington D.C.)
10. **Tiner BL**, Sha J, Kirtley ML, Ponnusamy D, Fitts E, Chopra AK. (2013) Outer Membrane Proteins of *Yersinia pestis* as Virulence Factors: Could Deletion of Such Genes Lead to the Development of a Suitable Live-attenuated Plague Vaccine? (Poster; 2013 Institute of for Human Infections & Immunity McLaughlin Colloquium on Infection & Immunity)